GENETIC AND MOLECULAR STUDIES OF MAMMALIAN HEART DEVELOPMENT

A Dissertation

Presented to the Faculty of the Graduate School

of Cornell University

in Partial Fulfillment of the Requirements for the Degree of

Doctor of Philosophy

by

Seung-Woo Jung

August 2009

GENETIC AND MOLECULAR STUDIES OF MAMMALIAN HEART DEVELOPMENT

Seung-Woo Jung, Ph.D.

Cornell University 2009

The genetic and molecular basis of mammalian cardiac development was studied in two model systems: German shepherd dogs (GSDs) afflicted with inherited juvenile ventricular arrhythmias and the dark-like (*dal*) mutant mouse, which I identify as a new model for studying myocardial development.

GSDs with inherited juvenile ventricular arrhythmias and sudden cardiac death are an established model for studying cardiac ventricular arrhythmias. The inheritance of this disease in GSDs is consistent with a major gene that allows a dog to be affected and modifiers that influence severity. Genome-wide linkage analysis was performed to identify the loci responsible, but no strong evidence of linkage was detected. As altered calcium homeostasis has been observed in the hearts of these dogs, I examined cardiac expression levels of genes implicated in calcium handling. A significant inverse correlation was observed between the levels of *ATP2A2* RNA and its protein product, SERCA2, and severity of ventricular arrhythmias, but no mutations were found in the *ATP2A2* coding sequence. SERCA2 is a calcium pump located on the sarcoplasmic reticulum (SR) that sequesters cytosolic calcium back to the SR. My work indicates that SERCA2 is a molecular determinant of severity of ventricular arrhythmias in GSDs and suggests that at least one of the causative genes acts upstream of *ATP2A2* transcription.

Mice homozygous for the *dal* mutation are small and have darkly pigmented fur. A spectrum of previously unrecognized developmental cardiac abnormalities was observed in *dal* mutant embryos, including a thickening of ventricular walls, atrial and ventricular septal defects, and enlarged endocardial cushions. No significant differences were detected in the proliferation status of mutant and control embryonic ventricles, but *dal* mutant embryonic cardiomyocytes were significantly larger than those of controls. This indicated that the thickened ventricles of *dal* mutant embryos result from developmental cardiac hypertrophy. Functional consequences associated with hypertrophy included early afterdepolarizations (EADs) and significant irregularities in the Ca^{2+} transient interval. Positional cloning identified a four base pair deletion in the *peptidase D* (*Pepd*) gene and morpholino knockdown of *Pepd* expression in zebrafish confirmed that *Pepd* loss of function disrupts normal myocardial development, pigmentation and body size. *Pepd* encodes prolidase, an enzyme involved in collagen metabolism. I hypothesized that loss of prolidase function in *dal* mutant embryos causes cardiac hypertrophy by disrupting the extracellular matrix and integrin signaling. Accordingly, I demonstrated reduced expression of integrin transducers and disrupted cytoskeletal organization in *dal* mutant embryonic hearts. My work provides a novel understanding of the genetic and molecular basis of developmental cardiac hypertrophy and has implications for the mechanisms that control the normal postnatal transition from proliferative to hypertrophic cardiomyocyte growth. These studies provide important insights into the genetic and molecular mechanisms underlying developmental cardiac disorders and will provide useful insights into understanding the pathogenesis of similar human heart diseases.

BIOGRAPHICAL SKETCH

Seung-Woo Jung was born in Seoul, Korean on August 13, 1976. He attended the College of Veterinary Medicine in Seoul National University, and received the degree of Doctor of Veterinary Medicine (D.V.M.) in 2001. While he pursued his clinical careers as an internist at Veterinary Teaching Hospital in Seoul National University during his master's degree, he was granted an opportunity to gain experience in the advanced veterinary cardiology clinic at Cornell University through the support of the Brain Korea 21 foundation in 2003. After additional training in Cardiology clinic in 2004, he decided to pursue Ph.D. degree in physiological genomics, and began graduate school at Cornell University in 2005 under mentorship of Dr. Teresa M. Gunn. His research focuses on genetic and molecular mechanisms underlying cardiovascular diseases of animals.

This dissertation is dedicated to my Lord and my Family.

I believe I can do everything through him who gives me strength (Philippians 4:13).

I am so much blessed to be a son of my parents, Kyu Jin Jung and Ok Hwa Kim.

My biggest heart and love goes to my dearest wife, Kyung Ha Lee.

ACKNOWLEDGEMENTS

There may be so many elements that make our life happy and fulfilled. Among them, I believe that “people” is one of the most important components in our life. Looking back the last 4 years of graduate study at Cornell University, I have to confess that I have been so much blessed to have so many great people around me. Without them, I would not have been able to go through those years and to dream the dream that I have for the future.

I really would like to take a moment to express my sincerest and deepest gratitude to my advisor, Dr. Teresa M. Gunn. She provided me the best guidance and opportunity of great learning. More importantly, it is Teresa’s inspiration and encouragement that made me continue to pursue my dream and not forget about it. Her patience, sacrifice, consistency, protection and devotion for me will be remembered forever.

I also would like to thank my committee members, Drs. John C. Schimenti, Robert F. Gilmour and N. Sydney Moïse for their support, help and valuable advice that made me succeed in my graduate study. Particularly, I would love to deliver special thanks to Dr. Moïse. She gave a life-changing opportunity to me. Words are not enough to describe how much I am grateful and touched by her constant and even continuously growing love onto me.

I also want to thank my colleagues, friends and family for their prayers and cheers for me. My biggest thoughts and gratitude always go to my wife, Kyung Ha Lee who makes my heart run.

My LORD, I bring all the glory to you and praise your name.

TABLE OF CONTENTS

LIST OF FIGURES

LIST OF TABLES

LIST OF ABBREVIATIONS

agouti …….…. (Ag)

Alpha-melanocortin stimulating hormone ……..……. (a-MSH)

Atrial septal defect ……..…… (ASD)

Attractin ……..……..… (Atrn)

Backcross ……...… (BC)

Base pair ……..……..…. (bp)

Bromo-2'-deoxy-uridine ……...…….…… (BrdU)

Calcium …… (Ca)

Calcium-induced calcium release …….. (CICR)

Calsequestrin ……...… (CASQ)

Cardiac myosin light chain ……..… (CMLC)

Celsius ……..….. (C)

Centimorgan …….…….……. (cM)

dark ……..…….…… (da)

dark-like ……..…… (*dal*)

days post fertilization …….……..…. (dpf)

Early afterdepolarization …… (EAD)

East campus research facility ……..…….…… (ECRF)

Embryonic day …….…..... (E)

Epithelial-to-mesenchymal ……..…….…… (EMT)

Extracellular matrix ……....…….…… (ECM)

Focal adhesion kinase ……..……..…….. (FAK)

German shepherd dog ……..……...… (GSD)

Glucose-6-phosphate isomerase ……..……..... (GPI)

Glyceraldehyde-3-phosphate dehydrogenase …… (GAPDH)

Green fluorescent protein ……..… (GFP)

Hematoxylin and Eosin ……..……. (H&E)

Identity-by-descent ……..……..……... (IBD)

Kilobases ……..……..……. (kb)

Kilo*dal*tons……..…... (kDa)

Late afterdepolarization ……..… (DAD)

Left ……..…… (L)

Left ventricle ……... (LV)

Left ventricular anterior apical …… (LVAA)

Lethal yellow agouti ……..... (A^y)

Logarithm of the odds ……..……..... (LOD)

L-type calcium channel …… (LTCC)

Mahogunin Ring Finger-1 ……..…. (Mgrn1)

Megabases ……..… (Mb)

Melanocortin-1 receptor ……..……. (Mc1r)

Morpholino ……..….. (MO)

Peptidase D ……..…. (Pepd)

Phosphate buffered saline ……. (PBS)

Phospholamban ……..…… (PLB)

Polymerase chain reaction …… (PCR)

Premature ventricular complexes …… (PVC)

Quantitative real time Polymerase chain reaction …… (qRT-PCR)

Quantitative trait loci ……..…… (QTL)

Relative quantification ……..…….. (RQ)

Reverse transcriptase ……... (RT)

Reverse transcriptase Polymerase chain reaction ……..…..…… (RT-PCR)

Right ……..…… (R)

Room temperature ……....…..……. (RT)

Ryanodine receptor ……..……... (RyR)

Sarcoplasmic reticulum ……..….. (SR)

Sarcoplasmic reticulum calcium ATPase …….. (SERCA)

Severely affected ……..….. (SA)

Single nucleotide polymorphism ……..… (SNP)

Small interfering RNA ……..……..…….. (siRNA)

Sodium/calcium exchanger ……..…. (NCX)

Sudden cardiac death ……..……...……... (SCD)

Triadin ……... (TRDN)

Unaffected ……..…. (UA)

Vascular endothelial growth factor ……..... (VEGF)

Ventricular arrhythmias ……..……..… (VA)

Ventricular septal defect ……..…. (VSD)

Ventricular tachycardia ……...…….. (VT)

Wild-type ……..…….. (WT)

CHAPTER 1

LITERATURE REVIEW

Normal cardiac development

Cardiac morphogenesis is a complex process. The earliest cardiac progenitors arise from lateral plate mesoderm under the control of proteins secreted from the adjacent endoderm. These proteins include fibroblast growth factors (FGFs), bone morphogenetic proteins (BMPs), and Wnt proteins (Srivastava, 2006). *Nkx2.5* is a transcription factor necessary for specification of the cardiac lineage. It directly activates transcription of the *Mef2* (myocyte enhancer factor 2) gene, which is involved in myocyte differentiation. Cardiac progenitors are arranged in bilateral fields on either side of the prechordal plate and rostral notochord. These fields contain both myocardial and endocardial precursor cells (Tam et al., 1997). The bilateral fields of the cardiogenic mesoderm merge at their anterior margins to form the cardiac crescent (Brown et al., 2005). A second type of heart field is located medially in the splanchnic mesoderm, adjacent to the cardiac crescent. The cells from this anterior heart-forming field are fated to generate anterior heart structures of the outflow tracts (Kelly and Buckingham, 2002). The earliest steps of assembly of the heart tube, initiated by the fusion of the bilateral heart primordial along the midline, are controlled by the GATA transcription factor (Bisaha and Bader, 1991). The beating tubular heart is composed of an external myocardial and an internal endocardial layer. It also possesses a polarity along the anteroposterior axis, where the prospective tissues of the

outflow tract, right ventricle, left ventricle, and atria are arranged in an anterior to posterior order along the heart tube (Christoffels et al., 2000).

The tubular heart undergoes a process called rightward looping, which is essential for proper orientation of the right and left ventricles and for alignment of the heart chambers with the vasculature. The direction of cardiac looping is determined by the asymmetrical expression of *Sonic hedgehog* (*Shh*) and *Nodal*, a member of the transforming growth factor-β (TGF-β) family, and affects the position of the internal organs. Left-right signals are translated to the organ primordia by the transcription factor *Pitx2*, which is expressed along the left side of developing embryo (Okada et al., 2005). Further septal division of the chambers and formation of cardiac valves are essential steps leading to the formation of an integrated 4-chambered heart. Regulatory genes encoding transcription factors such as Gata4, Gata5, Gata6, Tbx1(also known as Brachyury), Tbx5 and Nkx- 2.5 are involved in specification, trabeculation, and differentiation of the heart (Anversa and Nadal-Ginard, 2002; Zaffran and Frasch, 2002). In mammalian hearts, the transcription factors HAND1 and HAND2 are expressed predominantly in the primitive left and right ventricular segments, respectively (Srivastava et al., 1995). Interestingly, only the right ventricular marker HAND2 is expressed in zebrafish heart, which consists of one ventricle and one atrium.

Prior to trabeculation (development of the finger-like projections comprised of ventricular cardiomyocytes), the heart tube consists of an outer myocardial layer that is separated from an inner endocardial cell layer by an intervening matrix called cardiac jelly. Signaling from the endocardium to the ventricular

myocardium initiates the conversion of the myocardium into a thickened ventricular myocardial chamber wall capable of contraction. This process includes the proliferation, differentiation, and migration of cells out of the myocardial layer into the lumen of the ventricle to form trabeculae at the outer curvature of the looped heart tube (Icardo and Fernandez-Teran, 1987).

The trabecular myocardium is largely responsible for the maintenance of blood flow during development. Several signal transduction pathways are involved in formation of myocardial trabeculation and myocardial growth. These include the retinoic acid (RA), neuregulin/ErBb, serotonin, vascular endothelial growth factor (VEGF), and bone morphogenic protein-10 (BMP-10) pathways. Neuregulin growth factor, secreted from the endocardium, and its myocardial receptors, ErbB2 and ErbB4, are required for development of trabeculae (Lee et al., 1995). Transgenic mice over-expressing the cardiac-specific growth factor BMP-10 developed hyper-trabeculated hearts (Chen et al., 2006). Further analysis of these mutants showed that BMP-10 plays a critical role in formation of the trabeculated myocardium by regulating both the proliferation of cardiomyocytes and postnatal hypertrophic growth to provide appropriate numbers of cells to the compact ventricular wall critical for normal heart function (Chen et al., 2006).

Blood flow through a chambered heart requires synchronized pumping between different heart chambers. Proper formation of the cardiac valve is critical to ensure that blood flows in one direction and to prevent backflow in the opposite direction. The precursors of valves, called cardiac cushions, form between atria and ventricles within the atrioventricular canal. In the AV canal,

cushion formation begins when the cardiac jelly expands and swells into the cushion primordial that becomes cellularized via the influx of mesenchymal cells (Eisenberg and Markwald, 1995). These cells come from the endocardial cell layer from which they have delaminated after undergoing an epithelial-to-mesenchymal transformation (EMT) process. The signals that direct the endocardium to form AV endocardial cushions include BMP-2, Wnt, Notch, TGF-β, vascular endothelial growth factor (VEGF), neurofibromin, and extracellular matrix (ECM) produced by endocardial cells (Ramsdell et al., 1998). The successful integration of these various signaling pathways is crucial to heart development since abnormalities of the myocardium and valves comprise the majority of congenital heart defects.

The development of the sympathetic nervous system is a coordinated process for the sympathetic lineage and expression of catecholaminergic and neuronal traits. Neural crest cell-derived precursor cells migrate ventrally, aggregate adjacent to the dorsal aorta and ultimately differentiate into catecholaminergic neurons (Anderson, 1993). Transcription factors whose expression coincide with these differentiation events are *MASH1, eHAND, dHAND, Phox2a*, and *Gata-2* (Groves et al., 1995). Cell number is refined during a period of cell death when neurotrophic factors, such as nerve growth factor (NGF) and neurotrophin (NT-3), determine the number of neuronal precursors and neurons that survive (Groves et al., 1995). Sympathetic neurons transport NGF from target tissues, and application of NGF to nerve terminals maintains sympathetic neurons. During development, increasing NGF levels rescues sympathetic neurons that normally die, whereas decreasing NGF causes destruction of the sympathetic nervous systems (Albers et al., 1994). NT-3

acts later in development to maintain dividing sympathetic precursors that are not responsive to NGF, and NT-3 increases the survival of precursors isolated from embryonic sympathetic ganglia (Verdi et al., 1996).

Embryonic cardiac growth is mainly accomplished by hyperplasia of myocardial cells, and further hypertrophic growth of the heart after birth makes the heart 30- to 40-fold larger during postnatal maturation (Figure 1.1) (Oparil et al., 1984). The molecular and genetic mechanisms of this transition process from hyperplasia to hypertrophy remain largely unknown. A role for cardiac fibroblasts was elucidated in embryonic myocardial development (Ieda et al., 2009). This study suggested that cardiac fibroblasts are not merely a supportive structure, but rather provide a microenvironment, via the secretion of growth factors and extracellular matrix proteins, that allows cardiomyocytes and cardiac fibroblasts to communicate. This group found that embryonic cardiac fibroblasts regulate the proliferation of cardiomyocytes through the secretion of extracellular matrix proteins (collagen, fibronectin), and that β1 integrin signaling plays a critical role in this process.

Congenital cardiac defects arise from abnormal heart development during embryogenesis. Even subtle perturbations in cardiogenesis can cause cardiac malformations with devastating consequences. While some of the genetic and molecular mechanisms have been identified, much remains to be learned.

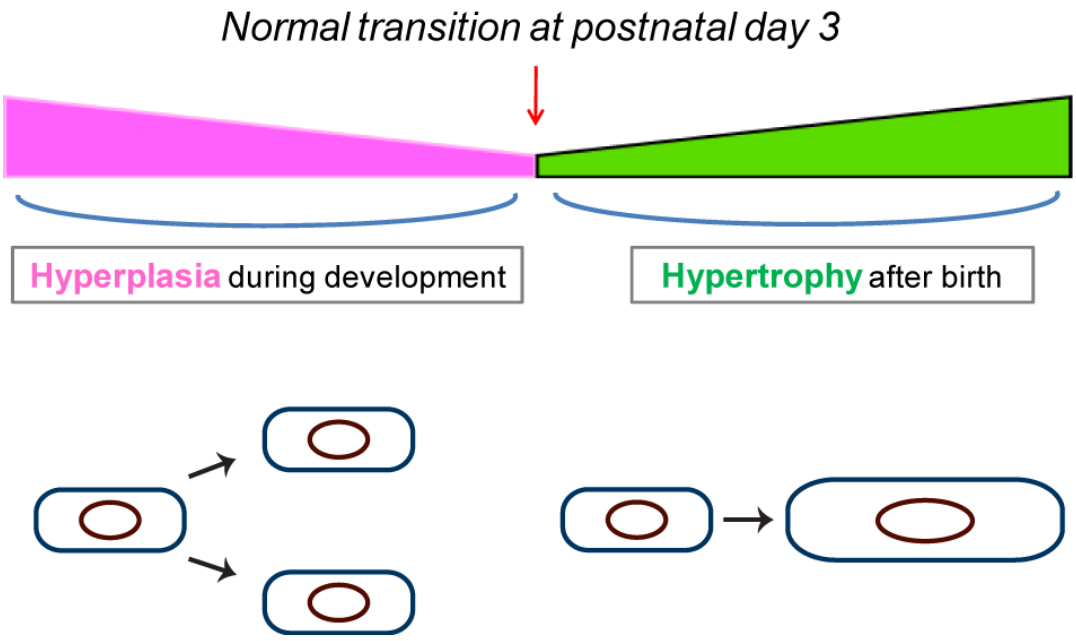

Figure 1.1. Normal transition of cardiomyocyte growth from hyperplasia to hypertrophy. Myocardial growth during prenatal developmental stages is mainly accomplished by hyperplasia, which increases the number of cardiomyocytes. Shortly after birth (postnatal day 3 in mice), cardiac hyperplasia is terminated and cardiomyocytes undergo hypertrophic changes, which make the heart 30- to 40-fold larger during postnatal maturation.

Abnormal cardiac development I: Ventricular arrhythmias and sudden cardiac death

The heart spontaneously and repetitively generates electrical impulses. These electrical impulses organize the sequence of muscle contraction under the control of the autonomic (sympathetic and parasympathetic) nervous system during each heartbeat, which is vital to optimize the cardiac stroke volume. Cardiac electrical excitation originates in the sinoatrial node and activates the atria. The impulse then traverses the bundle of His, bundle branches and the Purkinje system to activate the ventricular myocardium, which generates strong forces to pump blood into the circulatory system. A laminar electrical propagation through this tightly orchestrated electrical system is fundamental to all cardiac function. The resting intracellular transmembrane voltage is negative and the magnitude of the negativity varies for different cells. The magnitudes for the sinoatrial nodal cell and Purkinje fiber are -60mV and -90mV, respectively. Activation of a cell is associated with a sudden and rapid reversal of the intracellular negativity during phase 0 (a sudden influx of sodium reverses the intracellular negativity) and phase 1 (the positive overshoot). Phase 2 is fairly stable and any changes during this phase are due to slow calcium channel fluxes, which play a significant role in the generation of the action potential of sinoatrial (SA) and atrioventricular (AV) nodal cells. The transmembrane negativity is restored during phase 3 with efflux of potassium. Phase 4 follows to restore normal ionic concentration and to finish a cycle of electrical and contraction coupling (E-C coupling). Phase 0 represents cardiac electrical depolarization, while repolarization encompasses phases 1 through 4 (Figure 1.2). Deregulation of this electrical system impairs

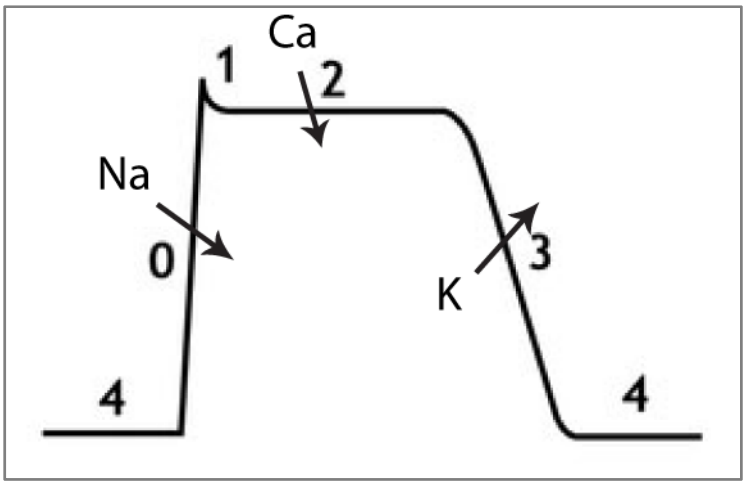

Figure 1.2. Cardiac action potential. Ion channels play important roles in generating the cardiac action potential. Sodium influx into cardiomyocytes triggers phase 0 depolarization, followed by phase 1 through 4 repolarization periods via calcium and potassium currents.

normal electrical propagation in the heart and manifests as rhythm disturbances (cardiac arrhythmias), where the heart's ability to pump enough blood to systemic circulation and maintain adequate coronary circulation is debilitated.

Among the types of cardiac arrhythmias, polymorphic ventricular arrhythmias (torsades de pointes) often accompany more detrimental consequences, such as syncope (loss of consciousness) or sudden cardiac death, than supraventricular arrhythmias. Various genetic diseases can predispose to fatal inherited ventricular arrhythmias. Inherited ventricular arrhythmic disorders are divided into two subgroups: familial electrical disorders and arrhythmogenic cardiomyopathies (Roberts and Brugada, 2003). The primary electrical disorders, where organic heart disease is not detectable, include long QT syndrome, Brugada syndrome, idiopathic ventricular fibrillation, catecholaminergic polymorphic ventricular tachycardia (CPVT) and idiopathic right ventricular outflow tract tachycardia (RVO-VT). Arrhythmogenic cardiomyopathies, where a primary myocardial disease manifests with ventricular arrhythmias, include hypertrophic cardiomyopathy (HCM), dilated cardiomyopathy (DCM), and arrhythmogenic right ventricular cardiomyopathy (ARVC). These cardiomyopathies primarily result from mutations in genes that encode sarcomeric proteins, which generate the mechanical contraction of cardiomyocytes (HCM) (Marian and Roberts, 1995) cytoskeletal proteins, which coordinate and transmit the forces to the next cells (DCM) (Olson et al., 1998), or ion channels, which regulate electrical activity in the heart (familial arrhythmias) (Roden et al., 1996). A failure to coordinate ion channels, ion currents, and structural proteins leads to perturbed transmission of electrical

and mechanical impulses across cardiomyocytes. This can degenerate into fatal ventricular arrhythmias and cause cardiac sudden death.

Despite genetic and phenotypic heterogeneity in the etiology of inherited ventricular arrhythmias, the mechanism underlying arrhythmogenesis generally falls into one of three categories: i) increased automaticity; ii) electrical re-entry; or iii) triggered activities such as early afterdepolarizations (EADs) or delayed afterdepolarizations (DADs). Abnormal cardiac sympathetic innervation has been documented in long QT and Brugada syndromes (Vincent, 1998). Modulation of the autonomic tone is considered to be an important modifier in triggering polymorphic ventricular arrhythmias with ion channel defects. Cardiac electrical re-entrant waves can be generated by several predisposing substrates, such as cardiac scar formation, ischemia, inflammation, increased wall stress (hypertrophy) due to pressure or volume overload, or heterogeneous refractoriness across the myocardium. In particular, maintenance or sustainability of arrhythmias predominantly depends on this re-entrant mechanism. Early afterdepolarizations (EADs) are one form of triggered activity that can occur during phase 3 of the cardiac action potential. Delayed afterdepolarizations (DADs) are another form of triggered activity that can take place during phase 4. These afterdepolarizations from the myocardium or purkinje fibers during the early (EADs) or late (DADs) repolarization period can provide substrates to provoke new action potentials and degenerating torsades de pointes.

There is a close relationship between intracellular calcium handling and triggered activities, as demonstrated by the example of digitalis toxicity. DADs

occur in conditions of intracellular calcium overload due to digitalis overdose by inhibiting the sodium-potassium ATPase pump (Clusin, 2003). DAD-dependent ventricular arrhythmias are one of the common side effects in cardiac patients with digitalis administered. This indicates that disturbed calcium homeostasis plays a pivotal role in the genesis of triggered activities and resultant ventricular arrhythmias. In addition, spontaneous calcium release in cardiomyocytes or purkinje fibers can also lead to afterdepolarizations with sufficient amplitude to trigger an ectopic beat (Michael et al., 2009). Furthermore, patients with end-stage heart failure or cardiac hypertrophy often develop fatal ventricular arrhythmias where a considerable prolongation of calcium transients and a drastic decline in the activity of the sarcoplasmic-endoplasmic reticulum calcium ATPase (SERCA) pump are demonstrated (Berridge, 2006).

Abnormal cardiac development II: Integrin signaling and hypertrophic remodeling

Integrins comprise a large family of cell surface receptors that exist as heterodimers of α and β subunits. Vertebrates express 18 different integrin α-subunits and 8 β-subunits, making integrins the most structurally and functionally diverse family of cell-adhesion molecules (Howe et al., 1998). Importantly, integrins (one of the predominant ECM receptors) function as mechanotransducers, converting mechanical forces to biochemical signals. The large extracellular domain of the integrin receptor complex binds various ECM proteins (collagen, laminin and fibronectin), while a short cytoplasmic domain interacts with the cytoskeleton within the cell, influencing myofibrillar

and cytoskeletal assembly in cardiomyocytes (Hilenski et al., 1991). The cytoplasmic domains of integrins also bind directly to several protein tyrosine kinases, including focal adhesion kinases (FAK), Src family kinases, paxillin, and integrin-linked kinase (ILK), which play essential roles in orchestrating multiple functions in cell growth, differentiation, migration, and organogenesis (Figure 1.3) (Curley et al., 1999). Thus, the binding of a specific ECM ligand (such as collagen) to an integrin receptor elicits the activation of intracellular signaling, cytoskeletal reorganization and changes in cell adhesion or migration (DeSimone et al., 1987).

An altered balance of numerous different stimuli, such as mechanical forces, neurohormonal activation, growth factors, and cytokines can trigger a defective hypertrophic response and cardiac remodeling (Frey and Olson, 2003). In cardiomyocytes, integrin-dependent pathways mediate hypertrophic responses to mechanical stimuli and are required for stimulation of hypertrophy in response to trophic agents such as phenylephrine or endothelin (Aikawa et al., 2002). Mechanical stress-induced increases in sarcomere length change the spatial arrangement of the actin filament network that link z-discs (Bloom et al., 1996). Over-expression of β_1-integrin in cardiomyocytes was found to increase atrial natriuretic peptide (ANP) levels (ANP is a marker of hypertrophic changes), which demonstrates that integrins influence the hypertrophic response in cardiomyocytes (Kuppuswamy et al., 1997). FAK is also implicated in cardiac development as conditional knockout of FAK in mouse cardiomyocytes resulted in cardiac defects and ventricular hypertrophy (Peng et al., 2008).

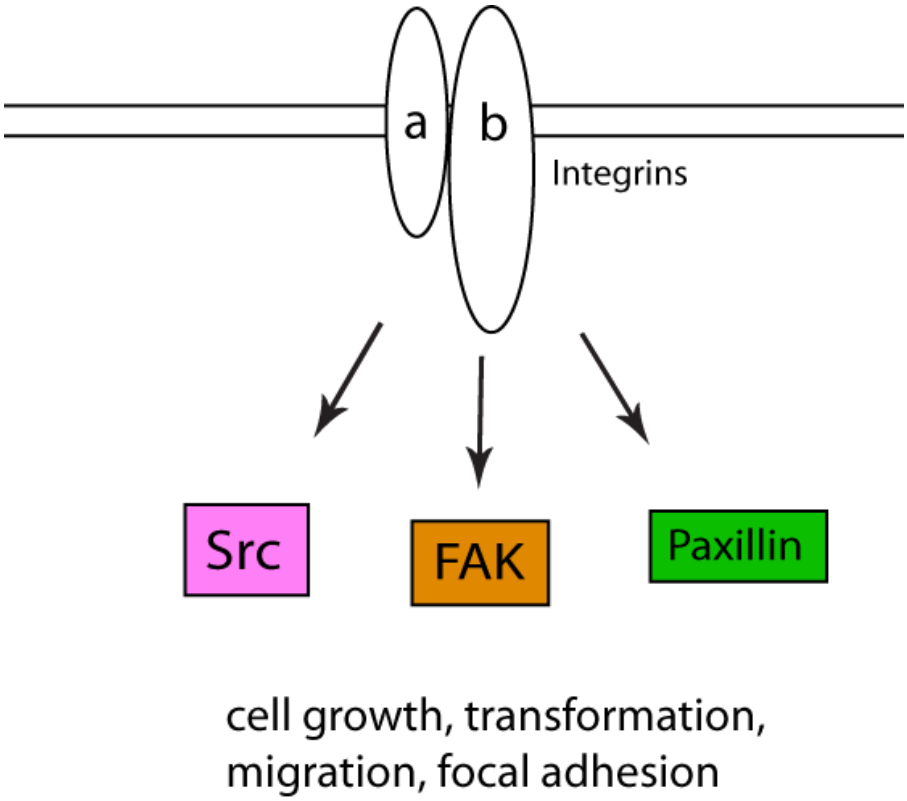

Figure 1.3. Integrin activation mediates downstream signaling cascades. Integrins are heterodimers consisting of noncovalently-associated alpha (a) and beta (b) subunits. They mediate adhesion of cells to the ECM and cell to cell interactions. Integrin receptors are considered to provide a cellular link between the ECM and the cytoskeleton. The downstream signals that follow integrin activation trigger modifications of signal-transducers, including FAK (focal adhesion kinase), Src and Paxillin, which leads to alterations in cell morphology, cell growth, or cell migration as well as the regulation of cell cycle progression.

Many genetic and molecular mechanisms in cardiac development and congenital heart diseases, however, still remain determined. Forward genetic approaches where a phenotypic characterization is followed by the identification of the mutated gene will determine genes and pathways that underlie developmental cardiac disorders.

Approaches for mapping phenotypic trait loci

Phenotypic trait loci vary from major gene mutations causing simple Mendelian trait differences to quantitative trait loci (QTLs) that underlie complex traits. Phenotypic traits can be either monogenic (under the control of a single gene locus) or multigenic (under the control of more than one locus). There are two major approaches for mapping phenotypic trait loci: the candidate gene approach and genome-wide linkage analysis. The candidate gene approach can be a powerful and effective method for gene discovery. The disadvantage of the candidate gene approach, however, is its reliance on existing knowledge about the biology of the phenotype since molecular details of most biological phenomena remain largely unknown. In comparison, genome-wide linkage analysis usually proceeds without presumptions regarding known functional features of the trait and identifies chromosomal regions responsible for the trait in pedigree- or population-based structures, which eventually provides a large number of candidate genes for mutation screening within the candidate interval.

‘Linkage’ defines the situation where two loci are inherited together because

they are close to each other on a chromosome. Two linked loci tend to be co-inherited because crossing-over is unlikely to occur between them in a given meiosis, because of their physical proximity. The closer two loci are to each other, the lower the probability of recombination between them. ‘Linkage analysis’ is a test for detecting co-segregation of a chromosomal region (i.e. a marker) with a trait of interest, which is determined by variation/ mutation in a specific gene or genes. The aims of linkage analysis are to narrow down the genomic region responsible for the phenotype, and ultimately to identify the causative mutation.

Mapping loci using inbred mice which are homozygous at virtually every locus has a unique advantage since highly divergent inbred lines can be mated to produce mice segregating different alleles at the target locus and at DNA markers throughout the genome. Two types of crosses are generally used in mouse genetics: backcross (BC) and intercross (F_2). In a backcross, F_1 hybrids produced from mating two different inbred strains are mated back to one of the parental strains. In an intercross, F_1 hybrids are mated to each other to produce an F_2 population. After genotyping outcross mice for selected DNA markers, genotype data can be analyzed to map the chromosomal region linked to the trait where genotypes at mutation (based on phenotypes) correlates with genotypes at markers. Animals with recombination events between each marker and the target locus can be identified to map the recombination breakpoints and define the smallest common haplotype block, which is indicative of candidate interval harboring the locus.

Mendelian traits are comparatively easy to study, but account for a small

proportion of human and animal diseases, most of which are multigenic in nature, exhibiting quantitative variation. These include cardiovascular disease, seizure, obesity and cancer (Wright et al., 2003). Complex traits are analyzed by linkage analysis to detect linkage between genetic markers and the loci responsible for the phenotypic variation. The variance component method, in particular, has gained wide popularity and is a way to assess the amount of variation in a dependent variable that is associated with a random-effects variable (Visscher et al., 1999). This method can be used to analyze a large pedigree without knowing the mode of inheritance (Blangero et al., 2000) and allele sharing statistics are based on identity by descent (IBD) at the marker locus, where IBD analysis estimates the probability that two individuals share marker alleles that are inherited from a common ancestor within the pedigree (Almasy and Blangero, 1998). Since all linkage techniques are essentially designed to test for a statistical association between inheriting a specific parental allele at a genetic marker and the mutation that underlies a phenotypic trait, statistical power for detecting linkage is influenced by pedigree size and structure, sample size, marker informativeness, penetrance, distance of marker from the disease locus, genetic heterogeneity and the magnitude of the genetic effect.

The dog genome is less diverged from the human than the mouse genome and has approximately the same number of genes as humans. Long linkage disequilibrium (LD) and haplotype blocks in most canine breeds allows for genome-wide association mapping studies with fewer markers and fewer individuals compared to human (Lindblad-Toh et al., 2005). In association mapping, two groups (affected and unaffected) are compared to identify

haplotype blocks that are frequently observed in the affected group but not in the unaffected group. Sequence information from several breeds of dogs has enabled the identification of more than 2 million single nucleotide polymorphisms (SNPs) in the canine genome that can be used for association mapping. It is estimated that a SNP occurs every 1000 bases in dogs (Lindblad-Toh *et al.*, 2005). In contrast to microsatellite markers, which are less abundant and display multiple alleles, SNPs are the most common type of polymorphism in the genome and are biallelic. Canine SNP chips harboring about 27,000 SNPs that provide uniform genome coverage are now commercially available. Since many human diseases also affect dogs, mapping disease loci in dogs can identify genes and pathways relevant to human disease.

Summary

Congenital heart defects are the most common birth defects. Dissecting the genetic and signaling pathways important for heart development and function will not only help to better understand disease pathogenesis, but also have clinical applications such as early diagnostic testing and therapeutic interventions, which will eventually benefit animal health as well as human well-being. Animal models provide excellent opportunities to study the genetic and molecular basis of cardiovascular diseases. The following chapters will present the studies of developmental cardiac disorders in canine and murine models.

CHAPTER 2

INHERITED VENTRICULAR ARRHYTHMIAS IN GERMAN SHEPHERD DOGS

Introduction

Cardiovascular disease is known as the most common cause of mortality and morbidity. In particular, sudden cardiac death is responsible for a substantial portion of total mortality in cardiac patients. A recent report estimated the annual incidence of sudden cardiac deaths to be in the range of 180,000 to 250,000 in the United States (Chugh *et al.*, 2008). The most important pre-existing etiology of sudden cardiac death is malignant polymorphic ventricular arrhythmias, for which the pathophysiologic and genetic mechanisms remain to be elucidated.

Ventricular arrhythmias can be acquired or inherited. Acquired ventricular arrhythmias are commonly associated with underlying diseases, including cardiomyopathies, coronary artery diseases, heart failure, hypertension, diabetes mellitus, and renal failure. Since primary inherited ventricular arrhythmias were first diagnosed in a human family with long QT syndrome in 1957 (Jervell and Lange-Nielsen, 1957), extensive efforts have been made through basic research and clinical studies to dissect the genetic risk factors that cause inherited forms of ventricular arrhythmias to degenerate into sudden arrhythmic death. Currently, familial hereditary ventricular arrhythmias in human medicine include long QT syndrome, Brugada syndrome, short QT

syndrome, and polymorphic ventricular tachycardia. Underlying mutations have been identified in genes encoding sodium channels, potassium channels, gap junction proteins, and the ryanodine receptor. It has been noted, however, that disease penetrance is incomplete and the phenotypic spectrum varies (for example, some individuals die suddenly while family members carrying an identical mutation are asymptomatic). This indicates that familial hereditary ventricular arrhythmias in human are not simple autosomal traits (Cheng et al., 2003). Further investigations need to be carried out to identify genetic modifiers that contribute to the wide spectrum of phenotypic expression of arrhythmias using animal models with spontaneous ventricular arrhythmias and sudden death. Murine cardiac physiology somewhat differs from human, however, with regard to heart size, heart rate, developmental aspects, ion channel compositions, and action potential characteristics, which makes a large animal model (i.e., dogs) more suitable for conducting complex physiological studies.

A colony of German shepherd dogs (GSDs) with a genetic predisposition to spontaneous ventricular arrhythmias and sudden death has been established by Dr. N. Sydney Moïse at Cornell University (Moise *et al.*, 1994). Quantitative phenotypic variation in the number and frequency of ventricular arrhythmias is evident in these dogs, ranging from very few ectopic beats to life-threatening cardiac rhythm disturbances. A window of vulnerability for the presence of ventricular arrhythmias and sudden cardiac death exists between 12 and 50 weeks of age, with peak affectedness occurring between 20 and 28 weeks. Interestingly, affected dogs rarely continue to have this disease after 18 to 24 months of age (Moise *et al.*, 1997a). When it occurs, death is unexpected and

most frequent during rapid eye movement sleep or at rest after exercise. Although echocardiographic and post-mortem examinations revealed no functional or structural abnormalities in the hearts of affected GSDs, examination of cardiac innervation revealed sympathetic denervation in the left anterior apical regions of affected GSDs (Dae *et al.*, 1997).

Multiple subcellular abnormalities have been identified in the hearts of affected GSDs. Cardiac electrophysiological analysis revealed abnormal calcium oscillation, calcium overload, prominent early afterdepolarizations (EADs), as well as delayed afterdepolarizations (DADs) and decreased density of potassium channels (Sosunov et al., 1999; Steinberg et al., 2002). These abnormalities are considered to be responsible for the modification of cardiac repolarization in the region of sympathetic denervation, which could provide substrates for developing ventricular arrhythmias. Phenotypic similarities between GSDs with ventricular arrhythmias and humans with familial ventricular arrhythmias include sudden death during sleep or at rest after exercise, young age of onset of arrhythmias, a broad phenotypic spectrum, heterogeneous sympathetic innvervation, abnormal repolarizations (EADs and DADs), altered ion channel functions, and normal cardiac structure and hemodynamics. This makes the GSD particularly suitable for studies to understand the genetic and molecular mechanisms of arrhythmogenicity in human populations.

Calcium cycling regulates excitation-contraction (E-C) coupling. Calcium entry through the L-type calcium channel stimulates calcium-induced calcium release from the sarcoplasmic reticulum calcium store via the ryanodine

receptor (RyR). During diastole, calcium is removed from the cytoplasm by resequestration back into the SR through sarcoplasmic-endoplasmic reticulum calcium ATPase (SERCA) and Na/Ca exchanger (NCX) located in the sarcolemma. Phospholamban inhibits the SERCA pump via phosphorylation, and calsequestrin stabilizes intra-SR calcium. Signaling between the RyR and SR luminal calcium is mediated by two small SR proteins, junctin and triadin. Prolonged action potential duration caused by Na^+- or K^+-channel dysfunction allows excessive calcium entry through L-type calcium channels and manifests EADs (Sicouri et al., 1997; Thomas et al., 2007). Excessive doses of digitalis produce calcium overload in the SR, which in turn induces spontaneous release of calcium (DADs) through RyRs (Sicouri and Antzelevitch, 1993). These findings suggest that abnormal calcium cycling can be a substrate to trigger afterdepolarizations (EADs and DADs). I therefore hypothesized that abnormal expression of the calcium handling genes described above may be responsible for abnormal calcium cycling seen as EADs and DADs in the GSD model of spontaneous ventricular arrhythmias.

A previous study had suggested that arrhythmic phenotypes in GSDs do not follow simple dominant or recessive inheritance, but rather complex mode of inheritance (Cruickshank et al., 2009). Crosses between mildly affected dogs produced severely affected offspring, as well as unaffected dogs. Breeding severely affected dogs to severely affected dogs produced unaffected dogs, as well as severely affected ones. Mating unaffected GSDs with affected GSDs produced offspring with a full range of affectedness (from unaffected to severely affected). These observations are consistent with inherited ventricular

arrhythmias in GSDs being caused by a major gene for susceptibility and a small number of modifier genes that determine severity.

The goals of this study were to: 1) map the underlying genetic mutations that contribute to ventricular arrhythmias in GSDs and 2) determine whether the expression of major cardiac calcium handling genes (*ATP2A2, NCX1, RYR2, CASQ2, PLB, LTCC, and TRDN*) differ between unaffected and affected GSDs in the least innervated region of the myocardium. While the mapping studies did not identify strong regions of linkage, the results of the second study provide evidence that SERCA2 levels are a key determinant of the severity of inherited ventricular arrhythmias in GSDs.

Materials and Methods

Dogs and tissues

All dogs were housed and fed in controlled conditions in AAALAC-approved facilities at Cornell University. All experimental procedures using animals in this study were performed according to protocols approved by the Cornell University Institutional Animal Care and Use Committee. A closed colony of purebred GSDs with ventricular arrhythmias has been established and has produced more than 400 dogs over 7 generations. One hundred and forty GSDs and their parents whose blood samples were available in the archive were selected from three sire families (Max, Harvey and Dr. Pepper). As the incidence of developing severe arrhythmias increased in GSD colony over 7 generations of breeding, a pedigree with higher genetic and phenotypic heterogeneity was required for linkage analysis. Thus, a backcross pedigree was generated to introduce genetic and phenotypic diversity (Table 2.1). A severely affected female GSD from purebred GSDs was out-crossed to a male Greyhound dog to produce F_1 dogs. Although the arrhythmic phenotypic information of this Greyhound dog was not available, this dog was considered to be an unaffected, normal dog because Greyhound dogs are not generally predisposed to any types of inherited cardiac disorders. Two unaffected F_1 hybrids were crossed back to female and male GSDs with severe ventricular arrhythmias.

A total of 13 GSDs, 9 BC and 1 beagle samples were randomly selected from the archive of liquid nitrogen snap-frozen cardiac tissues for gene expression

Table 2.1. Phenotype data for 38 backcross dogs and their parents

dog ID	sire	dam	sex	breed	#Single PVCs	#couplets	#triplets	#runs
Pollux	*	*	M	GH	*	*	*	*
S292	S254	S099	F	GSD	26521	22	3	2
S306	S297	S270	F	GSD	5000	1434	729	17
S313	S297	S154	M	GSD	5000	4384	108	12
S419	Pollux	S292	F	F1	4	0	0	0
S420	Pollux	S292	F	F1	12	0	0	0
S421	Pollux	S292	M	F1	352	0	0	0
S422	Pollux	S292	M	F1	0	0	0	0
S423	Pollux	S292	M	F1	28	0	0	0
S482	S422	S292	F	BC	29079	428	153	4
S483	S422	S292	F	BC	112	2	0	0
S484	S422	S292	F	BC	2405	4	0	0
S485	S422	S292	M	BC	0	0	0	0
S487	S422	S306	M	BC	0	0	0	0
S488	S422	S306	M	BC	21	0	0	0
S489	S422	S306	F	BC	8	4	3	0
S506	S422	S292	F	BC	1	0	0	0
S507	S422	S292	F	BC	0	0	0	0
S508	S422	S292	F	BC	378	0	0	0
S509	S422	S292	M	BC	6	0	0	0
S510	S422	S292	M	BC	2	0	0	0
S511	S422	S292	M	BC	204	0	3	16
S512	S313	S419	M	BC	15081	77	0	2
S513	S313	S419	M	BC	4	0	0	0
S514	S313	S419	M	BC	1168	84	6	0
S515	S313	S419	M	BC	20388	4346	714	89
S516	S313	S419	F	BC	2331	2	0	0
S517	S313	S419	F	BC	306	0	0	0
S518	S313	S419	F	BC	2697	179	29	0
S519	S313	S419	F	BC	2	0	0	0
S520	S313	S419	F	BC	103655	1592	158	22
S521	S422	S306	F	BC	2	0	0	0
S522	S422	S306	F	BC	29580	19957	1094	114
S523	S422	S306	F	BC	0	0	0	0
S524	S422	S306	F	BC	7478	203	3	0
S525	S422	S306	F	BC	88	0	0	0
S526	S422	S306	F	BC	0	0	0	0

Table 2.1. Phenotype data for 38 backcross dogs and their parents (Continued)

dog ID	sire	dam	sex	breed	#Single PVCs	#couplets	#triplets	#runs
S562	S422	S292	F	BC	0	0	3	2
S563	S422	S292	F	BC	3125	825	6	0
S564	S422	S292	F	BC	1634	22	0	1
S565	S422	S292	M	BC	28272	0	0	0
S566	S422	S292	M	BC	1	0	0	0
S567	S422	S292	M	BC	0	0	0	0
S574	S422	S306	F	BC	1	2	0	0
S575	S422	S306	F	BC	0	0	0	0
S576	S422	S306	M	BC	870	0	0	0
S577	S422	S306	M	BC	2343	0	0	0

studies (Table 2.2). All dogs were 5 months of age when tissue was collected. Affectedness score for each dog was determined based on the classification in Tables 2.3 and 2.4. The beagle sample was used as a calibrator for qRT-PCR. This dog was euthanized for reasons unrelated to this study. It had no history or clinical signs of heart disease or conditions likely to cause abnormal cardiac electrophysiology.

Phenotypic quantification of ventricular arrhythmias

The incidence and severity of arrhythmias peak at 5~7 months of age and decline over the period of puberty. Surviving dogs grow out of the arrhythmias by 12~18 months of age (Moise et al., 1997b). Phenotype data are collected from 24 hour Holter recordings performed at about 5 months of age, to diagnose and quantify ventricular arrhythmias. In cases where multiple recordings were available for a given dog, its worst Holter recording

Table 2.2. Holter recordings and affectedness category for 22 dogs used for quantitative RT-PCR

ID #	Breed	Single	Couplet	Triplet	Run	Score	Category
S 509	BC	44	0	0	0	1	mild
S 519	BC	25	0	6	0	5	mild
S 450	GSD	33621	285	0	0	4	mild
S 413	GSD	100	0	0	0	1	mild
S 466	GSD	147	0	3	0	1	mild
S 511	BC	204	0	3	16	13	moderate
S 476	GSD	1264	44	1822	0	11	moderate
S 469	GSD	796	284	60	9	13	moderate
S 412	GSD	36635	6096	216	5	16	severe
S 517	BC	5150	11	20	6	14	severe
S 477	GSD	6860	1290	297	13	22	severe
S 439	GSD	46534	24924	8967	400	26	severe
S 449	GSD	24594	288	32	49	20	severe
S 440	GSD	13145	48184	387	286	22	severe
S 457	GSD	64904	18134	702	166	26	severe
S 453	GSD	20026	248	17	17	20	severe
S 522	BC	29580	19957	15588	8441	16	severe
S 523	BC	2	0	0	0	0	UA
S 521	BC	2	0	0	0	0	UA
S 507	BC	2	0	0	0	0	UA
S 506	BC	3	0	0	0	0	UA
S 451	GSD	3	0	0	0	0	UA

Table 2.3. Cutoff values for scoring affectedness

Category	Score*
Unaffected (UA)	0
Mildly affected	1~5
Moderately affected	6~13
Severely affected (SA)	≥14

* : a cumulative value from four ordinal trait scores for each dog

Table 2.4. Affectedness categorization of ventricular arrhythmias

	Range	Score	Range	Score	Range	Score
Singles	≤5	0	5< X ≤5000	1	>5000	2
Couplets	≤5	0	5< X ≤500	2	>500	4
Triplets	≤5	0	5< X ≤500	4	>500	8
Runs	<1	0	1≤ X ≤10	6	>10	12

(i.e., giving the most severe phenotype) was selected as the phenotype data. The phenotypic spectrum of ventricular arrhythmias was categorized into 4 different traits: single premature ventricular complexes (PVCs), couplets (two consecutive PVCs), triplets (three PVCs in a row), and runs of ventricular tachycardia (more than 3 consecutive PVCs). The number of ventricular ectopic beats for each trait (single PVCs, couplets, triplets, and runs of VT) was counted after manual review of every single beat by experienced technicians. For quantitative real time PCR analysis, each individual's phenotype was classified as an ordinal trait (mild, moderate, severe, unaffected) after calculating the affectedness score based on the classification proposed in Tables 2.3 and 2.4. Except for the presence of fatal ventricular arrhythmias, no hemodynamic or structural abnormalities were documented in

the pedigree of GSDs. Pedigree analysis also revealed no sex effect on affectedness (Cruickshank et al., 2009).

Multiplex PCR and fragment analysis

Genomic DNA from 140 German shepherd dogs (GSDs), 38 BC dogs and their parents and grandparents were isolated from whole blood leukocytes using a standard ammonium acetate/ethanol protocol. A genome wide screen was performed using 320 microsatellite markers that comprise the Minimal Screening Set 2 (MSS2), for which the average marker distance is 9 Mb and average heterozygosity is 0.73 (Clark et al., 2004). Primer sequences are available at (http://research.nhgri.nih.gov/dog_genome). Primers were synthesized by Sigma Aldrich. Forward primers were labeled with one of four fluorescent dyes: 6-FAM (blue), NED (yellow), PET (red), or VIC (green). These markers can be combined into 96 multiplexed panels with 3 to 6 markers in each panel, grouped together based on compatible annealing temperatures, dye colors and allele sizes (Clark et al., 2004). All multiplex sets were amplified with an identical step-down thermal cycling program: 5 min at 95°C followed by 4 cycles of 30s at 95°C, 20s at 58°C, and 20s at 72°C and an additional 30 cycles of 20s at 95°C, 20s at 56°C, and 20s at 72°C, with a final extension of 5 min at 72°C. A single master mix, excluding primers, was used for all multiplex and individual reactions. Amplified PCR products were mixed with an internal size standard (GeneScan 500 LIZ, Applied Biosystems) and formamide in a MicroAmp optical 384-well reaction plate, denatured at 95°C for 3 minutes and chilled on ice for 5 minutes. Plates were then submitted to the BioResource Center at Cornell University for analysis on an

ABI 3730 automatic sequencer (Applied Biosystems). Assignment of the allelic peaks was confirmed by a manual inspection of each eletrophoretogram with GeneMapper 3.5 software (Applied Biosystems).

Linkage Analysis

Parametric and non-parametric linkage analyses were conducted to increase the chance of detecting genomic region(s) responsible for ventricular arrhythmias in GSDs. It was hoped that common or overlapping regions of linkage would be identified by both approaches.

I: Parametric SUPERLINK linkage analysis

Genotypes were checked for Mendelian inheritance errors using the Pedigree Check program in Pedtool (http://bioinfo.cs.technion.ac.il/superlink-online/makeped/pedcheck). The Parametric SUPERLINK program (http://bioinfo.cs.technion.ac.il/superlink-online) was used to calculate multipoint logarithm of the odds (LOD) scores that tested for linkage between genotype at microsatellite markers and arrhythmic phenotypes in the BC pedigree. The GSD pedigree was too large to be compatible with this program. Since the specific mode of inheritance of the ventricular arrhythmias in the BC pedigree is not certain, linkage analysis was run (separately) for both dominant and recessive modes of inheritance. As the penetrance of inherited ventricular arrhythmias is also undetermined, it was set at 0.5. Marker allele frequencies were assumed to be equal. As parametric linkage analysis via SUPERLINK required designating disease status (either affected or

unaffected), the cutoff values for affectedness were set at >100 single PVCs, >8 couplets, >6 triplets, or >1 run of VT (N. Sydney Moïse, personal communication). Each individual dog's worst Holter record was used to determine its affectedness based on these cutoff values.

II: Non-parametric SOLAR linkage analysis

A pedigree-based multipoint variance component approach was used to test for linkage between genotype at marker loci and phenotype using the actual number of ventricular ectopic beats from each dog's worst Holter recording to map genomic region(s) responsible for arrhythmias in GSDs with the software program Sequential Oligogenic Linkage Analysis Routines (SOLAR) (Almasy and Blangero, 1998). SOLAR employs a maximum likelihood method. As the use of the variance component approach in Solar program required an estimate of the identity-by-descent (IBD) matrix in the pedigree, the program LOKI (Lee and Thomas, 2000), which employs a Markov chain Monte Carlo stochastic procedure, was used to compute the IBD allele sharing matrix from genotype data for each marker locus. Marker maps for 38 autosomes were generously provided by Dr. Rory Todhunter. Since pedigree information did not show a sex effect on affectedness (Cruickshank et al., 2009), sex chromosomes were excluded from linkage analysis.

Expression analysis of calcium handling genes

Total myocardial RNA from liquid nitrogen snap-frozen cardiac tissue taken from the anterior apical left ventricular wall was isolated using Qiagen RNeasy

Fibrous Tissue Mini kit. Total RNA was eluted into 50 µl of RNase-free water. RNA integrity and quality was determined using the Agilent 2100 Bioanalyzer (Agilent technologies, Santa Clara, CA) and the concentration measured using a Nanodrop ND-100 spectrophotometer (Thermo Scientific, Wilmington, DE). RNA samples were diluted to 22 ng/µl and 220 ng used in a 20 µl reverse transcription (RT) reaction along with 10X RT buffer, 25X dNTP mix (100mM), 10X RT random primers, 1 µl Multiscribe^{TM} reverse transciptase, and nuclease-free water using the ABI High Capacity cDNA Reverse Transcription Kit. The 2X RT master mix reactions were incubated at 25°C for 10 min, 37°C for 120 min, then 5 sec at 85°C. Transcribed cDNA samples were diluted 7-fold in nuclease-free water and stored at -80°C. The same cDNA samples were used for all subsequent PCR assays.

The Primer3 program (http://frodo.wi.mit.edu) was used to design primers to amplify a portion of 7 target genes involved in Ca^{2+} homeostasis: *ATP2A2, NCX1, RYR2, CASQ2, PLB, LTCC, and TRDN*. Primers were designed to amplify a 100-150 bp region of cDNA flanking at least one large intron, so that products amplified from cDNA could be distinguished from any amplified genomic DNA that might contaminate the RNA samples. Primers were also designed to amplify 101 bp of the Glucose-6-Phophate Isomerse (GPI) transcript, which was used as an endogenous control for normalization of cDNA input. The sequences of the PCR primers are listed in Table 2.5. Quantitative Real Time PCR (qRT-PCR) was performed using the ABI 7500 Real time PCR System and the Power SYBR green PCR master mix kit

Table 2.5. Primer sequences used to amplify cDNA of major calcium handling genes.

Genes	Primer Sequence
ATPA2[1]	F-CCTTGAGGACTCTGCCAACT
	R-CAGAGGAGGCCACTTCAATC
LTCC[2]	F-CAGCATCGTCGAATGGAAAT
	R-GTTCCAGGTTGGAATTGGTG
CASQ[3]	F-AAGTCGCGCAGAAACAGTTC
	R-GCTTCTTTCTTGGCATCCAC
NCX1[4]	F-AATGTGTCGTAGCCCTGAGC
	R-GAGGAGTGCAAACCCCACTA
PLB[5]	F-AACACCGATAAGACTTCATACAACTC
	R-CCAAATGTGAGCTCAACCAC
RYR2[6]	F-GCAACCATCCACAAAGAACA
	R-GCAGATGGAGAGGTCTGGAG
TRDN[7]	F-TCCAACCACCATGACTGAGA
	R-AGCACTTTTCCAGGGGATTT
GPI[8]	F-AGAACCTTGTGACCGACACC
	R-CGATCCTCCGTGAAGTTGAT

1: Sarcoplasmic-Endoplasmic Calcium ATPase
2: L-type Calcium Channel
3: Calsequestrin
4: Sodium-Calcium Exchanger
5: Phospholamban
6: Ryanodine Receptor
7: Triadin
8: Glucose-6-Phophate Isomerse

(Applied Biosystems, Foster City, CA). Each reaction was mixed with 5µl of 2X SYBR Green Master Mix, 1 µl of 10mM primer mix (forward and reverse), 1 µl of cDNA template, and RNase-free water up to 10 µl. Reactions were loaded into a MicroAmp 96-well plate and sealed with a MicroAmp optical cap. Each sample was assayed in duplicate. A negative control (nuclease-free water used as template in place of cDNA) was run with each set of experiments.

Reactions were incubated at 50°C for 2 min to activate uracil N'-glycosilase and then for 10 min at 95°C to inactivate the uracil N'-glycosilase and activate the polymerase, followed by 40 cycles of 15s at 95°C, 30s at 60°C, and 30s at 72°C. PCR reactions were then subjected to the 7500 Real Time PCR System heat dissociation protocol. As SYBR green dye can bind to all double-stranded DNA molecules including primer-dimers, melting curve analysis was conducted to distinguish any contaminating genomic DNA from the desired products. The fold change in target gene levels relative to the GPI endogenous control was determined by the $2^{-\Delta\Delta Ct}$ method, where $\Delta\Delta C_t = (C_{tTarget} - C_{tGPI})_{GSD} - (C_{tTarget} - C_{tGPI})_{beagle}$. The C_t (threshold cycle) value was calculated based on the time (measured in PCR cycle number) at which SYBR green fluorescent emission increased beyond a threshold bar and became visible to the system (Livak and Schmittgen, 2001).

A greater copy number of input mRNA target therefore results in a lower C_t value as a result of requiring fewer PCR cycles for SYBR green fluorescent intensity to reach the threshold. The calibrator sample (beagle) was included on every assay plate. The relative quantification (RQ) value for each sample was calculated as the ratio between the amount of target molecule and a reference molecule (GPI). The normalized RQ value was used for statistical analysis of differential gene expression using Spearman's rank correlation test and Student's *t*-test in the GraphPad Prism 5 statistical program. Spearman's rank correlation test was used to examine the relationship between two variables, RQ value and affectedness score. Student's *t*-test compared the mean of RQ values between unaffected and affected (mild, moderate or severe) GSDs. Since the same samples were used to estimate the expression

level of 7 genes, the correlation and mean difference were considered significant at p-value of 0.007 (=0.05/ 7 genes), determined by a Bonferroni correction for multiple testing.

Immunoblotting analysis of SERCA expression

Frozen heart tissue from the left ventricular anterio-apical (LVAA) region of 3 unaffected dogs (s507, s521, s523) and 3 severely affected dogs (s453, s457, s522) was homogenized with a Polytron homogenizer in RIPA buffer (50mM Tris HCl pH7.4, 150mM NaCl, 2mM EDTA, 1% NP-40, 0.1% SDS) supplemented with Complete protease inhibitor cocktail (Roche, Germany). Homogenates were centrifuged at 12000 rpm for 5 minutes at 4°C and the supernatant collected and stored at -80°C. Protein concentrations were determined by BCA protein assay (Pierce, Rockford, IL). Equal amounts of protein lysates (20 µg of total protein) were mixed with 2X SDS buffer (125 mM Tris-HCl, 10% glycerol, 10% SDS, 130 mM DTT), incubated at 70°C for 5 minutes and separated on 4% stacking, 8% SDS polyacrylamide gels. Proteins were transferred to Immobilon P membrane (Millipore, Bedford, MA) at 0.5 mA for 3 hours. The membrane was blocked with 5% dry milk in Tris-Tween Buffered Saline (TTBS) for 12 hours at 4°C and incubated for 3 hours at 4°C with an antibody against SERCA2 (cat#:ab2861, Abcam, Cambridge, MA) diluted 1:2000 in TTBS. The blot was washed, incubated with horseradish peroxidase (HRP)-conjugated anti-mouse secondary antibody (cat#:554002, BD Transduction Laboratories, San Jose, CA) in TTBS for 50 min at room temperature followed by three 15 min washes in TTBS. Antibody signal was detected by chemiluminescence (ECL Western Blotting Detection Reagent,

Amersham, UK) and visualized using the Versadoc Imaging system (Bio-Rad, Hercules, CA). The membrane was re-blotted with a HRP-conjugated antibody against GAPDH (cat#: ab9482, Abcam) to check for equal protein loading. Densitometry was performed using Quantity One Software (Bio-Rad). Differences between mean values was considered statistically significant at $p<0.05$.

ATP2A2 sequence analysis

Total RNA was extracted from 2 unaffected dogs (GS7, BC13) and 2 severely affected dogs (GS2, GS23). RT was performed using Superscript III First-Strand cDNA kit with an oligo-dT primer (Invitrogen). Eight pairs of overlapping primers spanning the full length *ATP2A2* cDNA were designed to generate ~700-1000 bp PCR products (Table 2.6). PCR was performed using i-Proof high fidelity DNA polymerase (Bio-Rad) with the following amplification conditions: denaturation at 94°C for 30s, annealing 64°C for 30s, and extension at 72°C for 90s for 40 cycles of amplification. PCR products were purified using the QIAquick Gel Extraction Kit (Qiagen) and PCR products sequenced from both forward and reverse directions on an ABI 3730 sequencer (Applied Biosystem) at the Sequencing Core Facility in the BioResource Center at Cornell University. SeqMan software (DNAStar Inc.) was used to align and compare sequence data for affected dogs against unaffected dogs and the boxer consensus sequence available at the Ensembl genome browser.

Table 2.6. Primers used to sequence cDNA of *ATP2A2* gene.

Primer name	Primer Sequence
ATP2A2_F1	GCAGGAGGAGGAGGAGGA
ATP2A2_R1	CGGATCTTGCCAATTTCTGT
ATP2A2_F2	GGGTGTATGGCAGGAGAGAA
ATP2A2_R2	GGGAGCAGCTATCACCTTCA
ATP2A2_F3	CAGCTTTCCAAAGTCATCTCC
ATP2A2_R3	CCTGGGGTCATAGGGACTT
ATP2A2_F4	GGATTACAATGAGGCGAAGG
ATP2A2_R4	AGGAGCATCATTCACACCATC
ATP2A2_F5	AATCTGACTTTCGTTGGATGC
ATP2A2_R5	GTGGCTCAGCTGGTAGAAGG
ATP2A2_F6	AAATGTGGGGGAGGTTGTCT
ATP2A2_R6	CACACAATGAGTTGGGGACTT
ATP2A2_F7	CCCCCTGGGAGAACATCT
ATP2A2_R7	GCACCAACATCTGTCTACTGCT
ATP2A2_F8	GAGGTTCCAAAACCTTATCTAAGAA
ATP2A2_R8	TTTACCTGAAACCATGTCTGTG

Results

Susceptibility to ventricular arrhythmias follows a complex mode of inheritance

Previous studies had suggested a complex mode of inheritance for ventricular arrhythmias in the closed colony of GSDs (Cruickshank et al., 2009). Crosses between mildly affected dogs produced severely affected offspring as well as unaffected dogs. Breeding severely affected dogs to severely affected dogs produced unaffected dogs as well as severely affected ones.

Mating unaffected GSDs with affected GSDs produced offspring with a full range of affectedness (from unaffected to severely affected GSDs). Genetic analysis also demonstrated a relatively high heritability for affectedness and severity of ventricular arrhythmias in GSDs.

In order to produce a BC population for linkage mapping, a severely affected female GSD (ID: s292) was outcrossed to a presumed unaffected male Greyhound dog (ID: Pollux) to produce 5 F_1 hybrids. Two F_1 were unaffected while 3 were mildly affected (Table 2.1). The fact that 3 F_1's were affected, albeit mildly, suggests that a dominant major locus determines susceptibility to ventricular arrhythmias. The unaffected F_1 hybrids were mated back to 3 severely affected GSDs, including the dam (s292) of F_1 hybrids. A total of 38 BC dogs were produced (Table 2.1). The cross between an unaffected F_1 and his mother (s292) produced 7 unaffected and 9 affected BC dogs. This is consistent with a dominant major gene for which the dam (s292) was heterozygous. Twenty three (61%) dogs in the BC population were affected: 7 dogs were severely, 2 moderately and 13 mildly. Affected BC dogs showed a wide spectrum of affectedness (from mild to severe). This implies the presence of a major gene with modifiers that influence severity. The settings for affectedness categorization, however, are somewhat arbitrary (Tables 2.3 and 2.4) and might under-represent severity for some dogs.

Mapping susceptibility loci for ventricular arrhythmias in GSDs

As pedigree analysis demonstrated an inherited genetic component for susceptibility of GSDs to ventricular arrhythmias, a genome-wide linkage

analysis was undertaken to map the loci responsible. Genotypes for 140 GSD, 38 BC dogs and their parents were determined for the MSS2 panel of microsatellite markers. Two separate linkage programs, SUPERLINK and SOLAR, were used for each pedigree to increase the chance of detecting genomic region(s) linked to the disease and the results were compared to try to find overlapping genetic region(s) common to the two pedigrees. In this way, it was hoped that false positive and negative results would be reduced or eliminated. Both programs run a pedigree-based analysis and all results are based on relationships within the pedigree. The former is a model-based parametric linkage analysis program which requires a parameter defining the mode of inheritance, whereas the latter is a non-parametric model-free method and thus better suited to a pedigree in which a complex trait is segregating.

Given the uncertainty regarding the mode of inheritance of ventricular arrhythmias in GSDs, a non-parametric multipoint linkage analysis was first used to test for linkage between marker loci and cardiac phenotype. Non-parametric approaches are often more powerful when some assumptions (such as mode of inheritance) that are important to the analysis are questionable or may not be met. Since SOLAR uses an IBD matrix calculated by LOKI (a Markov chain Monte Carlo procedure), the BC and GSD populations were analyzed separately. As shown in Table 2.7 and 2.8, none of the markers showed strong evidence of linkage to ventricular arrhythmias in either pedigree. The highest LOD score observed was ~2.3 for runs at 43 cM on CFA11 in the 140 GSDs (Table 2.8), but LOD scores for all traits across CFA11 in the BC pedigree were 0 (Table 2.8).

As the non-parametric approach was not successful in identifying significant linkage between affectedness for arrhythmias and any chromosomal region, a parametric linkage analysis was also performed using the SUPERLINK program. The large size of the GSDs pedigree was not compatible for use with this program, so SUPERLINK analysis was only run using data for the 38 BC dogs. The results for dominant and recessive modes of inheritance were equivalent. The highest LOD scores detected for each ordinal trait and their map positions are summarized in Table 2.9. It was interesting to note that all the suggestive or strong LOD scores (>2.2) were for triplets (Table 2.9). Potential loci for triplets mapped to the same positions on CFA 2, 3, 9, 15, 25 and 32 as more weakly suggestive LOD scores (values of 0.94-1.85) for couplets. Positive LOD scores (~0.7) were also observed for couplets, triplets and runs at the same position on CFA 23.

Overall, the linkage studies did not identify any consistent region(s) of linkage for the 4 ordinal traits. It is possible that one or more of the putative modifiers that influence severity map to one of the regions described above since a modifier might be expected to only influence a subset of the more severe traits. Several of the regions with suggestive LOD scores are likely to represent false positive results, however, since the number of potential loci identified exceeds the likely number of modifier loci.

ATP2A2 is differentially expressed in affected GSDs

As the genome-wide scan described above did not provide strong support for linkage between any chromosomal region(s) and susceptibility to ventricular

Table 2.7. Linkage analysis for *BC pedigree* by SOLAR program

	single		couplet		triplet		run	
	LOD	cM	LOD	cM	LOD	cM	LOD	cM
cfa1	0.198	47	1.025	1	1.729	31 (FH3413)	0.233	63
cfa2	0.581	66	0.005	31	0.046	50	0.000	0
cfa3	0.048	23	0.211	53	0.000	0	0.000	0
cfa4	0.000	0	0.015	63	0.023	62	0.327	31
cfa5	0.003	68	0.029	52	0.000	0	0.000	0
cfa6	0.707	35	0.151	76	0.000	0	0.000	0
cfa7	0.110	0	0.000	0	0.000	0	0.000	0
cfa8	0.000	0	0.623	73	0.000	0	0.000	0
cfa9	0.033	68	0.043	40	0.000	0	0.000	0
cfa10	0.233	72	0.549	63	0.940	72	0.040	52
cfa11	0.000	0	0.000	0	0.000	0	0.000	0
cfa12	0.146	62	0.468	46	0.000	0	0.000	0
cfa13	0.017	53	0.000	0	0.023	60	0.000	0
cfa14	0.059	55	0.026	47	0.000	0	0.000	0
cfa15	0.061	44	0.000	0	0.000	0	0.000	0
cfa16	0.407	40	0.886	30	0.242	7	0.000	0
cfa17	0.007	75	0.000	0	0.000	0	0.000	0
cfa18	0.076	40	0.019	40	0.000	0	0.000	0
cfa19	0.081	51	0.000	0	0.000	0	0.000	0
cfa20	0.000	0	0.113	23	0.112	23	0.000	0
cfa21	0.054	20	0.523	13	0.545	10	0.000	0
cfa22	0.000	0	0.000	0	0.000	0	0.000	0
cfa23	0.000	0	0.000	0	0.000	0	0.000	0
cfa24	0.000	0	0.000	0	0.027	7	0.000	0
cfa25	0.000	0	1.274	13	0.335	21	0.000	0
cfa26	0.000	0	0.192	22	0.000	0	0.000	0
cfa27	0.000	0	0.050	20	0.000	0	0.000	0
cfa28	1.164	44	0.379	44	1.587	44 (REN146G17)	1.216	31
cfa29	0.978	19	0.581	15	0.146	2	0.000	0
cfa30	0.012	34	0.008	14	0.080	25	0.000	0
cfa31	0.000	0	0.000	0	0.000	0	0.000	0
cfa32	0.002	22	0.000	0	0.000	0	0.000	0
cfa33	0.516	16	0.035	23	0.000	0	0.000	0
cfa34	0.784	0	0.356	0	0.049	0	0.000	0
cfa35	0.000	0	1.322	11	0.000	0	0.000	0
cfa36	0.052	14	0.088	1	0.000	0	0.000	0
cfa37	0.000	0	0.000	0	0.000	0	0.622	34
cfa38	0.000	0	0.007	36	0.211	33	0.169	33

Table 2.8. Linkage analysis for *GSD pedigree* by SOLAR program

	single		couplet		triplet		run	
	LOD	**cM**	**LOD**	**cM**	**LOD**	**cM**	**LOD**	**cM**
cfa1	1.5669	35 (FH3413)	0.6287	34	0.3565	34	0.2823	34
cfa2	0	0	0	0	0	0	0	0
cfa3	0.057	84	0	0	0	0	0.006	14
cfa4	0.4519	9	0.1941	85	0.6763	88	0.1017	87
cfa5	0.6469	89	0.4513	89	0.2904	102	0	0
cfa6	0.0731	11	0	0	0.0193	0	0.0366	0
cfa7	0.7603	85	0.6249	99	0.4524	86	0	0
cfa8	0.6725	55	0.0684	46	0	0	0.0929	33
cfa9	0.0081	41	0	0	0	0	0.0366	24
cfa10	0.0008	51	0	0	0.2528	48	0.4116	48
cfa11	0.8206	32	1.7446	30 (REN242K04)	1.554	31	2.2987	43 (FH2004 ,FH2319)
cfa12	0.4872	52	0.247	51	0	0	0	0
cfa13	0	0	0	0	0	0	0	0
cfa14	0.7708	13	0	0	0.4157	57	0.0501	47
cfa15	0.1473	51	0	0	0	0	0	0
cfa16	0.6944	0	0	0	0.0123	60	1.6389	2 (REN214L11)
cfa17	0	0	0	0	0	0	0.3	75
cfa18	0	0	0	0	0	0	0	0
cfa19	0	0	0.104	21	0.1625	19	0.3688	34
cfa20	0.3118	11	0.1437	49	0	0	0.4352	32
cfa21	0	0	0	0	0	0	0	0
cfa22	0	0	0.5775	60	0.2236	43	0	0
cfa23	0.2661	53	0.254	50	0.2021	12	0.6298	0
cfa24	0.1478	25	0	0	0	0	0	0
cfa25	0	0	0.7	43	0.4426	43	0.18	44
cfa26	0.5427	38	1.1247	38 (FH2130)	0	0	0	0
cfa27	0	0	0	0	0	0	0	0
cfa28	0	0	0	0	0	0	0	0
cfa29	0.3216	3	0.1372	7	0	0	0	0
cfa30	0	0	0	0	0	0	0	0
cfa31	0	0	0	0	0	0	0.3896	42
cfa32	0.8189	33	0	0	0	0	0	0
cfa33	0.3154	0	0.3699	0	0.4538	0	0.1142	0
cfa34	0	0	0	0	0	0	0	0
cfa35	0	0	0	0	0	0	0	0
cfa36	0	0	0	0	0	0	0	0
cfa37	0.0331	17	0	0	0.1308	4	0.3146	0
cfa38	0.0012	33	0	0	0.0019	44	0	0

Table 2.9. Linkage analysis for *BC pedigree* by SUPERLINK program

	single		couplet		triplet		run	
	LOD	**cM**	**LOD**	**cM**	**LOD**	**cM**	**LOD**	**cM**
cfa1	0	0	1.33	97.73 (FH2309)	1.13	57.62	0.53	57.62
cfa2	0	0	1.11	89.05 (C02.342)	2.29	89.05 (C02.342)	0	0
cfa3	0	0	1.31	3.76 (FH3396)	1.95	3.76	0	0
cfa4	0	0	0.40	56.79	0.40	56.79	0	0
cfa5	0	0	0	0	0	0	0	0
cfa6	0	0	0	0	0	0	0	0
cfa7	0	0	0	0	0	0	0	0
cfa8	0	0	0	0	0	0	1.12	18.74 (REN204K13)
cfa9	1.52	49.93 (FH3835)	1.27	76.06	2.97	76.06 (FH2885)	0	0
cfa10	0	0	0	0	0	0	0	0
cfa11	0	0	0	0	0	0	0	0
cfa12	0	0	0	0	0	0	0	0
cfa13	0	0	0	0	0	0	0	0
cfa14	0	0	0	0	0	0	0	0
cfa15	0	0	0.94	38.88	2.44	38.8 (FH3813)	0	0
cfa16	0	0	0	0	0	0	0	0
cfa17	0	0	0	0	0	0	0	0
cfa18	0.99	62.70	0	0	0.55	8.04	0	0
cfa19	0	0	0	0	0	0	0	0
cfa20	0	0	1.33	31.28 (REN100J13)	3.37	20.84 (FH2951)	0	0
cfa21	0	0	0	0	0	0	0	0
cfa22	0	0	0	0	0	0	0	0
cfa23	0	0	0.69	44.56	0.71	44.56	0.71	44.56
cfa24	0	0	0	0	0	0	0	0
cfa25	0	0	1.67	37.7	2.31	37.7 (FH2141)	0	0
cfa26	0	0	0	0	0	0	0	0
cfa27	0	0	0	0	0	0	0	0
cfa28	0	0	0	0	0	0	0	0
cfa29	0	0	0	0	0.91	7.4	0	0

Table 2.9. Linkage analysis for *BC pedigree* by SUPERLINK program (Continued)

	single		couplet		triplet		run	
	LOD	**cM**	**LOD**	**cM**	**LOD**	**cM**	**LOD**	**cM**
cfa30	0	0	0	0	0	0	1.14	32.07 (FH2290)
cfa31	0	0	1.00	13.87	0	0	0	0
cfa32	0	0	1.85	45.86	2.51	45.86 (AHT127)	0	0
cfa33	0	0	0.52	0	0	0	0.82	20.42
cfa34	0	0	0	0	0	0	0	0
cfa35	0	0	0.42	34.72	0.90	6.22	0.43	34.72
cfa36	0	0	0	0	0	0	0	0
cfa37	0	0	0	0	0	0	0	0
cfa38	0	0	0	0	0	0	0	0

arrhythmias in GSDs, an alternative candidate gene approach was used to identify the underlying genes. In human medicine, a significant correlation has been established between abnormal calcium signaling and heart failure. Importantly, altered calcium homeostasis has also been implicated in the genesis of ventricular arrhythmias (Goldhaber et al., 2005; Wan et al., 2005). As described in Introduction section, I hypothesized that differences in the expression of major calcium handling genes might underlie the abnormal calcium oscillation observed in the hearts of affected GSDs. Any genes differentially expressed in affected GSDs would be examined as candidate susceptibility loci.

Quantitative RT-PCR for *ATP2A2, NCX1, RYR2, CASQ2, PLB, LTCC,* and *TRDN* was performed on heart RNA isolated from colony GSDs and BC dogs that ranged in disease severity from unaffected to severely affected for ventricular arrhythmias. The RQ value was calculated for each gene. Student's

t-test was first performed to identify gene(s) that were differentially expressed between unaffected and affected dogs. Among the 7 candidate genes, only *ATP2A2* showed a statistically significant difference between mean RQ values (Table 2.10 and Figure 2.1A). *ATP2A2* encodes the SR/ER calcium ATPase pump (SERCA) that plays an essential role in calcium homeostasis by sequestering cytosolic calcium back into SR. Additional statistical analysis using Spearman's rank correlation coefficient tested whether there was a correlation between the RQ value and disease severity, which was estimated using an "affectedness" scoring system (Tables 2.3 and 2.4) that placed each dog into one of 4 groups (unaffected, mildly affected, moderately affected, and severely affected). Higher affectedness scores reflected more severe phenotypes. *ATP2A2* expression showed a significant (inverse) correlation with disease severity ($p<0.05$; Table 2.10): in other words, the lower *ATP2A2* expression, the more severely affected a dog was (Figure 2.1B and Table 2.10).

In order to test whether reduced *ATP2A2* expression in affected GSDs resulted in reduced SERCA2 protein levels, protein lysates from the hearts of 3 of the unaffected and 3 of the severely affected dogs that were used for quantitative RT-PCR were subjected to immunoblotting using an antibody against SERCA2a (the cardiac isoform). Consistent with the altered RNA expression of *ATP2A2,* SERCA2a levels were reduced by ~40% in the hearts of severely affected dogs relative to unaffected dogs (Figure 2.2).

The reduced expression of *ATP2A2* in affected GSDs identified this gene as a candidate locus for susceptibility to ventricular arrhythmias. It should be noted

that *ATP2A2* maps to 13.725 cM (11.167 Mb) on CFA 26, which was not identified as a region of linkage in the BC or GSD pedigrees (although positive LOD scores of 0.5 and 1.1 were observed at ~38 cM for singles and couplets, respectively, in SOLAR analysis of GSDs). The *ATP2A2* coding region was amplified by RT-PCR from heart RNA of 2 severely affected and 2 unaffected GSDs. The product sequences were compared to each other and against the boxer sequence in the Ensembl database. Some single nucleotide polymorphisms were identified between the affected GSD and boxer sequence and also between affected and unaffected GSD. Protein sequence, however, was not predicted to be altered. No other sequence changes were identified.

Table 2.10. Cardiac expression of *ATP2A2* was significantly reduced and correlated with affectedness in GSDs with ventricular arrhythmias.

	Spearman's rank correlation test		Student's *t*-test
Genes	**p-value**	**coefficient (*r*)**	**p-value**
ATP2A2	0.003 (*)	-0.7624	0.006 (*)
CASQ2	0.315	-0.1612	0.334
LTCC	0.637	-0.0991	0.455
NCX1	0.194	-0.3073	0.249
PLB	0.246	-0.2973	0.585
RYR2	0.12	-0.3655	0.257
TRDN	0.28	-0.2343	0.328

* Significant p<0.007

Figure 2.1. *ATP2A2* was differentially expressed in the hearts of affected and unaffected dogs. (A) A significant difference was detected in the mean level of *ATP2A2* expression between unaffected and affected dogs (* Student's *t*-test, p=0.0063). (B) Relative quantification (RQ) value for the mRNA expression level of *ATP2A2* was calculated for dogs with inherited ventricular arrhythmias. The RQ value of *ATP2A2* is plotted against severity of the trait. Spearman's rank correlation test revealed a significant inverse correlation between the expression level of *ATP2A2* and disease severity, with a p-value of 0.003 and correlation coefficient of -0.7624.

A.

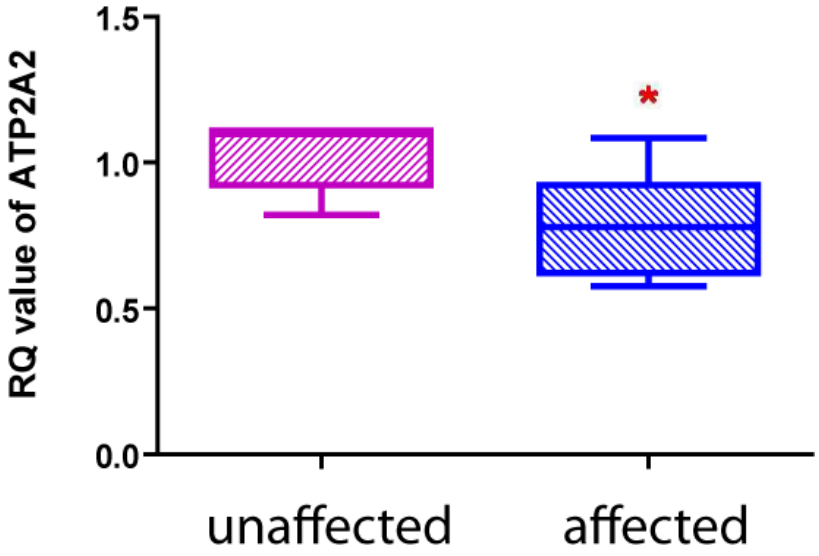
RQ value of ATP2A2
1.5
1.0
0.5
0.0
*
unaffected
affected

B.

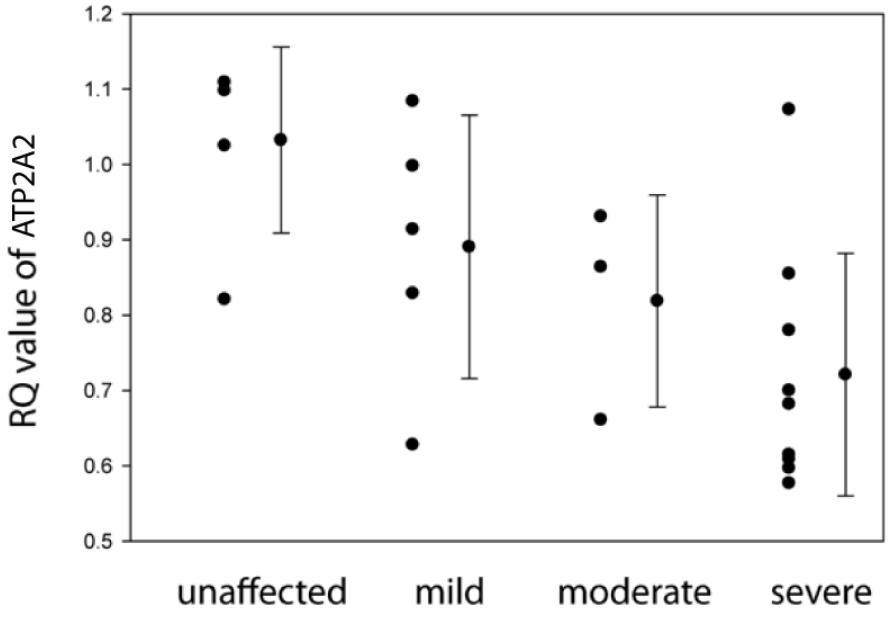
RQ value of ATP2A2
1.2
1.1
1.0
0.9
0.8
0.7
0.6
0.5
unaffected
mild
moderate
severe

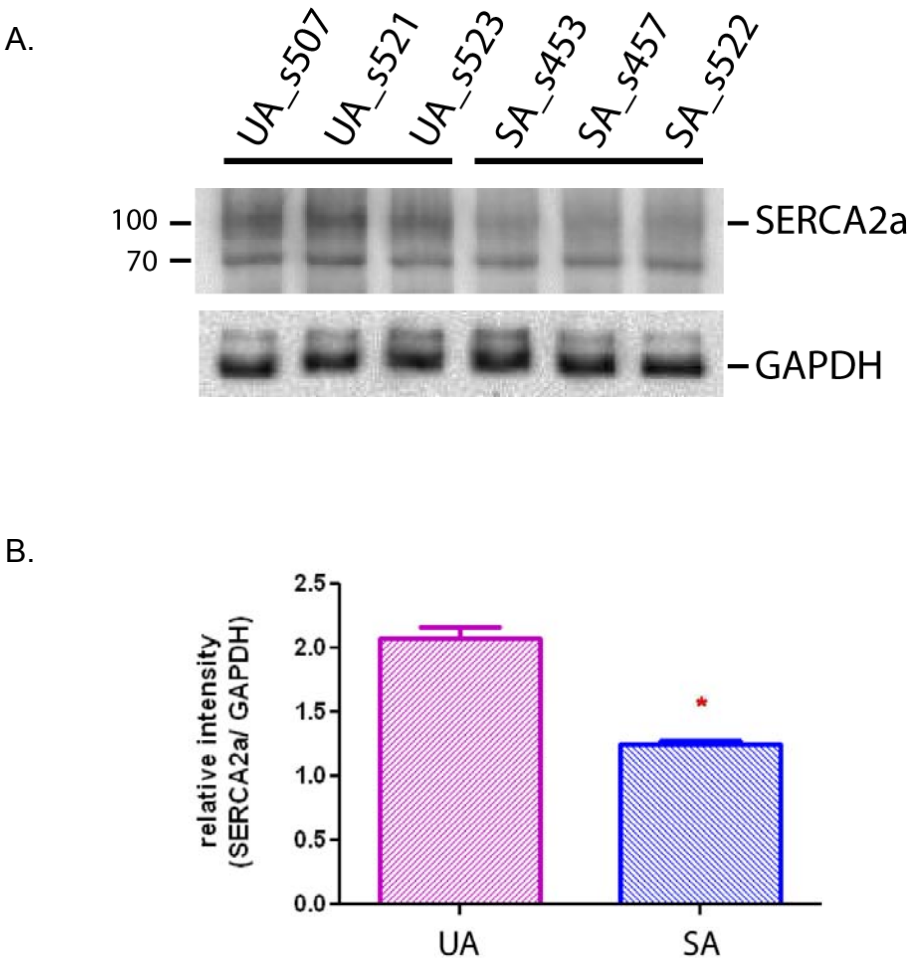

Figure 2.2. SERCA2a expression was significantly lower in affected GSDs than in unaffected GSDs. (A) Western blot analysis showed that severely affected GSDs had lower levels of SERCA2a (100 kDa band) than unaffected GSDs. (B) Intensity of SERCA2a signal was normalized against GAPDH. The mean relative intensity of SERCA2a in the hearts of unaffected GSDs was almost twice as high as that in severely affected GSD hearts (* Student's *t*-test p-value: 0.017).

Discussion

While the phenotype of the GSD model of ventricular arrhythmias is fairly well understood, the future value of this model in contributing to the understanding of the molecular basis of human arrhythmogenic disease requires that the causative mutations be identified. This chapter describes my efforts to do so.

Linkage analysis

The cardiac phenotype in GSDs can be measured as a quantitative and continuous trait, represented by the number of PVCs and whether they occur as singles, couplets, triplets or runs. Pedigree analysis indicated that there is a strong genetic component to susceptibility to ventricular arrhythmias in these animals, best fitting a mode of inheritance where a major locus determines disease susceptibility and modifiers modulate the severity of disease. A genome-wide linkage analysis was performed to identify chromosomal region(s) linked to the GSD arrhythmogenic phenotype.

I used both parametric linkage analysis (SUPERLINK) and non-parametric variance component linkage analysis (SOLAR) with multipoint IBD estimation by Markov chain Monte Carlo sampling method. SOLAR failed to identify any regions of significant linkage for any of the traits (single PVCs, couplets, triplets or runs), while SUPERLINK identified 1 significant and 5 suggestive regions of linkage, but only for triplets in the BC population. Triplets (three premature ventricular complexes in a row) are a more advanced type of ventricular ectopic beats than singles or couplets, which might indicate that at

least one of the loci with significant or suggestive LOD scores represents a modifier that influences disease severity in the BC population. It should be noted, however, that none of these regions were detected in the SOLAR analysis with GSDs or BC dogs, and parametric linkage analysis (SUPERLINK) is not ideal for the pedigree with complex mode of inheritance. Further studies are needed to test whether these regions contain modifying genes that provoke triplets by performing linkage analysis with additional microsatellite markers and/or SNPs in these and/or nearby the regions.

There are several prerequisites to performing successful linkage analysis for a complex trait. Statistical power is influenced by pedigree size and structure, sample size, distance of marker from the disease locus and the magnitude of the genetic effect. The phenotype data must be reliable, well-defined and quantitative. A pedigree should be designed to maximize the informativeness of genetic variation within the population. The density and polymorphic content of DNA markers and accuracy of genotype data is also important. Each of GSD and BC pedigree had pros and cons regarding power. Sample size was higher in the closed colony of GSDs (140) than BC population (38), but genetic heterogeneity was much higher in the BC population. Failure to detect loci might reflect any combination of phenotyping errors, low marker density, genotyping errors, low penetrance, epistasis, and/or limited statistical power due to small sample size, especially in the BC population.

GSDs with ventricular arrhythmias have no phenotypic abnormalities other than potentially fatal ventricular arrhythmias, which can only be reliably detected by Holter monitoring. An ambulatory 24 hour Holter recording has

been widely used to quantify and identify complex ventricular arrhythmias predictive of sudden cardiac death. The exact, quantitative phenotype data from Holter monitoring, however, can vary spontaneously from day-to-day (Spier and Meurs, 2004). The arrhythmias only occur in young animals: if an affected dog survives to 1-2 years of age, its arrhythmias disappear (Moise et al., 1997b). This makes accurate phenotyping one of the biggest challenges facing genetic mapping studies of this trait in GSDs. An important question is whether total number of PVCs is an appropriate way to define the arrhythmogenic phenotype for linkage analyses. For dogs whose Holter recordings were performed multiple times, their affectedness phenotype (total number of PVCs) was consistent with respect to a dog being categorized as unaffected or severely affected. For GSDs categorized as mildly or moderately affected, however, the number of PVCs was not as consistent. This implies that using total number of PVCs is not the best representation of phenotype for dogs in these intermediate categories. Also, limited statistical power in linkage analysis can be associated with pedigree structure and sample size. The pedigree of 140 GSDs may not have had a useful degree of heterozygosity at the marker loci. Traditional genetic crosses (for example, in mice) use inbred strains, whereas these GSDs are not inbred lines. A backcross pedigree was generated in order to introduce more genetic variation, but the relatively small sample size (38) limits the statistical power, increasing the probability of type II (false negative) errors.

Microsatellite allele segregation analysis provides a useful tool in linkage analysis. I used 320 microsatellite markers for which the average marker spacing was 9 Mb and average heterozygosity was 0.73. The question

remains, however, as to whether this provided sufficient coverage of the canine genome and whether marker polymorphism was high enough in the GSD and BC pedigrees. A total of 73 of the 320 markers (23%) were not informative (only one or two alleles segregating in the pedigree). Moreover, microsatellites have their own intrinsic issues, as microsatellite “slippage” can occur during PCR amplification, and the length of microsatellite markers can change over time. Epistasis between susceptible loci and low heritability are other potential reasons for failure to detect linkage, although genetic analysis of ventricular arrhythmias in GSDs demonstrated a relatively high heritability of affectedness and severity of ventricular arrhythmias (Cruickshank et al., 2009).

A different approach, called association mapping, appears to be a more suitable for mapping complex traits, and is becoming one of the main tools for fine-mapping and identifying loci (Andersson, 2008). In this method, two groups (affected and unaffected animals) are compared to identify haplotype blocks that are frequently observed in the affected group but not in the unaffected group. A haplotype block is a series of alleles on a chromosome that are inherited together. Sequence information from several breeds of dogs has enabled the identification of more than 2 million single nucleotide polymorphisms (SNPs) in the canine genome that can be used for association mapping. It is estimated that a SNP occurs every 1000 bases in dogs (Lindblad-Toh *et al.*, 2005). In contrast to microsatellite markers, which are less abundant and display multiple alleles, SNPs are the most common type of polymorphism in the genome and are biallelic. Canine SNP chips harboring about 27,000 SNPs that provide uniform genome coverage are now commercially available. Therefore, an alternative approach that could be used

in the future is to perform a genome-wide association mapping study using SNP chips to identify haplotype blocks associated with ventricular arrhythmias in GSDs. Given ambiguities in defining correct affectedness for mildly or moderately affected dogs, I would recommend SNP genotyping only with definitively unaffected and severely affected dogs in the GSD pedigree. This would eliminate issues related to incorrect phenotyping and genotyping errors, and significantly increase marker density and genome coverage, which allows for fine-mapping in the initial genome-wide screen. The BC pedigree could be used for further fine mapping, as these animals carry recombination breakpoints that could help refine the position of the underlying mutation(s).

In the meantime, a candidate gene approach may prove useful in identifying the genetic and molecular basis of ventricular arrhythmias in GSDs. Previously reported information (Sosunov et al., 1999) that GSDs manifested afterdepolarizations associated with calcium cycling led me investigate the expression of calcium handling genes.

Differential ATP2A2 (SERCA2a) *expression is implicated in aberrant calcium handling and severity to ventricular arrhythmias in GSDs*

Intracellular calcium dynamics have been extensively explored in models of inherited arrhythmias and heart failure (Clusin, 2003). For example, mutations in *RYR2* have been identified in inherited catecholaminergic polymorphic ventricular arrhythmias (Katz *et al.*, 2009). Extra diastolic calcium waves such as EADs and DADs are known to cause familial ventricular arrhythmias (Sato et al., 1993). Increased diastolic calcium leakage from the SR contributes both

to a decrease in SR calcium content and an increased susceptibility to ventricular arrhythmias in heart failure. However, the expression of calcium handling genes and their relationship to arrhythmogenicity has not been examined in models of familial ventricular arrhythmias. The Cornell GSD colony provides a unique opportunity to study calcium remodeling at the genetic and molecular level in familial ventricular arrhythmias.

Arrhythmias in GSDs are similar to those in human disease, where diastolic calcium waves are proposed to be the cause of triggering fatal arrhythmias (Sicouri and Antzelevitch, 1993; Sicouri et al., 1997; Thomas et al., 2007). During the diastolic phase, 90% of cytosoilc calcium is pumped back to the SR through SERCA, whereas only 10% is extruded out of the cell via NCX (Marks, 2000). SERCA pump function is thus positioned to be a critical determinant of intracellular calcium homeostasis. There are three different SERCA genes: SERCA1, SERCA2 and SERCA3, among which SERCA2a is the cardiac isoform. The roles of SERCA2a in the genesis of abnormal calcium handling and cardiac dysfunction have been studied. Seth *et al*. demonstrated that gene silencing of *Atp2a2* by siRNA resulted in abnormal calcium signaling, including increased NCX expression and activity as a compensatory response, increased cytosolic calcium and depletion of internal calcium store (Seth et al., 2004). This suggested that loss of SERCA2a function can trigger a cascade of abnormal calcium dynamics and calcium-related arrhythmias. Reduced expression of SERCA2a is a common finding in humans with heart failure and also accelerates the onset of heart failure (Lehnart et al., 1998; Schultz Jel et al., 2004).

Here, I report that among 7 candidate calcium handling genes, a significant correlation was observed only between *ATP2A2* transcript level and severity of ventricular arrhythmias: severely affected GSDs had the lowest *ATP2A2* expression levels, unaffected GSD had the highest, and mildly and moderately affected dogs had intermediate levels. Interestingly, however, the expression of *NCX* or *RYR2* did not show a significant difference between the unaffected and affected. This might suggest that *ATP2A2* is the direct target of upstream genetic mutation in GSDs and *ATP2A2* is a critical determinant of severity. These findings not only identify GSDs as an exceptional animal model to study calcium-related ventricular arrhythmias, but also reveal a unique signature of this particular disease.

Mice deficient for the Sp1 transcription factor displayed ventricular arrhythmias and sudden death (Nguyen-Tran *et al.*, 2000). Sp1, Sp3 and GATA4 are known to regulate *ATP2A2* expression (Brady et al., 2003; Takizawa et al., 2003). Since it failed to identify any strong region(s) of linkage on chromosome 26 where *ATP2A2* gene is located at 11.167 Mb (13.725 cM), it might be worthwhile to sequence the genes that encode these transcription factors as additional candidates for susceptibility to ventricular arrhythmias in GSDs. In fact, complex traits result from non-coding regulatory variants more often than from coding sequence variants (Mackay, 2001). While complete loss-of-function of these genes would be expected to cause systemic and/or structural disorders, which are not observed in the GSDs, it is possible that a hypomorphic mutation could have a more specific effect on *ATP2A2* expression. Since significant portions of cardiac ventricles in GSDs lack

sympathetic innervation, sequence analysis for genes involved in sympathetic nerve development in the hearts should also be considered.

A process called calcium-induced calcium release (CICR) triggers a robust calcium release into the cytosol to elevate intracellular calcium levels during systole. Intracellular calcium handling relies heavily on SR calcium content, as the SR is a major intracellular calcium reservoir. Finding reduced expression of *ATP2A2* gene products in GSDs with ventricular arrhythmias, both at the RNA and protein level, suggests a partial loss of SERCA2a pump function. When SERCA2a function is disrupted, calcium ions which are supposed to be re-sequestered into the SR lumen during diastole would be expected to stay in cytosolic compartments far longer. SR calcium would become depleted over time and intracellular calcium concentration would rise. The NCX would then be hyper-activated in order to compensate for calcium overload inside the cells. Measuring the fluxes of the NCX and estimating SR calcium content would therefore be helpful in elucidating more detailed calcium dynamics at the cellular level in GSDs with ventricular arrhythmias.

Cardiac relaxation during diastole requires the removal of cytosolic calcium back to the SR via SERCA2a, as well as out of the cell through the NCX. Previous studies, however, showed no evidence of systolic or diastolic dysfunction in GSD colony dogs (Moise *et al.*, 1997b). Further investigations into the physiological consequences of reduced SERCA2a levels (expected to cause a partial loss of function of the SERCA pump) need to be performed to examine whether there is diastolic dysfunction in GSDs. This could be

accomplished by Tissue Doppler Echocardiography, which can detect subtle or early cardiac diastolic dysfunction (Chetboul *et al.*, 2006).

Summary

This chapter describes genetic and molecular studies of the GSD model of inherited ventricular arrhythmias. Genome-wide linkage analysis was performed but failed to definitively detect genomic region(s) associated with ventricular arrhythmias in young GSDs. In a complimentary candidate gene approach, the expression level of *ATP2A2* (SERCA2a) was found to be significantly inversely correlated with the severity of arrhythmias in GSDs. This work suggests that the mechanism underlying ventricular arrhythmias in GSDs involves abnormal calcium handling due to reduced levels of SERCA2. While future genetic studies are needed to identify the causative gene(s), my work indicates that genes upstream of *ATP2A2* expression might act as modifiers that modulate the disease severity in GSDs.

CHAPTER 3

DEVELOPMENTAL CARDIAC DEFECTS IN DARK-LIKE MICE

Introduction

Over the last century, the mouse has been developed into a useful model organism for genetic and biomedical research. Pigmentation disorders were one of the earliest genetic diseases studied in the mouse model system. Today, over 130 genes and 1,000 alleles have been identified that regulate pigmentation phenotypes (Steingrimsson et al., 2006). Mammals make two types of pigment: black/brown eumelanin and yellow/red pheomelanin. In many mammals, the “normal” coat hairs are black with a subapical band of yellow that results when hair follicle melanocytes switch between the production of eumelanin to pheomelanin during the mid-portion of the hair growth cycle, then back again. This phenotype is referred to as agouti. The switch from synthesis of eumelanin to pheomelanin is controlled by a number of gene products, including the melanocortin-1 receptor (MC1R) and its two ligands, alpha-melanocyte-stimulating hormone (α-MSH) and agouti signaling protein (ASP). Activation of MC1R via binding of the agonist α-MSH or constitutive basal activity causes an increase in intracellular cyclic adenosine monophosphate (cAMP) levels to result in the production of eumelanin. ASP acts as an inverse agonist and when it binds MC1R, cAMP levels are reduced and pheomelanin is produced (Figure 3.1).

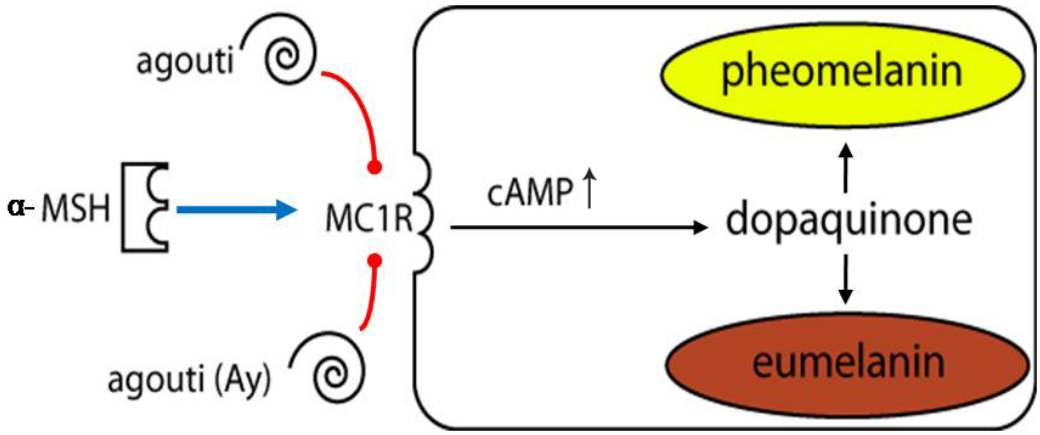

Figure 3.1. Basic pigment-type switching in mice. Constitutive activity and/or binding of the agonist α-MSH to the MC1R results in increased intracellular cAMP levels, which leads to the synthesis of black/brown eumelanin. Binding of the inverse agonist agouti (ASP) to the MC1R results in reduced levels of cAMP and synthesis of red/yellow pheomelanin. Mice lacking agouti or with constitutively active/hyperactive MC1R are black, while mice that ubiquitously express agouti or are homozygous for a loss-of-function allele of *Mc1r* are completely yellow.

Loss-of-function of *Mc1r* (*Mc1r*^{e}, previously called *recessive yellow, e*) gives rise to mice with completely yellow fur, while gain-of-function (i.e. *Mc1r*$^{E\text{-}tob}$ or *Mc1r*$^{E\text{-}so}$) results in mice with completely black hair. ASP is encoded by the *a* (*agouti*) locus. A gain-of-function mutation that results in ubiquitous over-expression of ASP (*lethal yellow, A*^{y}) results in mice that are completely yellow, while loss-of-function mutations produce mice with solid black hairs.

Pigmentation mutations often have pleiotropic effects on multiple body systems. Coat color is a visible marker, which helps identify genes that may cause underlying systemic diseases. Studying pigmentation mouse mutants often provides valuable insights into the function of genes with diverse physiological functions and the related systemic disorders, in addition to pigment-type switching. Loss-of-function mutations in genes contributing to the production of eumelanin and pheomelanin, such as *attractin* (*Atrn*) or *mahogunin ring finger-1* (*Mgrn1*), have been well studied in the context of developmental defects and systemic organ dysfunctions.

Atrn encodes a type I transmembrane protein with a short cytoplasmic tail and a large ectodomain. Mice with loss of function mutation in *Atrn* have phenotypes that include dark coat color and vacuolation of the central nervous system and testes (Bronson et al., 2001; Cota et al., 2008; He et al., 2001; Kuramoto et al., 2001; Miller et al., 1997). The neurological phenotype is associated with tremor, hyperactivity, and reduced body weight and adiposity (Gunn et al., 2001). While the function of ATRN in the nervous system remains unknown, in pigment-type switching it has been implicated as a low-affinity accessory receptor for ASP (He et al., 2001). It was also observed that some

mice homozygous for loss of both *Atrn* and its homolog, *Atrnl1* (*Atrn*$^{mg\text{-}3J/mg\text{-}3J}$; *Atrnl1*$^{tar/tar}$ double mutants) develop a progressive adult-onset cardiomyopathy (Walker et al., 2007).

MGRN1 is a RING finger domain-containing protein with ubiquitin ligase (E3) activity (He et al., 2003; Kim et al., 2007). *Mgrn1* null mutant mice show multiple phenotypic defects including completely black coat hairs, progressive adult-onset neurodegeneration associated with mitochondrial dysfunction, abnormal patterning of the left-right body axis that leads to congenital heart defects such as septal and AV cushion defects, reduced viability, and craniofacial defects (Cota et al., 2006; He et al., 2003; Jiao et al., 2009; Sun et al., 2007). Approximately 50% of *Mgrn1* null mutants die before or shortly after birth. A very small number of surviving null mutants display complete *situs inversus*, and *in-situ* hybridization analysis detected abnormal expression of genes involved in left-right patterning. Histological analysis for mid-to-late gestation *Mgrn1* mutant embryos revealed a high frequency of congenital heart defects, including atrial septal defects, ventricular septal defects, and atrio-ventricular cushion defects (Cota et al., 2006).

Cardiocutaneous syndromes have also been identified in human diseases. Multiple lentigines syndrome (MLS) manifests generalized lentiginosis (lentigines are dark or brown macules characterized by accumulation of melanin granules), hypertrophic cardiomyopathy, atrial septal defects, malignant arrhythmias resulting in sudden cardiac death and genital hypoplasia (Abdelmalek et al., 2002). Patients carry a missense mutation in *Ptpn11* gene which encodes Src homology 2 domain-containing protein-

tyrosine phosphatase (Lehmann et al., 2009). A common embryological origin of melanocytes and cardiomyocytes might explain the relationship between pigment phenotypes and cardiac defects (Jiang et al., 2000). Derivatives from neural crest cells give rise to many different cell types such as cardiomyocytes, melanocytes, bones, connective tissues and neurons. Coordinated neural crest cell migration is critical in order to accomplish successful organ development and function. Thus, mutations in genes that regulate neural crest migration, survival, proliferation and/or differentiation can affect multiple neural crest lineages to cause pleiotropic phenotypes in different tissues or organs simultaneously.

Mice homozygous for the recessive *dark* (*da*) mutation were identified in the 1950's and reported to have dark dorsal hairs and reduced growth rate and fertility (Falconer, 1956). This mutant appears to be extinct, but a new spontaneous mouse mutant with a similar phenotype that maps to the same general chromosomal location (proximal chromosome 7) arose at The Jackson Laboratory in the 1980's. Since *da* is extinct, an allelism test could not be performed and the new mutant was named dark-like (*dal*) (Harris, 2003). Mice homozygous for the *dal* mutation were reported to be easily distinguished from wild-type mice by 14 days of age due to their small body size and dark dorsal hairs, although the coat color phenotype was less apparent as animals aged. Genetic crosses were used to investigate the epistatic relationships between *dal* and other pigment-type switching genes (Cota et al., 2008). Double mutants were generated by crossing *dal* mutants (dark coat color) to A^y and $Mc1r^e$ mutants. A^y mice homozygous for *dal* had brown backs and yellow

bellies, while *Mc1r*$^{e/e}$*; dal/dal* mice were yellow. These observations place *dal* downstream of *agouti* transcription and upstream of *Mc1r*.

In addition to coat color, other phenotypes have been reported in *dal* mutants. Male and female *dal* mice were reported to breed normally until 5 months of age, but by 7 months of age, the reproductive performance of both sexes was reduced. Preliminary studies identified reproductive degeneration characterized by the absence of follicles and presence of many corpora lutea in 7-month old females and mild testicular degeneration with increased Leydig cells in 7-month old males (Harris, 2003). Studies to further analyze the reproductive degeneration in male *dal* mutant mice revealed vacuoles in *dal* mutant testis and reduced serum testosterone levels. Mating *dal* mutants to *Atrn* null mutants revealed an additive effect of these mutations on pigmentation and testicular and CNS vacuolation (Cota et al., 2008). Azouz and colleagues previously reported that loss of lipid raft domains was correlated with vacuolation in *Atrn* mutant brains (Azouz et al., 2007) and a similar phenomenon was observed for lipid rafts in the testes of *dal* mutant mice. These observations suggest that *dal* and *Atrn* act in a common pathway in pigment-type switching and vacuolation.

In performing the genetic crosses described above, it was noted that *dal/dal* pups were observed at lower than expected proportions and those that were born were more likely to be very small and often died before weaning (Teresa Gunn, personal communication). As congenital heart defects are a common cause of embryonic lethality and growth retardation, I hypothesized that the *dal* gene plays a pivotal role in cardiac development. A comprehensive

histological analysis revealed multiple heart defects including thickened cardiac ventricular walls, which I confirmed to be the result of developmental cardiac hypertrophy. I identified the gene mutated in *dal* mice as *peptidase d (Pepd)*, which encodes the enzyme prolidase, and demonstrated that loss-of-function of *Pepd* in zebrafish also causes pigmentation and cardiac defects. Prolidase is involved in collagen biosynthesis and recycling, and I demonstrated that disrupted integrin signaling underlies the cardiomyocyte hypertrophy observed in *dal* mutant embryos. This study introduces the *dal* mutant mouse as a novel model for studying myocardial development and the transition from proliferative to hypertrophic cardiomyocyte growth. It also presents the first examination of the function of *Pepd* in regulating the extracellular collagen matrix, integrin signaling and cytoskeletal organization in cardiomyocytes.

Materials and Methods

Mice

All mice were maintained under standard conditions in the Transgenic Mouse Core and East Campus Research Facilities at Cornell University. C3H/HeJ mice were originally obtained from the Jackson Laboratory (Bar Harbor, Maine) and maintained by brother-sister inbreeding. Mice carrying the pCAGGS-GCaMP transgene were generously provided by Dr. Michael Kotlikoff. Homozygous CBA/J-*dal*/*dal* mice were obtained from The Jackson Laboratory. The reproductive performance of CBA/J-*dal/dal* mice was very poor, the darkened coat color phenotype was not very strong and tended to disappear by the time mice were 6 months of age, and other pigment-type switching mutations in the Gunn laboratory are generally studied on the C3H/HeJ strain background (as it accentuates darkened coat color phenotypes). For these reasons, CBA/J-*dal*/*dal* mice were mated to C3H/HeJ mice to generate heterozygous F_1 progeny. Brother-sister pairs were set up from this and subsequent generations to produce intercrossed C3.CB-*dal/dal* and *dal/+* pups; mice from generations $F_{5\text{-}7}$ were used in the studies described below. Some C3.CB F_1 animals were also backcrossed to C3H/HeJ mice for up to 6 generations (N_6) to create incipient congenic mice that carry >98% of their genome from the C3H/HeJ background. The pre- and peri-natal lethality of these mice was much higher than that observed in the CBA/J-*dal/dal* or intercrossed C3.CB-*dal/dal*, consistent with anecdotal reports that heart defects are often more severe on the C3H/HeJ strain background.

F_1 progeny generated by breeding a female pCAGGS-GCaMP mouse to a male F_7 C3.CB-*dal/dal* mouse were backcrossed to F_7 C3.CB-*dal/dal* mice. From this cross, female *dal*/*dal* mice carrying the pCAGGS-GCaMP transgene were used for timed-matings with F_7 C3.CB-*dal/dal* males to produce *dal/dal*; pCAGGS-GCaMP(+) embryos. Genotypes of these mice and embryos were confirmed by PCR analysis as described below.

C3H/HeJ and C3.CB-*dal*/*dal* embryos for phenotypic analyses were collected from timed pregnancies. Male C3.CB-*dal/dal* mice were caged individually and given 2-3 mature (≥6 week-old) female mice. Females were checked for copulation plugs between 9 and 10 AM every day to determine whether mating had occurred. Noon of the day of the plug was considered day 0.5 of embryonic gestation (E0.5). Mice were euthanized by carbon dioxide inhalation, the uterus removed and embryos dissected under phosphate buffered saline (PBS).

Mouse genotyping

Once the *dal* mutation was identified, mice and embryos were genotyped by PCR amplification using forward primer AGCGCATCGATGAACCTG and reverse primer TCCAAGAGGTGGTCAATGAA under the following conditions: initial 5 minute denaturation at 95°C, then 35 cycles at 95°C for 30 seconds, 57°C for 30 seconds, and 72°C for 30 seconds, followed by a final extension at 72°C for 10 minutes. Products were separated on 5% low melting Nusieve agarose gels. Mice carrying the pCAGGS-GCaMP transgene were identified by performing PCR using forward primer AAGGGCGAGGAGCTGTTCA and

reverse primer CGATCTGCTCTTCAGTCAGTTGGT under the same amplification conditions described above.

Positional cloning

In order to identify the *dal* gene by position cloning, a mapping cross was established by mating a CBA/J-*dal*/*dal* male mouse to CAST/EiJ female mice. CAST/EiJ is a wild-derived inbred strain that has a high degree of genetic variation relative to C3H/HeJ and CBA/J mice. F_1 hybrid males and females were mated to CBA/J-*dal/dal* or C3.CB-*dal*/*dal* (N_3F_1, $F_{5\text{-}7}$) mice to produce the first generation interspecific backcross (BC_1) population. A second generation BC_2 population was also generated by mating some non-recombinant agouti (*dal/*+) BC_1 mice to F_5 or F_7 C3.CB-*dal*/*dal* mice. At 14-21 days of age, the genotype of BC pups at the *dal* locus was inferred by examining coat color (*dal* vs. agouti). DNA was isolated from tail tips using a standard protocol with proteinase K digestion, chloroform extraction and ethanol precipitation.

DNA from the parental strains, F_1 hybrids, BC_1 and BC_2 pups was used as template for polymerase chain reaction (PCR) amplification of D7Mit114 and D7Mit228, which are polymorphic among CAST/EiJ, CBA/J and C3H/HeJ, and encompass the candidate interval defined by Harris *et al*. (D7Mit294 to D7Mit247) (Harris, 2003). BC animals with recombination events between D7Mit114 and D7Mit228 were genotyped for 11 informative microsatellite markers (D7Mit267, D7Mit210, D7Mit246, D7Mit344, D7Mit155, D7Mit79, D7Mit269, D7Mit225, D7Mit78, D7Mit309 and D7Mit25) that lie between D7Mit114 and D7Mit228 to refine the map position of recombination

breakpoints. Primer sequences for these markers are listed in Table 3.1. All amplifications were performed under the same conditions: initial 5 minutes denaturation at 95°C, then 35 cycles of 95°C for 30 seconds, 55°C for 30 seconds, and 72°C for 30 seconds, followed by a final extension at 72°C for 10 minutes. Products were separated on 3% Nusieve, 1% agarose gels.

Total RNA was extracted from the hearts of E15.5 *dal/dal* and C3H/HeJ embryos, and also from testis of 3-month old homozygous *dal/dal* and C3H/HeJ mice using Trizol (Invitrogen, Carlsbad, CA). Genomic DNA from CBA/J, homozygous *dal/dal* and heterozygous *dal/+* mice was purchased from the DNA Resource at The Jackson Laboratory. Total RNA was transcribed into cDNA using ABI High Capacity cDNA Kit (Applied Biosystem, Foster city, CA). Overlapping primers were designed to amplify the cDNAs of candidate genes; the same primers were used to sequence the products (Table 3.2). Amplification conditions were as follows: initial 5 minutes denaturation at 95°C , then 35 cycles of 95°C for 30 seconds, 58°C for 30 seconds, and 72°C for 1 minute, followed by a final extension at 72°C for 10 minutes. PCR products were cleaned by incubating them with 2 μl ExoSAP-IT^{TM} reagent (USB, Cleveland, OH) at 37°C for 15 minutes followed by 80°C for 15 minutes. Five microliters of treated product was used in each sequencing reaction. All PCR products were sequenced from both directions with ABI 3730 sequencer (Applied Biosystem) at the Sequencing Core Facility in the BioResource Center at Cornell University.

Once the *Pepd* deletion mutation was identified in the cDNA of *dal* mutants, it was confirmed by PCR amplification and sequencing of this region from

Table 3.1. Primer sequences for microsatellite markers across the *dal* candidate interval

marker	Primer sequence
D7Mit114	F-TGGAGGGGAAATGGCAAG
	R-ACCTTCTATTTCTTGCCTATGCC
D7Mit267	F- CTCTTTCTGTTACATGGTTAGATTTCC
	R- AAAGACAGTTGAAGTTGACTTCTGG
D7Mit210	F-TCCCCAGGAAAGTGTTTGTC
	R-TTAAGCCCTTTAGATATACAGGTGTG
D7Mit246	F-CACACAAAGCCGCAGTTCTA
	R-TTGTTACGTGGCCTAGATTGG
D7Mit344	F-CAAGACCAGCCTGGGATG
	R-TACAAGCATGCAGGCAGAAC
D7Mit155	F-GTTGGAGAAATGACACCATGG
	R-ACTTTACACACTGATCACTTTTCAGC
D7Mit79	F-GGTGCAGGAGGGACACTTAA
	R-CACCACACCCAGCAGATTTA
D7Mit269	F-ATGGTGGCAGGTGCATCT
	R-TCTTTCAACCACTTATTGCGG
D7Mit225	F-TTAACCTGGACTGTACAAAGAGACC
	R-GAGATGAAGGGAGATGGAAGG
D7Mit78	F-ATGACACCCAAGGGCTAGC
	R-ATAAAGCCCAGCATGCTTTG
D7Mit309	F-TGATAAGGACCCTACAAGCACC
	R-CACAGAGATGGACAGATACAGACA
D7Mit25	F-AGGGGCACATGTTCAACTATG
	R-GGTTGTTTCCAGCTTTGGG
D7Mit228	F-ATTCTTGGCCTTTTCTTGTAACA
	R-AAACCTCCACACTGACTTCCA

Table 3.2. Primers used to amplify candidate gene cDNAs

Gene name	Primer name*	Primer sequence
Pepd[1]	Pepd-1F^{t1}	GAGTGAACATGGCGTCCAC
	Pepd-1R^{t1}	GCAGGTGATGTCAGAAGCAA
	Pepd-2F^{t1}	CAATGACCGGACGATCAAG
	Pepd-2R^{t1}	TTCGATTTCCTCCACAGTCC
	Pepd-3F^{t1}	TTCATTGACCACCTCTTGGA
	Pepd-3R^{t1}	GCAAATTCCATTCTGCATGTT
	Pepd-1F^{t2}	TCTCCCTGGGGAATGAGAC
	Pepd-1R^{t2}	GGGAAGGAGCAGGTGATGT
	Pepd-2F^{t2}	CAATGACCGGACGATCAAG
	Pepd-2R^{t2}	TTCGATTTCCTCCACAGTCC
	Pepd-3F^{t2}	TGGAGCCAGGCATCTACTTC
	Pepd-3R^{t2}	GCAAATTCCATTCTGCATGTT
Lrp3[2]	Lrp3-1F^{t1}	AGCGACGCACCCTCGTAG
	Lrp3-1R^{t1}	GACCAGCACTGCGAGCAC
	Lrp3-2F^{t1}	CTTCGGACCTTCACTGCAC
	Lrp3-2R^{t1}	ACAGACAGGGGCAATGAGAC
	Lrp3-1F^{t2}	AGCGACGCACCCTCGTAG
	Lrp3-1R^{t2}	GACCAGCACTGCGAGCAC
	Lrp3-2F^{t2}	CTTCGGACCTTCACTGCAC
	Lrp3-2R^{t2}	CAGAAGGGCCTCATCATCAC
Ccdc123[3]	Ccdc-1F	CTAGGCTGTGGGGAGCTGT
	Ccdc-1R	AAGCCTTTTCCGTCTCCTTC
	Ccdc-2F	CCAAAGAAAAGTTTGCGGAGT
	Ccdc-2R	AGCAGGCTCTTCTTCTGCAC
	Ccdc-3F	TGGATAGCAAGATCGCAGTG
	Ccdc-3R	TCCCTTGCCTATGACACTCA
Cepbg[4]	Cepbg-1F	GCGCAGGTACATGTGAAGATT
	Cepbg-1R	TCCAGGAATTTTGTTTTAACGAT

1: Peptidase D

2: Density lipoprotein receptor-related protein 3

3: Coiled-coil domain containing 123

4: CCAAT/enhancer binding protein (C/EBP), gamma

* Superscript t$^{\#}$ identifies alternatively spliced transcripts.

Table 3.2. Primers used to amplify candidate gene cDNAs (Continued)

Gene name	Primer name	Primer sequence
Gpatch[5]	Gpatch-1F^{t1}	AGTGACAGCGACGAGGATCT
	Gpatch-1R^{t1}	GAGCTGTCCAGCCATAGAGG
	Gpatch-2F^{t1}	AGAAAACTGGGCATTTCTGG
	Gpatch-2R^{t1}	ATCTTCACAGCCGACTGCTT
	Gpatch-3F^{t1}	CAAGGAGGAGGAGGATTCAG
	Gpatch-3R^{t1}	CAGCCTCCTGAGAGCCTTTA
	Gpatch-4F^{t1}	ACGCCCAGACACGACTGTA
	Gpatch-4R^{t1}	TCCTTCTAACATGGACTGAAGTT
	Gpatch-1F^{t2}	AGTGACAGCGACGAGGATCT
	Gpatch-1R^{t2}	GAGCTGTCCAGCCATAGAGG
	Gpatch-2F^{t2}	AGAAAACTGGGCATTTCTGG
	Gpatch-2R^{t2}	ATCTTCACAGCCGACTGCTT
	Gpatch-3F^{t2}	CAAGGAGGAGGAGGATTCAG
	Gpatch-3R^{t2}	CAGCCTCCTGAGAGCCTTTA
	Gpatch-4F^{t2}	ATCTTCGCCAGTTCCTCTGA
	Gpatch-4R^{t2}	TCAGCCATCACATGATTTTG
Chst8[6]	Chst8-1F	GCGGGGAAGAGACAGGAC
	Chst8-1R	CCTGCCTTGGGTACTTCACA
	Chst8-2F	CGCACCATGGACAGTCGT
	Chst8-2R	AAGTCGTAGGTTCGCTGTCG
	Chst8-3F	CTTCTTCCTGCGTCTCATCC
	Chst8-3R	CCCTGGGTCATAGAAAAGCA
Cebpa[7]	Cebpa-1F	GAGCCAGTTGGGGCACTG
	Cebpa-1R	GCTGTTCTTGTCCACCGACT
	Cebpa-2F	CCACTTGCAGTTCCAGATCG
	Cebpa-2R	CGGGATCTCAGCTTCCTGTA
	Cebpa-3F	CAGGGCAGGAGGAAGATACA
	Cebpa-3R	AAGAGAAGGAAGCGGTCCAG

5: G patch domain containing 1

6: Carbohydrate (N-acetylgalactosamine 4-0) sulfotransferase 8

7: CCAAT/enhancer binding protein (C/EBP), alpha

Table 3.2. Primers used to amplify candidate gene cDNAs (Continued)

Gene name	Primer name	Primer sequence
Kctd15[8]	Kctd15-t1-1F[t1]	CTTGGAGAAGCGGGTCAAT
	Kctd15-t1-1R[t1]	CAGCCAGGGGAGACACAG
	Kctd15-t1-2F[t1]	ATGGAAGCCTAGATGCCTCA
	Kctd15-t1-2R[t1]	CCCAGCAGAGGACGCTATAC
	Kctd15-t1-3F[t1]	GTGTCCACGGAAGGACTGTT
	Kctd15-t1-3R[t1]	GCGTTCTTTATGGCATGAACC
	Kctd15-t2-1F[t2]	GGGGGCGAGAGAGAAAGTAA
	Kctd15-t2-1R[t2]	CAGCCAGGGGAGACACAG
	Kctd15-t2-2F[t2]	ATGGAAGCCTAGATGCCTCA
	Kctd15-t2-2R[t2]	CCCAGCAGAGGACGCTATAC
	Kctd15-t2-3F[t2]	GTGTCCACGGAAGGACTGTT
	Kctd15-t2-3R[t2]	GCGTTCTTTATGGCATGAACC
	Kctd15-t3-1F[t3]	GCGCTCGTCCAGGAAATG
	Kctd15-t3-1R[t3]	CAGCCAGGGGAGACACAG
	Kctd15-t3-2F[t3]	ATGGAAGCCTAGATGCCTCA
	Kctd15-t3-2R[t3]	CCCAGCAGAGGACGCTATAC
	Kctd15-t3-3F[t3]	GTGTCCACGGAAGGACTGTT
	Kctd15-t3-3R[t3]	GCGTTCTTTATGGCATGAACC
Rhpn2[9]	Rhpn2-1F	TCCAGGCACAGAAACAGTCA
	Rhpn2-1R	GAAGCCTCTGGATGTTGGAG
	Rhpn2-2F	TTTATTGAGGCCCATGGTGT
	Rhpn2-2R	ATCATCGCCATCATCTAGCC
Riken clone C28005212	Riken clone-1F	CTTGCGAGAGCTTGTCCTCT
	Riken clone-1R	GAGCTAGGTGGGAAGGATGG
	Riken clone-2F	ATGTTCTGTCCCCTCACAGG
	Riken clone-2R	GAAGGTGGGCAAGAACTGTC
Slc7a10[10]	Slc7a10-1F	GGTAGCGCAGGGAACTGG
	Slc7a10-1R	CCTGGATGAGGTGAACAGGT
	Slc7a10-2F	GAGAAGCTGCTGGGCTACTTT
	Slc7a10-2R	CAGCAACAACCAGCCCTGT

8: Potassium channel tetramerisation domain containing 15

9: Rhophilin, Rho GTPase binding protein 2

10: Solute carrier family 7 (cationic amino acid transporter), member 10

genomic DNA using forward primer AGCGCATCGATGAACCTG and reverse primer TCCAAGAGGTGGTCAATGAA.

Quantitative real time PCR

Wild type and *dal/dal* embryos were dissected in ice-cold PBS. Total RNA from each embryonic heart was extracted using Trizol (Invitrogen) according to the manufacturer instructions, and 10 nanogram of total RNA was reverse transcribed in a final volume of 20 µl using ABI High Capacity cDNA Kit. All PCR reactions were performed using the ABI 3700 Real Time System. Each sample was analyzed in triplicate on the same plate. PCR reactions containing 1 µl cDNA template, 10mM of each primer and 2X SYBR green PCR master mix (Applied Biosystems) were incubated at 50°C for 2 minutes, then denatured for 10 minutes at 95°C. Following initial incubation, 40 cycles of 95°C for 15 seconds and 60°C for 1 minute were performed. Primer sequences are listed in Table 3.3. The expression levels for genes of interest (*Pepd, ANP, BNP*) normalized to the housekeeping gene *GPI* were determined using comparative C_t method of relative quantification (Livak and Schmittgen, 2001). The RQ value of each gene of interest was expressed as the fold change relative to that of endogenous control gene. Student's *t*-test was utilized to compare the mean difference in transcript level between controls and *dal/dal* mutants.

Histological studies

Embryos were harvested in ice-cold PBS, fixed in 10% buffered formalin for at

Table 3.3. Primer sequences used for quantitative real time PCR

Gene name	Primer sequence
Pepd[1]	F- GAAGGCCATCTACGAAGCAG
	R- CTCCAGGTGGATACGGTCAG
GPI[2]	F- CAACTGCTACGGCTGTGAGA
	R- CTTTCCGTTGGACTCCATGT
ANP[3]	F- CCTTGATGTCTTTGGGGAGA
	R- GATTTGGGGGTTCTCGGTAT
BNP[4]	F- TGCTTTGGGCACAAGATAGA
	R- AGACCCAGGCAGAGTCAGAA

1: Peptidase D
2: Glucose-6-Phophate Isomerse
3: Atrial natriuretic peptide
4: Brain natriuretic peptide

least 12 hours, then dehydrated through an ethanol series and cleared in xylene. Prepared embryos were placed in molds, paraffin-embedded, and allowed to set in cold plates. Six to ten micrometer (μm) transverse serial sections were made, mounted on Superfrost slides, processed for dewaxing, stained with hematoxylin and eosin (H&E) , then mounted in aqueous media (Permount, Invitrogen) using standard protocols. Mounted slides were dried at room temperature overnight and viewed and photographed at 10X magnification on a Leica DMRE fluorescent microscope (Leica, Germany).

Picrosirius red staining is a commonly used method to detect extracellular collagen. Five hearts (each) from 2 month-old *dal/dal* and C3H/HeJ mice were collected, embedded in paraffin and sectioned at 7 μm. Slides were stained

with Picrosirius red solution (0.1% Sirius Red F3BA, Sigma, St.Louis, MO) in saturated aqueous picric acid, rinsed in 0.01N HCl for 2 minutes, dehydrated, and mounted with cover slips. Mounted slides were dried at room temperature overnight and viewed and photographed at 20X magnification on a Leica DMRE fluorescent microscope (Leica, Germany).

BrdU incorporation assay

Cell proliferation was assayed on paraffin-embedded sections of E12.5 embryos using 5-bromo-2'-deoxy-uridine (BrdU). One hour prior to euthanasia, pregnant mice were injected peritoneally with 100 µg BrdU (Invitrogen) per gram (g) of body weight diluted in PBS. Embryos were fixed, embedded in paraffin and sectioned, as described above. Sections were deparaffinized in xylene, rehydrated through an ethanol series, washed in PBS, denatured in 2N HCL for 30 minutes at room temperature, neutralized by washing in PBS, and incubated in blocking solution (1% bovine serum albumin (BSA), 0.2% low fat milk and 0.3% Triton X-100) for 15 min at room temperature. Mouse monoclonal anti-BrdU antibody (BrdU Staining Kit, Invitrogen) diluted 1:100 in blocking solution was added and slides were incubated with Cy3-conjugated anti-mouse antibody diluted 1:1000 in blocking solution at room temperature for 1 hour, washed in PBS, and mounted with Paramount mounting media (Invitrogen). Sections were examined and photographed digitally using a Leica DMRE fluorescent microscope (Leica, Germany). The number of BrdU positive cells was quantified within the interventricular septum under 100X magnification from a minimum of three separate areas and within endocardial cushion area under 40X magnification for each wild type and *dal/dal*

embryonic heart. The proportion of BrdU positive cells was analyzed using z-test with significance set at $p<0.05$.

Cardiomyocyte isolation

Embryonic cardiomyocytes were isolated from E15.5 *dal* homozygous mutant and C3H/HeJ control embryos. Hearts were visualized and harvested through an incision through the anterior chest wall, placed on ice and washed in ice-cold PBS. Ventricular tissues were selectively separated. The ventricles were dissociated by serial enzymatic digestion with collagenase B (Roche, Germany) in a shaking water bath at 37°C and 100 rpm. The isolated cells were immediately collected by centrifugation at 1400 rpm and resuspended into culture medium containing DMEM (Cellgro, Manassas, VA), 20% FCS and 100 µg/ml penicillin/streptomycin (Cellgro). Suspended cells were seeded onto culture plates and maintained in a humidified atmosphere of 5% CO_2 at 37°C overnight. All pictures of beating individual cardiomyocytes were taken under the same magnification. Cell surface area was measured using polygon selections in the ImageJ software program. Parameter adjustments with 180 of distance in pixels and 20 of known distance were set for all pictures to synchronize the scale between each picture.

Actin cytoskeletal staining and confocal microscopy analysis

Cardiomyocytes isolated from E15.5 *dal/dal* and C3H/HeJ embryonic hearts (as described above) were grown on poly-L-lysine-coated glass coverslips overnight. Cells were then washed with ice-cold PBS, fixed with 4%

paraformaldehyde in PBS, permeabilized with Triton X-100 in PBS (0.1%) for 30 minutes and treated with a blocking solution of 7% BSA in PBS for 30 minutes at room temperature. For staining of polymerized actin filaments, cells were incubated with alexa 647-conjugated phalloidin (Alexa Fluor 647, Invitrogen) for 1 hour and then rinsed in PBS. Coverslips were mounted onto microscope glass slides with Vectashield anti-fade mounting medium. Phalloidin labeling was visualized using an Olympus IX70 confocal imaging system (Olympus, Center Valley, PA) and images captured as a stacked series (1 mm Z steps). Image-acquisition settings (laser intensity, iris size, magnification, and amplifier gain) were maintained constant for all images to allow for comparisons between groups. The intensity of alexa-phallodin-stained actin was determined using Fluoview v5.0 software (Olympus, Germany).

In vivo calcium imaging

E12.5 embryos were collected from pregnant C3.CB-*dal*/*dal*; pCAGGS-GCaMP(+) females. Embryos were maintained in embryo holding solution (NaCl 136mM, KCl 5.4mM, $MgCL_2 \cdot 6H_2O$ 1mM, NaH_2PO_4 0.33mM, $CaCl_2 \cdot 2H_2O$ 2.5mM, Glucose 10mM and 4-(2-hydroxyethyl)-1-piperazineethanesulfonic acid 10mM) on ice throughout the study. After exposing an embryonic heart via opening the chest cavity, fluorescence of calcium transients was imaged using an Olympus MVX10 inverted microscope (Olympus, Germany) and intensified using a charge-coupled device camera (Andor Technology, UK). Image acquisition and data analysis were performed using Metafluor 5.0 and ImageJ software programs. After image analysis was

completed, each embryo was fixed in 10% buffered formalin for histological analysis (following the protocol described above) in order to examine the correlation between calcium transients and cardiac structure.

Antisense morpholino oligo microinjection

An antisense morpholino oligonucleotide [5'-ACACCCTACACAACACACAGATGAG-3'] that specifically binds to the splice acceptor sequence of exon 20 [5'-ctcatctgtgtgttgtgtagGGTGT-3'; intronic sequences in lower case, exonic sequence in upper case letters] of the zebrafish *Pepd* gene was designed and designated as Pepd_MO. A standard control morpholino [5'-CCTCTTACCTCAGTTACAATTTATA-3'] against a random sequence not present in the zebrafish genome was purchased (Gene Tools, Philomath, OR) and designated as Control_MO. Each morpholino (Pepd_MO and Control_MO) was injected into the yolk sac of at least 20 wild-type embryos from 7 different clutches on different days. Embryos at the 1- or 2-cell stage (when the chorion is intact) were injected with 0.5 mM of morpholino oligos under the settings of 3 msec injection time and 30 mmHg injection pressure. Injected embryos were raised at 28.5°C to 5 days post-fertilization (dpf), by which time cardiac development is largely complete (Sprague et al., 2001). Successful pre-mRNA modification was monitored by RT-PCR across exon 20 using forward primer GGGGTGAAGTGGACAGACAT (in exon 19) and reverse primer TTGGACTGAAGGGTTTGGAC (in exon 21) using total RNA extracted from morpholino-injected embryos using Trizol (Invitrogen) as template. Embryos were examined under the light microscope for gross phenotypes, particularly body size and pigmentation. In order to

evaluate myocardial development and ventricular wall thickness, Pepd_MO and Control_MO were injected into the yolk sac of transgenic zebrafish embryos carrying a cardiac myosin light chain promoter-driven green fluorescent protein transgene (CMLC-GFP), which drives GFP expression in the heart. At 5 days post-injection, embryonic hearts were examined by confocal microscopy (Axiovert 200M, Zeiss, Germany) to image cardiac GFP expression. Images were analyzed using the LSM510 Meta software program.

Western blotting

Hearts from E15.5 *dal/dal* and C3H/HeJ embryos were collected, washed in PBS, and homogenized in RIPA buffer (50mM Tris HCl pH7.4, 150mM NaCl, 2mM EDTA, 1% NP-40, 0.1% SDS) containing Complete protease inhibitor (Roche, Germany) using a polytron homogenizer. Phosphatase inhibitor (Invitrogen) was added to lysates when phospho-specific antibodies were used for western blotting. Homogenates were cleared by centrifugation at 12000 rpm for 5 minutes at 4°C. The supernatant was collected and stored at -80°C. Protein concentrations were determined by BCA protein assay (Pierce, Rockford, IL). Equal amounts of protein lysates (15 µg for total protein and 300 µg for phosphorylated protein assays) were mixed with 2X SDS buffer (125 mM Tris-HCl, 10% glycerol, 10% SDS, 130 mM DTT), incubated at 70°C for 5 minutes and separated on 4% stacking, 8% SDS polyacrylamide gels. Proteins were transferred to Immobilon P membrane (Millipore, Bedford, MA) at 0.5 mA for 3 hours. Successful transfer was verified by Ponceau S staining. Blots were blocked in 5% milk in Tris-Tween Buffered Saline (TTBS) buffer for an hour at room temperature and incubated with anti-mouse or rabbit primary

antibody in TTBS at 4°C overnight. After washing three times (10 min each), blots were incubated in horseradish peroxidase (HRP)-conjugated anti-mouse (cat#:554002, BD Transduction Laboratories) or anti-rabbit secondary antibody in TTBS for 50 min at room temperature followed by three 15 min washes in TTBS. Antibody signal was detected by chemiluminescence (ECL Western Blotting Detection Reagent, Amersham, UK) and visualized using the Versadoc Imaging system (Bio-Rad, Hercules, CA). Protein signal intensity was quantified using ImageJ software (NIH) and the mean values analyzed by Student's *t*-test. Differences between mean values was considered statistically significant at $p<0.05$.

Primary antibodies used in the present study were against focal adhesion kinase (FAK) (cat#:3285, Cell Signaling Technology, Danvers, MA), phospho-FAK (cat#:3283, Cell Signaling Technology), Src (cat#:2109, Cell Signaling Technology), phospho-Src (cat#:2101, Cell Signaling Technology), Paxillin (cat#:610568, BD Transduction Laboratories, San Jose, CA), F-Actin (cat#:RDI-PRO61075, Fitzgerald, Concord, MA) and SERCA2a (cat#:ab2861, Abcam, Cambridge, MA). Membranes were re-blotted with HRP-conjugated GAPDH (cat#:ab9482, Abcam) to verify equal protein loading.

Results

Characterization of developmental cardiac phenotypes in dal embryos

Mice homozygous for the *dal* mutation had previously been reported to be smaller than their wild-type littermates (Harris, 2003). In BC mice generated by mating CAST/EiJ x C3.CB-*dal/dal* F1 mice back to C3.CB-*dal/dal* mice, the average weight of postnatal day 14 homozygous *dal* mutant pups was 6.2 g (n=30), which was significantly less than that of their heterozygous littermates, which 9.2 g (n=62) (Figure 3.2). In addition, a high rate of embryonic and perinatal lethality had previously been observed for *dal/dal* animals (Teresa Gunn, personal communication). For example, 27% of implantations in litters of mid-to-late gestation *dal* embryos were dead and/or resorbed, and 5.9% of surviving embryos were developmentally delayed (small body size relative to other littermates) (Table 3.4). As cardiac defects are the most common cause of mid-to-late gestation lethality and growth retardation (Takahashi et al., 2004), I hypothesized that the *dal* mutation disrupts normal cardiogenesis. I performed a comprehensive histological analysis of mid-to-late gestation (E12.5, E15.5, and E18.5) *dal/dal* and control embryos to detect the presence and frequency of cardiac structural abnormalities in *dal* embryos (Table 3.5). The most striking cardiac abnormality, observed in 67.6% of *dal/dal* mutant embryos, was a substantially increased thickness of the ventricular wall (Figure 3.3). Augmented ventricular thickness was most prominent at the interventricular septum. The interventricular septum of *dal/dal* embryonic hearts was significantly thicker (~1.6 fold) than that of controls (p=0.0002, Figure 3.4).

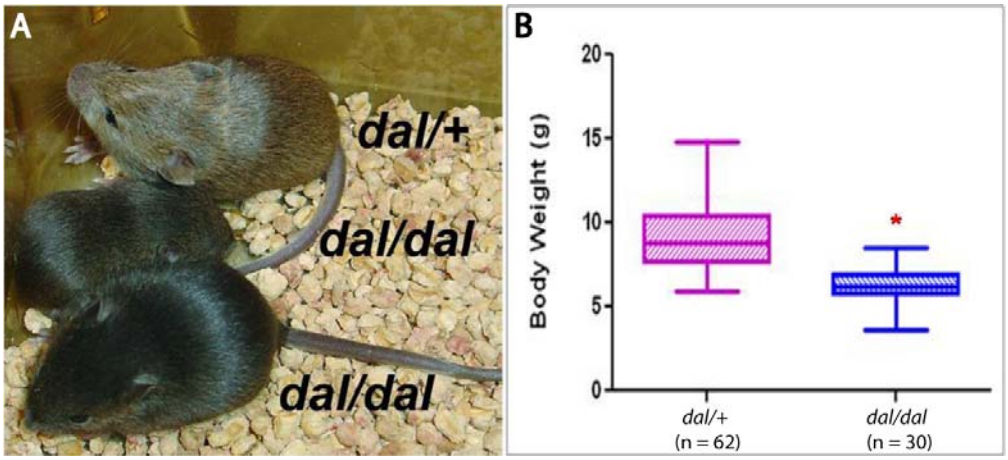

Figure 3.2. Gross phenotypes of *dal* mutant mice. (A) Mice homozygous for the *dal* mutation are generally small in size and have dark fur. Heterozygotes are indistinguishable from wild-type mice (not shown). (B) In a CAST x *dal* backcross, the mean body weight of two week-old *dal/dal* mice (6.2g) was significantly lower than that of *dal*/+ mice (9.2g) (*Student's *t*-test with Mann-Whitney correction : $p<0.0001$).

Table 3.4. Reduced viability in *dal/dal* mutant embryos

Stage	embryos n	growth delayed n (%)	dead or resorbed n (%)
E13.5-14.5	89	6 (6.7%)	17 (19.1%)
E14.5-18.5	63	3 (4.8%)	24 (38.1%)
Total	**152**	**9 (5.9)%**	**41 (27.0%)**

Table 3.5. Cardiac structural defects present in *dal/dal* mutant embryos

Strain	**Age**	**Normal thickness**	**Increased ventricular mass**
dal/dal	E12.5 (n=9)	3	6 (2ASD, 1 VSD)
	E15.5 (n=12)	3	9 (1 ASD)
	E18.5 (n=13)	5	8 (2 ASD)
C3H/HeJ	E12.5 (n=4)	4	-
	E15.5 (n=5)	5	-
	E18.5 (n=5)	5	-

Figure 3.3. Developmental cardiac defects in *dal* mutant mice. (A-B) H&E stained sections of E12.5 wild-type (A) and *dal*/*dal* (B) hearts showed atrial and ventricular septal defects (*) and markedly enlarged endocardial cushions (black arrow) in *dal* mutants. (C-D) H&E stained ventricular sections of E16.5 wild-type (C) and *dal*/*dal* (D)hearts showing significantly thickened ventricular walls (black arrow) and an atrial septal defect (*) in *dal* mutants. (E-F) High magnification view of ventricular septum of 3-month old wild-type (E) and *dal*/*dal* (F) mice demonstrating myocytic and myofibrillar disarray in mutant hearts (F).

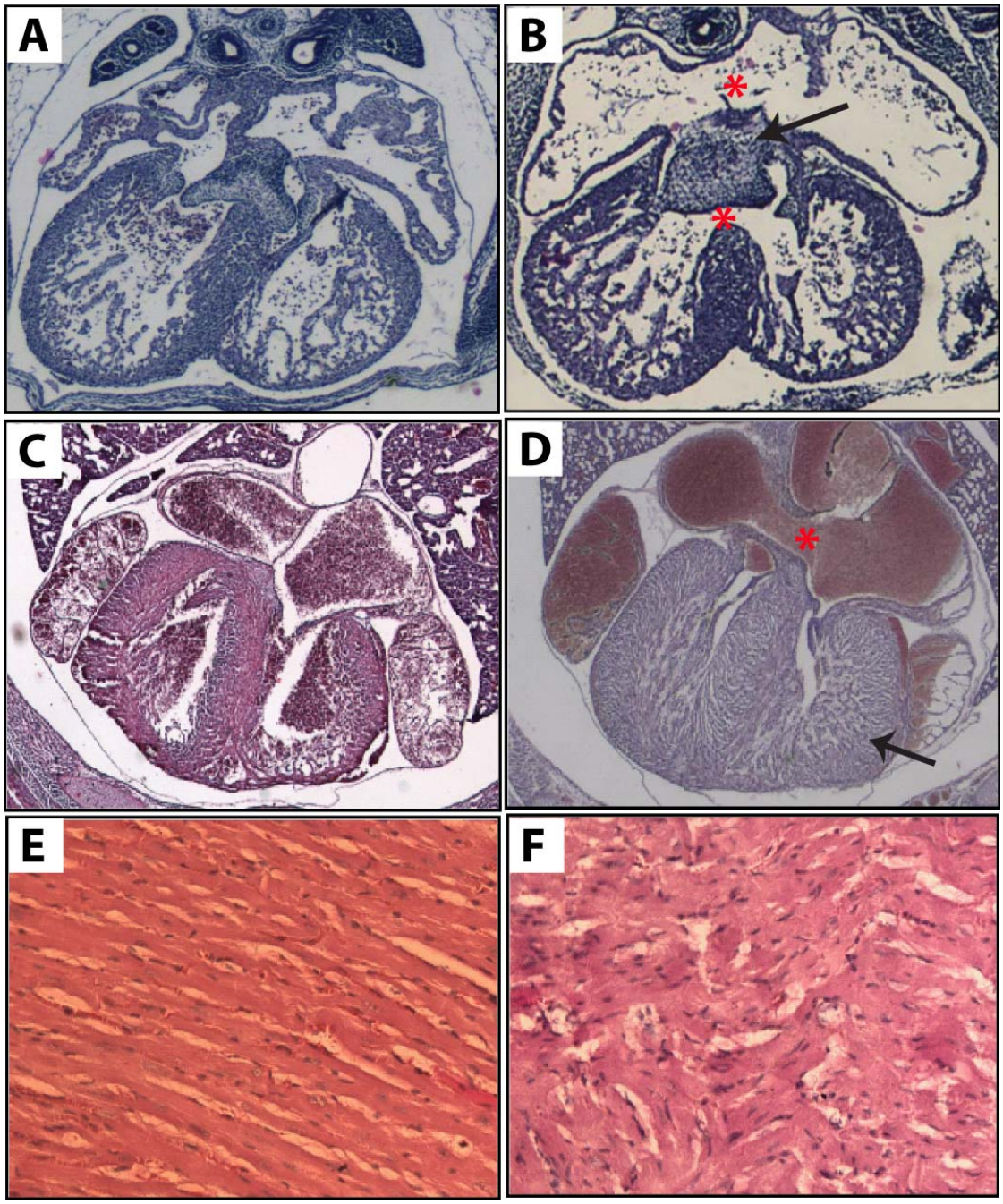
A
B
C
D
E
F

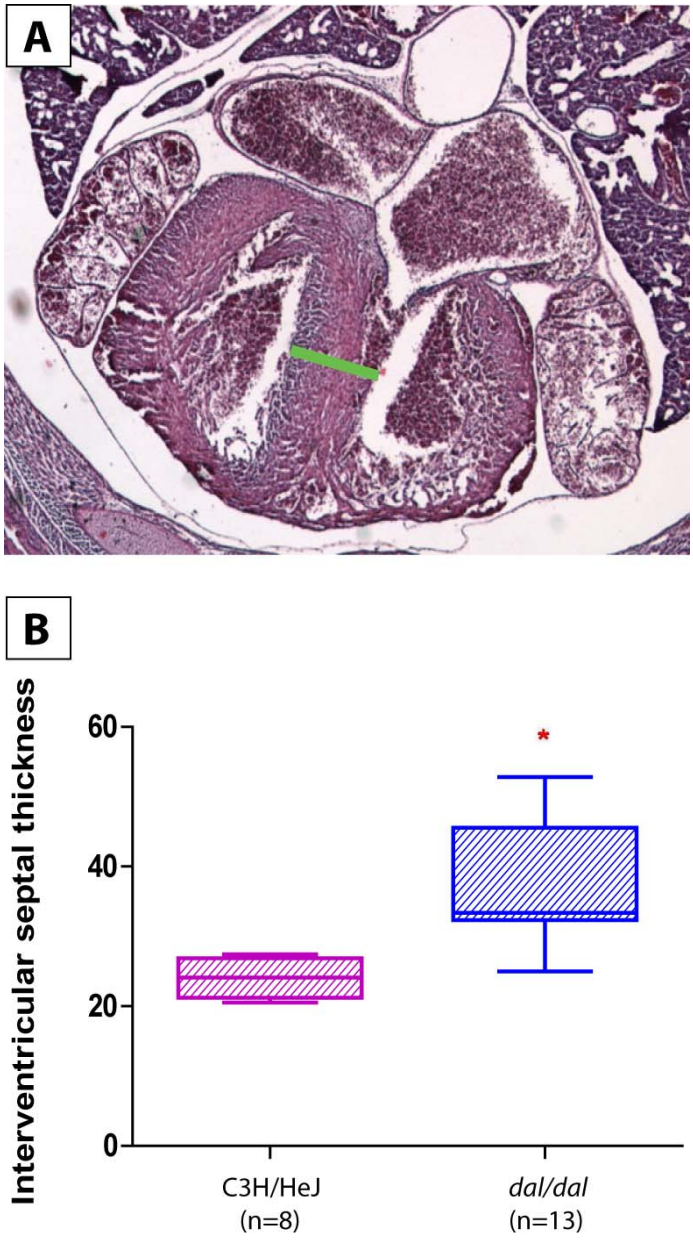

Figure 3.4. Interventricular septum is thicker in *dal/dal* embryonic hearts. (A) The thickness at the mid portion of interventricular septum was measured (as indicated by green bar). (B) Interventricular septum of *dal/dal* embryonic hearts (38 units) was significantly thicker than that of wild-type embryonic hearts (24 units) (* Student *t*-test p=0.0002).

Atrial septal defects (ASD) and/or ventricular septal defects (VSD) were observed in 15% of *dal/dal* mutant embryos (Table 3.5). The endocardial cushion area also appeared enlarged in some mid-gestation *dal* mutant embryonic hearts, with no evidence of increased cellular proliferation or density (Figure 3.3 and 3.5). Over the course of late pregnancy, however, no obvious structural defects such as aplastic or dysplastic valve were seen at the AV junction area (Figure 3.6). No anatomical abnormalities were detected in the atrial tissue of *dal/dal* embryos, with atrial wall thickness and chamber dimension comparable between wild-type and *dal/dal* embryos (Figure 3.3). High power magnification of the region of thickened ventricles in 3 month-old adult *dal* mice showed a myocytic and myofibrillar disarray (abnormal disturbance of normally ordered cardiac cell alignment), which is the pathological hallmark of cardiac hypertrophy in humans (Figure 3.3) (Ly et al., 2005).

The heart defects observed in *dal* mutant embryos indicated that the gene mutated in these animals plays an important role in myocardial development. It was not clear, however, whether the increased ventricular mass reflected an increase in the number of cardiomyocytes (hyperplasia), their size (hypertrophy), or a combination of the two. In order to distinguish these possibilities, I first examined the effect of the *dal* mutation on cardiomyocyte proliferation. I performed a bromodeoxyuridine (BrdU) incorporation assay on paraffin-embedded heart sections of E12.5 and E15.5 *dal/dal* and control embryos. BrdU is a thymidine analogue that incorporates into the DNA of proliferating cells and substitutes for thymidine during DNA replication. No differences were observed in the number of replicating cardiomyocytes based

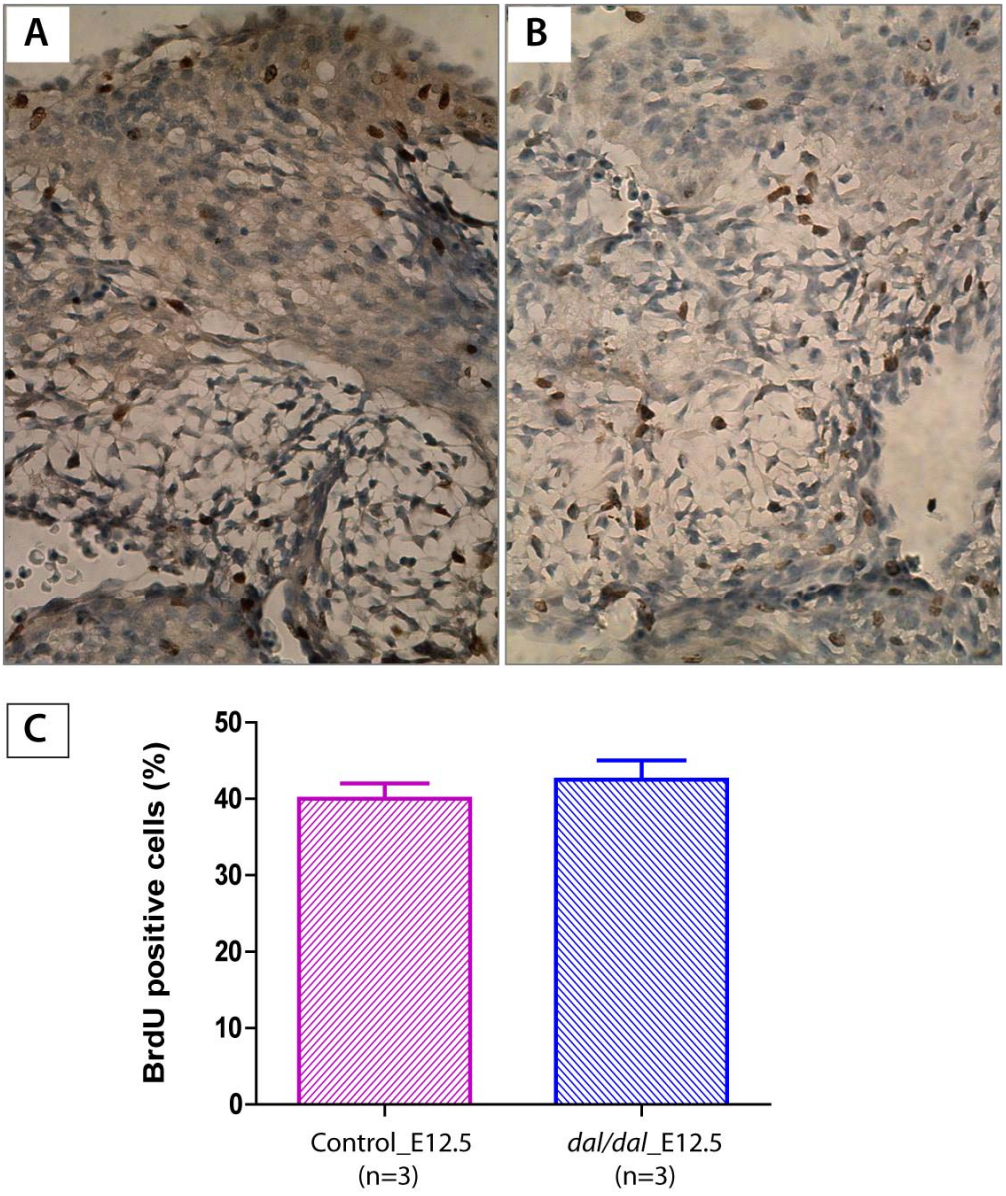

Figure 3.5. Normal cellular proliferation in the endocardial cushions of E12.5 *dal/dal* embryonic hearts. Cardiac sections stained with BrdU from E12.5 control (A) and *dal/dal* (B) embryonic hearts were examined under 40X magnification. (C) There was no difference in the proportion of BrdU positive cells between control (38%) and *dal/dal* mutant (40%) endocardial cushion areas (p=0.467).

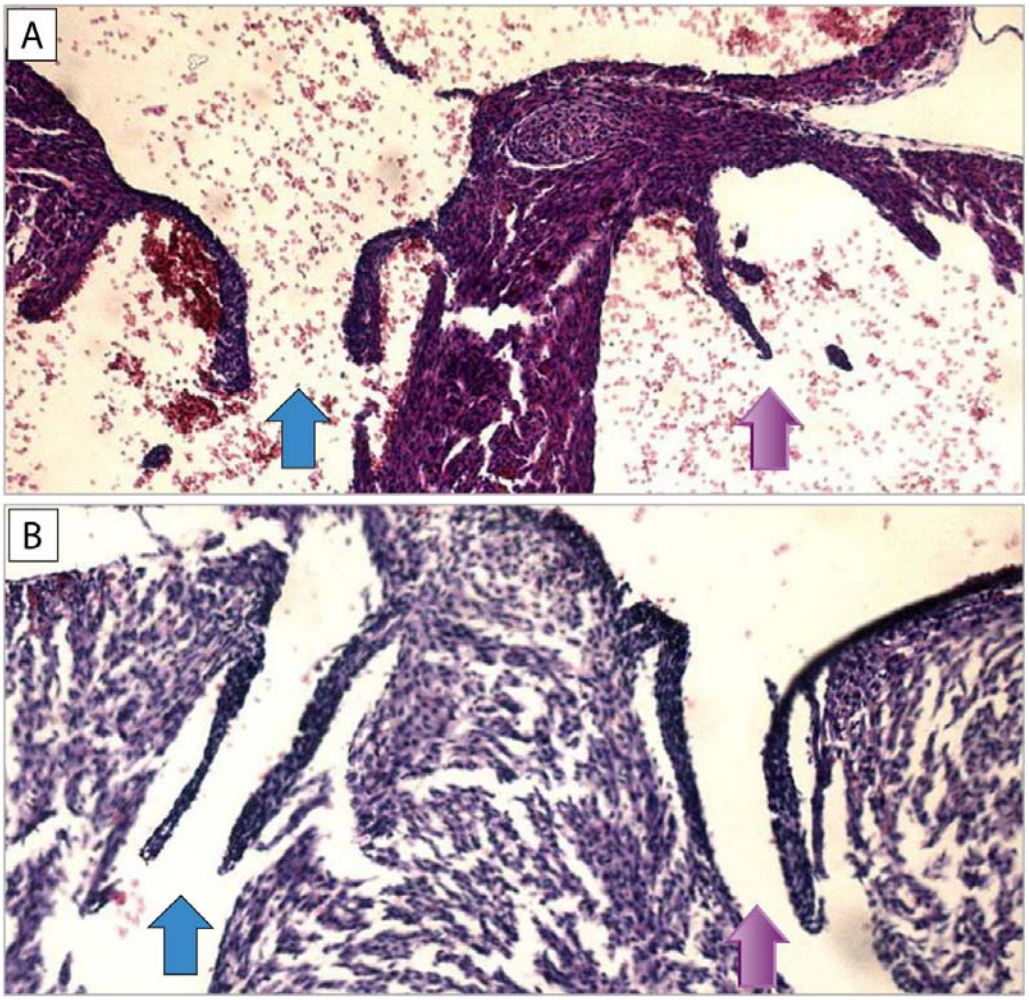

Figure 3.6. Cardiac valves were normally developed in *dal/dal* embryonic hearts. Histological examination of cardiac valve formation in E18.5 wild-type (A) and *dal/dal* (B) embryos showed that both the mitral (blue arrow) and tricuspid (purple arrow) valves were normally developed by late gestation. The thickened ventricular septum of *dal/dal* embryonic heart (B) is obvious.

Figure 3.7. The proliferation status of *dal* mutant cardiomyocytes was not altered. BrdU staining of E12.5 *dal*/*dal* and control embryonic hearts counterstained with hematoxylin. (A,B) E12.5 wild-type (A) and *dal* mutant (B) heart sections. The thickened ventricular wall of *dal* mutants is obvious. (C,D) High power (100X magnification) view of boxed areas in (A) and (B). The number of cells in the same field of view was lower in *dal/dal* hearts than controls (120 vs. 150 cells per field of view) and cells in *dal* mutants appeared to be more dispersed, with a greater spacing between nuclei than in control hearts. (E) Quantification of BrdU signals. There was no significant difference in the proportion of BrdU positive cells between *dal* mutant (30%) and control (28%) embryonic hearts (p=0.398).

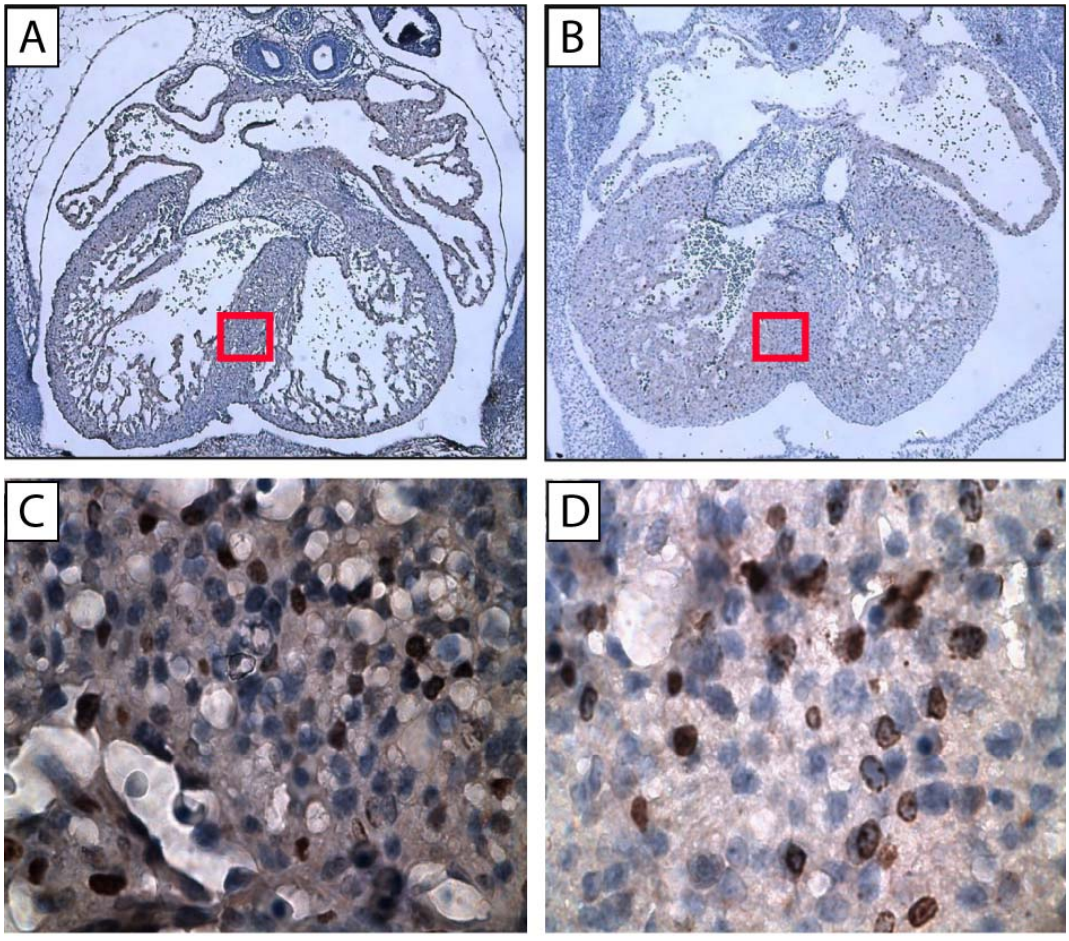
A
B
C
D

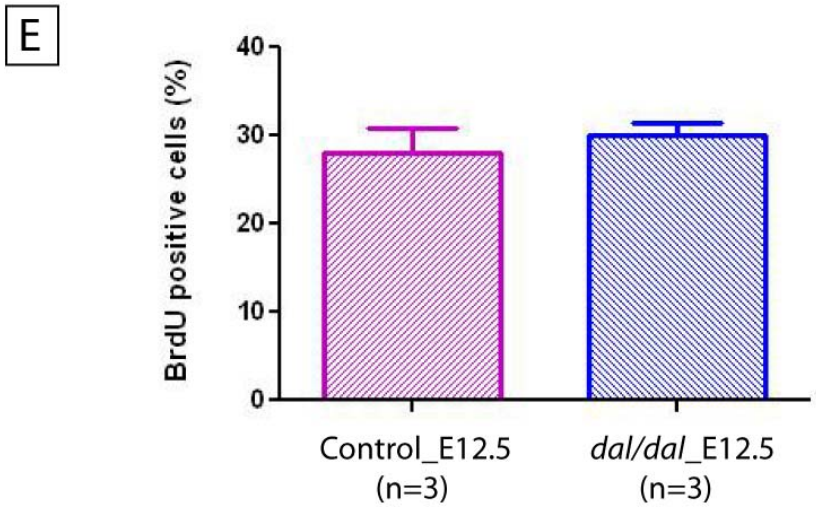
E
BrdU positive cells (%)
40
30
20
10
0
Control_E12.5
(n=3)
dal/dal_E12.5
(n=3)

on the proportion of BrdU positive cells out of the total number of cells within a given field of view (Figure 3.7): 30% (37/120) of cells were BrdU positive in *dal/dal* mutant hearts, while 28% (43/150) were positive in age-matched wild-type hearts. In analyzing the BrdU-stained sections, it was noted that sections of *dal/dal* hearts consistently had fewer cells in a given field of view, and their nuclei seemed to be more dispersed, suggesting the cells might be larger (hypertrophic). This observation prompted me to isolate and culture cardiomyocytes from control and *dal* mutant embryonic hearts and compare their surface area. Cardiomyocytes from *dal/dal* embryos were significantly larger (~1.7-fold) than those isolated from wild-type embryos ($p<0.0001$, Figure 3.8). The mean cell surface area of *dal/dal* and control cardiomyocytes was 317 and 187 (arbitrary units), respectively. Based on the result of this experiment, I concluded that the thickened ventricles in *dal/dal* mutants reflect bigger cardiomyocytes (hypertrophic changes during development).

Changes in the expression of the genes encoding the cardiac polypeptide hormones ANP and BNP are commonly used as a marker of cardiac hypertrophy. The expression level of these genes was therefore tested, with the expectation of their being elevated in the ventricles of *dal* mutant embryos. RNA was isolated from the hearts of 4 *dal* mutant and 4 wild-type E12.5 embryos and used as template for qRT-PCR. While *Anp and Bnp* were consistently expressed at higher levels in *dal* embryonic hearts than in controls, the differences were not statistically significant (Figure 3.9).

In order to examine the physiological consequences of cardiac hypertrophy, I analyzed calcium dynamics in *dal* embryonic hearts using pCAGGS-GCaMP

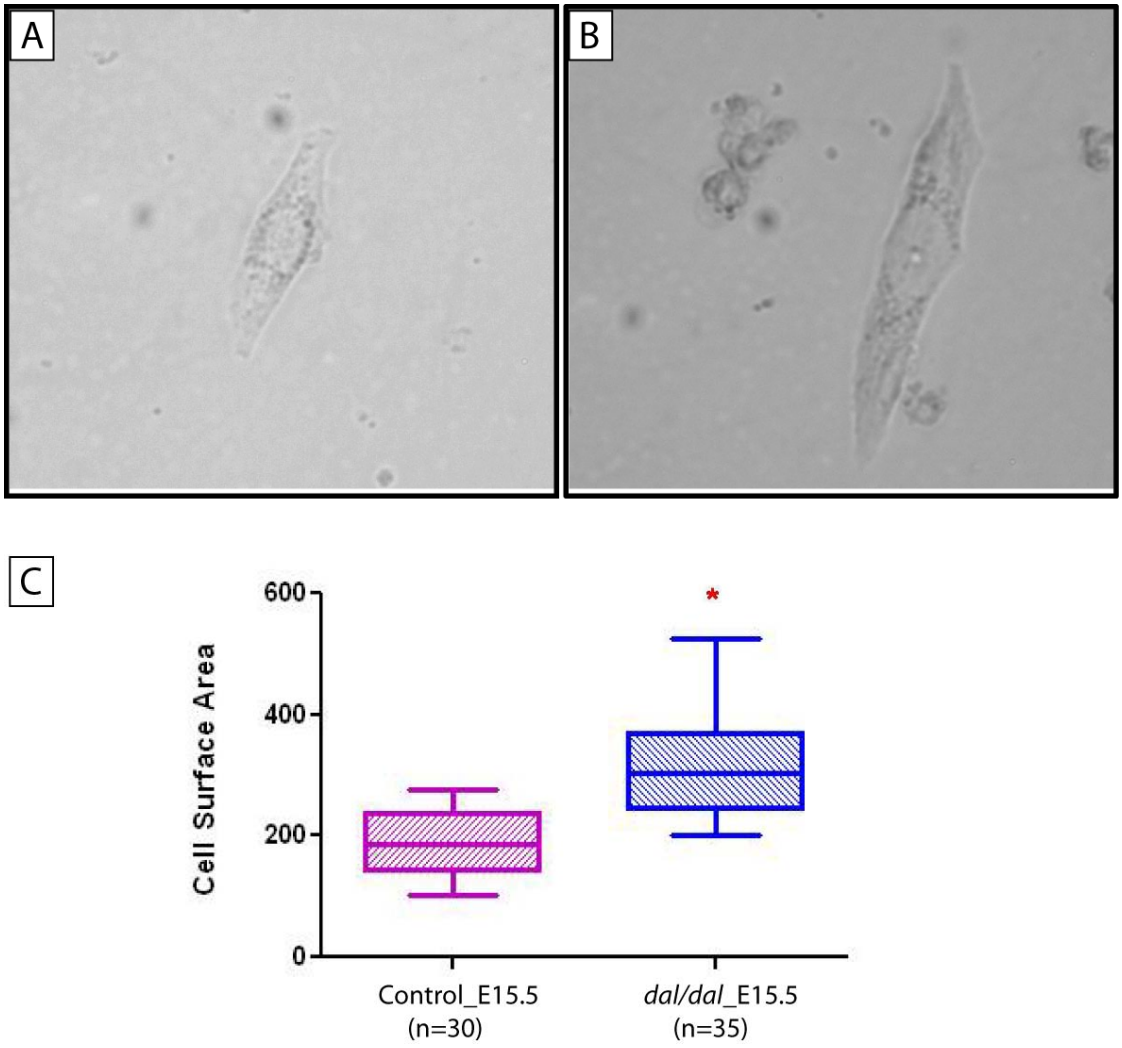

Figure 3.8. Cardiomyocytes from *dal* mutant embryos are hypertrophic. (A,B) Representative cardiomyocytes isolated from E15.5 *dal/dal* (A) and C3H/HeJ (wild-type control) (B) embryonic hearts. (C) The mean surface area of *dal/dal* cardiomyocytes (317 units) was almost 2-fold greater than that of wild-type cardiomyocytes (187 units) (* Student's *t*-test: $p<0.0001$).

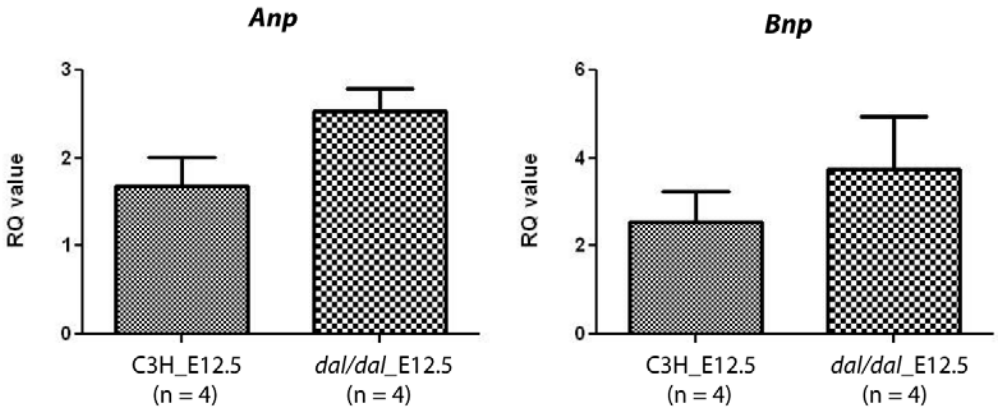

Figure 3.9. Expression of the hypertrophy markers *Anp and Bnp* appears to be elevated in some of *dal* mutant hearts. E12.5 *dal* mutant and control heart RNA was subjected to qRT-PCR for *Anp and Bnp*, which are commonly used markers of cardiac hypertrophy. Although the differences were not statistically significant ($0.2 \leq p < 0.5$), *Anp and Bnp* were consistently elevated in *dal* mutant hearts.

transgenic mice. The GCaMP transgene consists of the α-myosin heavy chain (MHC) promoter, enhanced green fluorescent protein (eGFP), calmodulin and RSET poly-His peptide (Tallini et al., 2006) (Figure 3.10). When calcium binds to calmodulin within the transgenic protein product during excitation-contraction coupling (E-C coupling), eGFP undergoes a conformational change and emits green fluorescent light. The intensity of the GFP signal is therefore an indicator of calcium cycling. This system enables one to visualize molecular calcium information for a beating heart.

While *dal/+* embryonic hearts exhibited normal, synchronous calcium transients in a constant interval, 3 out of 7 (43%) *dal/dal* embryos showed features of abnormal calcium transients that included abnormal ectopic depolarizations during the repolarization period (EADs) and significant interval irregularities (Figure 3.11). This suggests that *dal* neonates might be susceptible to developing fatal cardiac arrhythmias during postnatal maturation. The hearts of imaged embryos were subsequently sectioned to determine whether ventricular thickness was correlated with calcium handling defects. The ventricles of hearts from *dal/+* embryos and *dal/dal* embryos that had normal calcium transients were normal, while *dal/dal* embryos with altered calcium transients had thickened ventricular walls and septal defects (Figure 3.11). Western blot analysis for SERCA2, one of the major intracellular calcium handling proteins, showed no significant difference in expression level between control and *dal* mutant hearts (Figure 3.12).

Figure 3.10. The structure of the *in-vivo* calcium sensor encoded by the pCAGGS-GCaMP transgene. When calcium (orange dots) binds calmodulin, a conformational change causes eGFP to fluoresce. A high resolution camera is used to detect the signal, which is translated as molecular calcium signals.

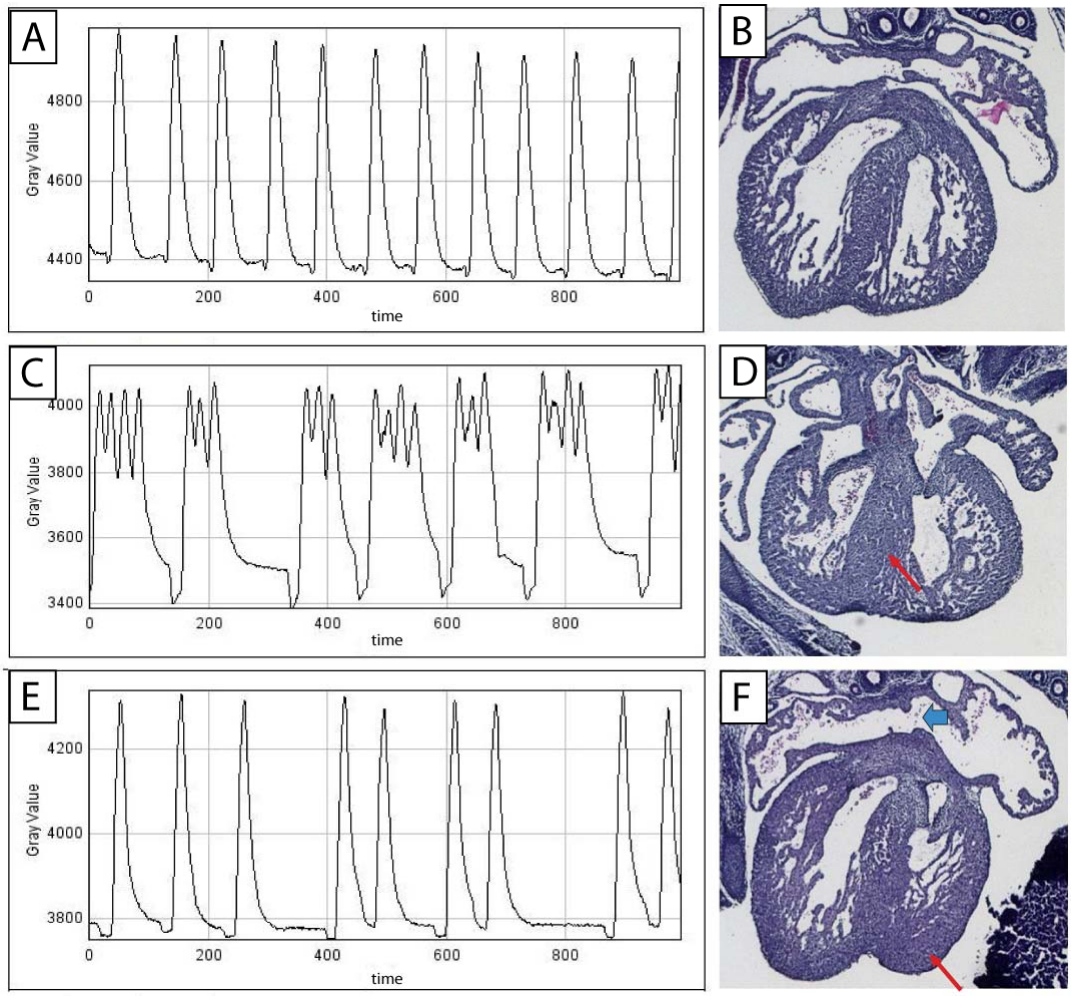

Figure 3.11. Abnormal calcium signaling is correlated with thickened ventricles in *dal/dal* mutant hearts. The hearts of *Tg.pCAGGS*; *dal*/*dal* and *Tg.pCAGGS*; *dal*/+ embryos were imaged to record GFP fluorescence that reflects calcium transients. (A, B) Normal calcium transients (A) and cardiac structure (B) in E12.5 *dal*/+ embryonic heart. (C-F) Altered calcium transients and corresponding thickened ventricles in E12.5 *dal*/*dal* embryonic hearts. Early afterdepolarization (EAD) (C) was observed in a *dal*/*dal* embryo with a prominent ventricular septum (red arrow in D). Irregular rhythm of calcium transients (E) was recorded from a *dal*/*dal* heart with thickened ventricles (red arrow in F) and ASD (blue arrow in F).

A.

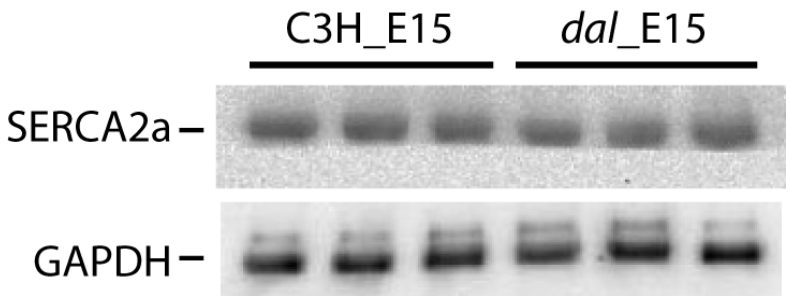

B.

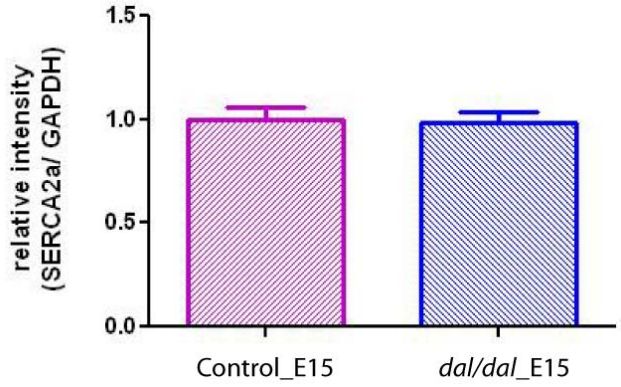

Figure 3.12. SERCA2a expression levels were not altered in E15.5 *dal* embryonic hearts. (A) No difference was observed upon Western blot analysis for SERCA2a between E15.5 control and *dal* embryonic hearts. (B) The mean relative intensity of SERCA2a signal, normalized to GAPDH loading control, showed no difference between controls and *dal* mutants (Student's *t*-test p=0.5629).

Identification of the dal gene

Identifying the gene mutated in *dal* mutant mice was the next logical step in understanding the mechanism underlying abnormal cardiomyocyte hypertrophy in *dal* embryonic hearts. Harris *et al.* (Harris, 2003) had mapped the *dal* mutation to a 9.9 Mb region between D7Mit294 and D7Mit247. This interval contains approximately 250 genes. In order to refine the candidate interval to a small enough region for mutation analysis, an interspecific backcross (BC) population was established by breeding male and female *dal/+* F1 (CBA/J-*dal/dal* x CAST/EiJ) mice to *dal/dal* mice (Figure 3.13). Some non-recombinant agouti (*dal/+*) BC mice were also mated to *dal/dal* mutants to generate additional recombinant animals when the breeding performance of F1 animals declined. The genotype of BC mice at the *dal* locus was inferred by coat color (agouti vs. dark). A total of 944 BC mice were produced, among which 397 mice were *dal* and 547 were agouti. It is worth noting that 13/547 agouti BC mice were homozygous for *dal* mutant strain alleles across the candidate interval. These 13 agouti BC mice were thus genotypically *dal/dal* but phenotypically agouti, indicating incomplete penetrance of the pigmentation phenotype. Penetrance of pigmentation phenotype was estimated to be 96.8% (=397/397+13) in this cross. In a BC, equal numbers of *dal/dal* and *dal/+* progeny are expected. Since 534 *dal/+* progeny were observed but only 410 *dal/dal* (by genotype across the candidate interval), this indicates reduced viability in this cross as well, with 124 (23%) of the expected *dal/dal* pups “missing” by 14-21 days of age.

Genotyping 944 BC mice with the flanking markers D7mit114 and D7mit228,

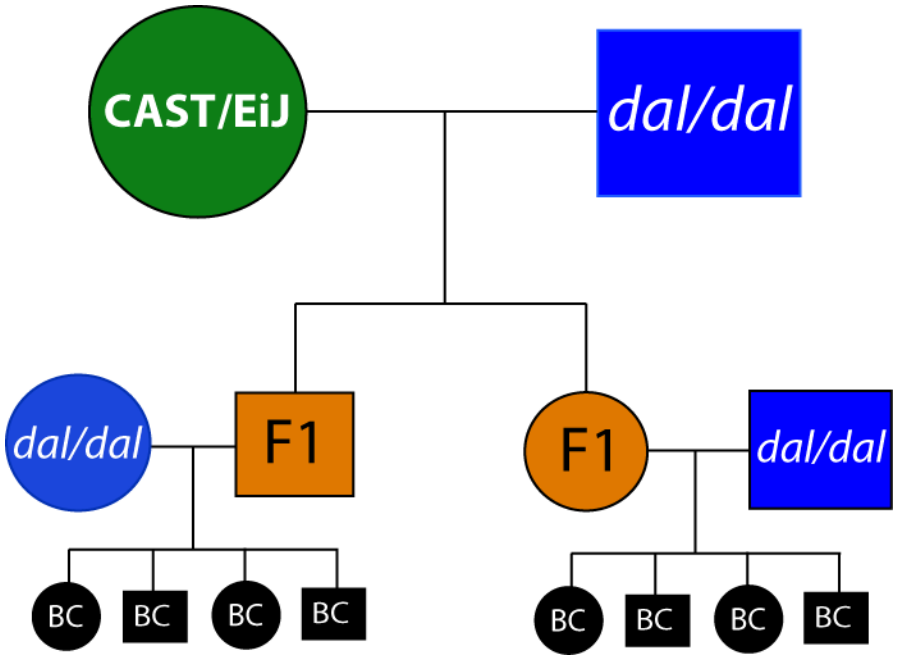

Figure 3.13. Structure of the backcross pedigree used to map the *dal* mutation. A homozygous CBA/J-*dal/dal* male was outcrossed to CAST/EiJ females to produce F_1 progeny. Male and female F_1s were backcrossed to CBA/J- or C3.CB-*dal/dal* mice to generate a backcross population of *dal/+* and *dal/dal* offspring.

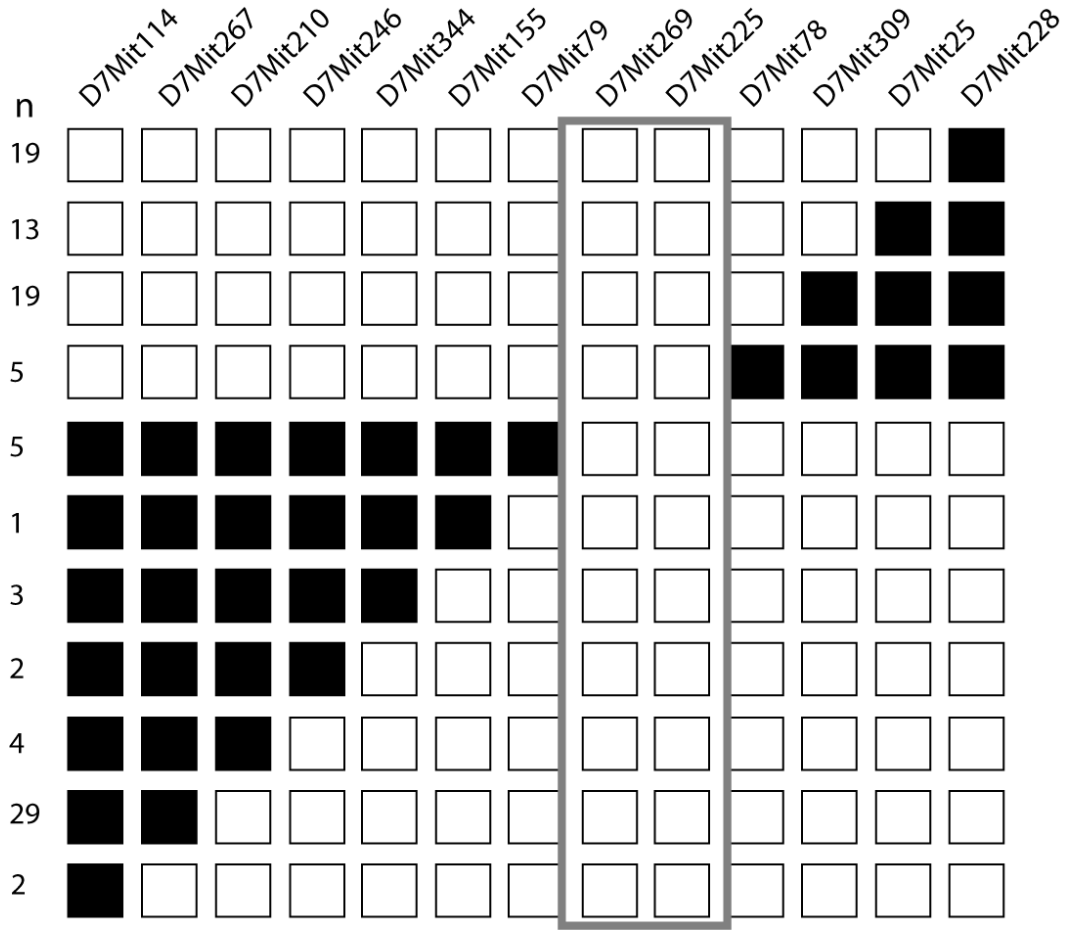

Figure 3.14. Recombination mapping of the *dal* mutation. Backcross mice with recombination breakpoints (illustrated by change from a white box to a black box along the horizontal axis) within the candidate interval refined the *dal* locus to a 1Mb interval between the markers D7Mit79 and D7Mit78. Markers are given across the top in the order in which they lie (proximal-to-distal) on chromosome 7. The number on the left (under "n") indicates how many backcross animals showed the recombination event represented to the right. The genotype of all BC animals was consistent with their phenotype (homozygous CBA when *dal*, heterozygous when agouti) at D7Mit269 and D7Mit225, indicated by the gray box.

which defined a 19.7 Mb candidate interval, identified 102 BC mice with recombination events between these markers. These recombinant animals were then genotyped for 11 polymorphic microsatellite markers that span the interval to identify the position of recombination breakpoints, to refine the candidate interval (Figure 3.14). The *dal* locus was mapped to a 1.0 Mb region flanked by D7mit79 and D7mit78 that contains 11 annotated genes (*Kctd15, Chst8, Pepd, Cebpg, Cebpa, Slc7a10, Lrp3, Gpatch1, Rhpn2, Riken clone C28005212* and *Ccdc123*) (Figure 3.15).

Primers were designed to amplify the cDNA of each gene from *dal/dal* embryonic heart RNA. The sequence of PCR products for *Pepd*, *Kctd15, Cebpg, Slc7a10, Gpatch1, Rhpn2, and Riken clone C28005212* were compared to the normal C57BL/6J sequence in the Ensembl database (http://www.ensembl.org/index.html). The only change identified was a 4 base-pair deletion in exon 14 of *Pepd* (Figure 3.16A). This difference was confirmed by amplifying and sequencing the same region from an adult *dal/dal* testis RNA sample as well as amplifying and sequencing the corresponding region from CBA/J-+/+ and CBA/J-*dal/dal* genomic DNA. To further confirm that this was the mutation, primers were designed to amplify a 109 bp product spanning this interval that would allow the wild-type and *dal* mutant products (109 and 105 bp in size, respectively) to be resolved on a 5% NuSieve gel (Figure 3.16B). Genomic DNA of CBA/J-+/+,CBA/J-*dal/*+ and CBA/J-*dal/dal* was amplified and examined. CBA/J-*dal/dal* samples were homozygous for the smaller product, wild-type (CBA/J-+/+) DNA produced a single larger band and obligate CBA/J-*dal/*+ samples had three bands (wild-type, dal and non-specific band) (Figure 3.16B).

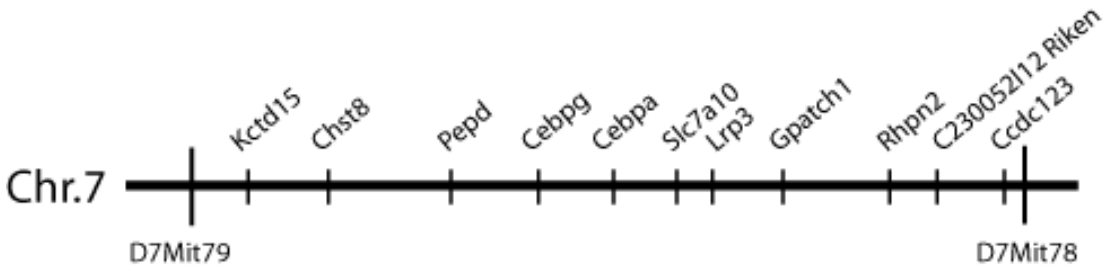

Figure 3.15. The *dal* candidate interval. Recombination mapping refined the map position of the *dal* locus to the 1 Mb interval between D7mit79 and D7mit78, which contains the 11 annotated genes illustrated.

Figure 3.16. The *dal* mutation is a 4 bp deletion in the *Pepd* gene.
(A) *Pepd* gene sequence comparison of Ensembl genome browser data, CBA/J (the strain of origin of the *dal* mutation) and *dal/dal* genomic DNA. A 4-bp deletion (ACTG) was detected in genomic DNA (and RNA from embryonic heart and adult testis) of *dal* mutant animals. (B) PCR analysis showing a 4 bp difference in the size of PCR products between CBA/J (109 bp) and *dal/dal* (105 bp) genomic DNA. Note that there are three bands for *dal*/+ samples. The lower two alleles represent wild-type and *dal* alleles, while the uppermost band is a non-specific band that was only observed in heterozygotes.

A

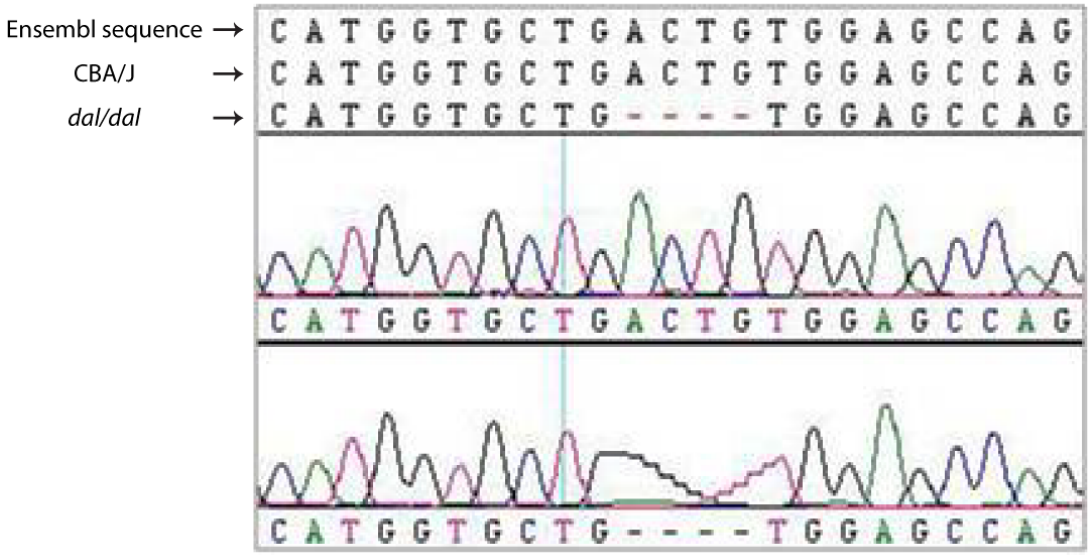
Ensembl sequence →
CBA/J →
dal/dal →
C A T G G T G C T G A C T G T G G A G C C A G
C A T G G T G C T G A C T G T G G A G C C A G
C A T G G T G C T G - - - - T G G A G C C A G
C A T G G T G C T G A C T G T G G A G C C A G
C A T G G T G C T G - - - - T G G A G C C A G

B

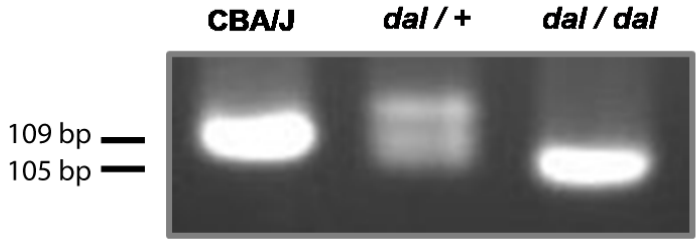
CBA/J
dal / +
dal / dal
109 bp
105 bp

Pepd encodes the enzyme prolidase, which is a metalloproteinase that metabolizes imidodipeptides containing a carboxy-terminal proline or hydroxyproline residue (such as those found on collagen degradation products and in dietary proteins) (Figure 3.17). This enzyme is a rate-limiting factor in collagen turnover and plays an primary role in recycling proline, which is required for collagen biosynthesis and cell growth (Lupi et al., 2008). Prolidase is highly conserved between vertebrate species.

Amino acid sequence alignments with ClustalW2 (http://www.ebi.ac.uk/Tools/clustalw2) demonstrated that mouse and human prolidase are 89% identical at the amino acid level, while mouse and zebrafish are 54% identical (Figure 3.18). The Ensembl database identifies only one *Pepd* ortholog in zebrafish. Bioinformatic analysis (http://elm.eu.org) predicted that mouse prolidase has a putative cortactin-interacting motif (VPRLPDSYAT). Cortactin is an actin binding protein and a target of the Src tyrosine kinase (a downstream transducer of the integrin signaling pathway). Two transcripts have been identified for mouse *Pepd*. One of the resulting PEPD protein isoforms (ENSMUSP00000075683) was predicted to contain a mitochondrial localization signal in its first 37 amino acids. Wild-type *Pepd* encodes a 493 amino acid protein, while the predicted *dal* mutant PEPD protein would have 455 amino acids. The 4 bp deletion identified in the *Pepd* gene in *dal* mice is expected to cause a frame shift after amino acid 410, with a novel 45 amino acids preceding a premature stop codon. A BLAST search for the novel portion of the *dal* mutant PEPD product (http://blast.ncbi.nlm.nih.gov/Blast) failed to detect any conserved domains.

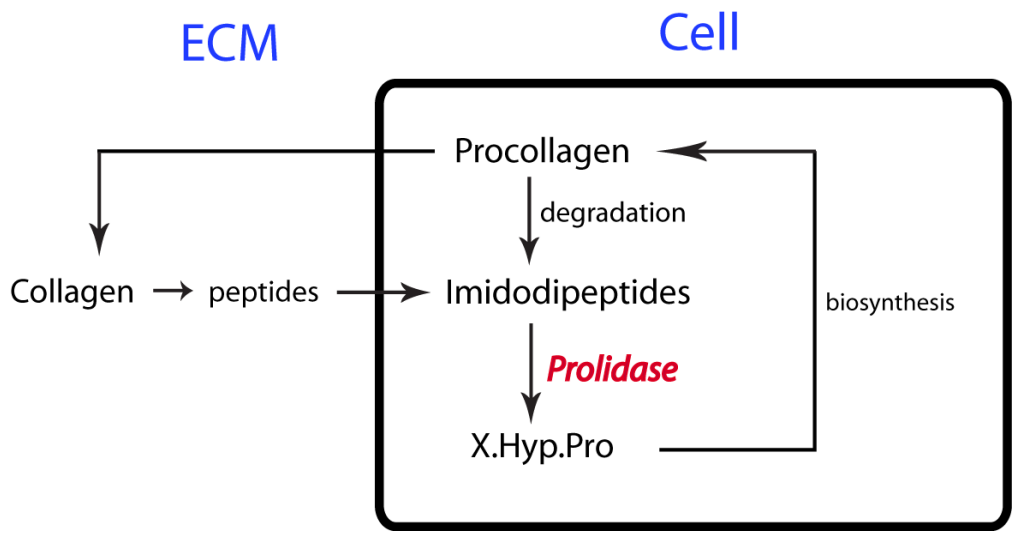

Figure 3.17. The role of prolidase in metabolism of collagen. The imidodipeptide targets of prolidase originate from intracellular degradation of procollagen, collagen, and other proline or hydroxyproline-containing peptides, including dietary proteins. Prolidase catalyzes the final step of their degradation into free amino acids in the cytoplasm. The primary biological function of prolidase in mammals is in the metabolism of collagen degradation products (imidodipeptides) and the recycling of proline from any amino acid containing proline-residues for collagen resynthesis. Imidodipeptides play important roles in collagen synthesis and degradation. In particular, imidodipeptides stimulate intracellular collagen degradation.

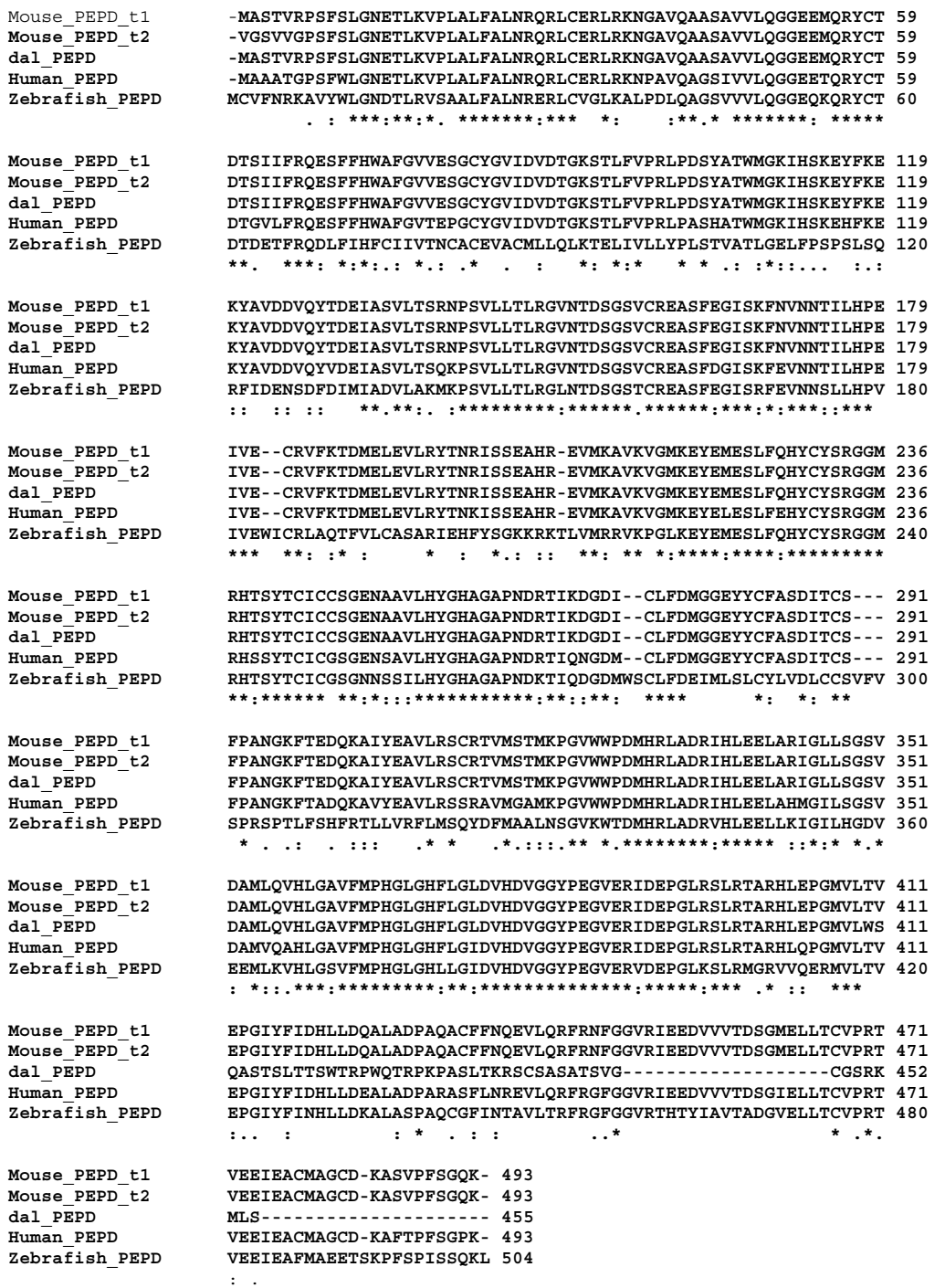

Figure 3.18. Comparison of mouse, human and zebrafish PEPD amino acid sequences. Amino acid sequence alignment showed that PEPD is highly conserved across species.

Premature stop codons often result in reduced mRNA expression level of a gene through a mechanism called nonsense-mediated decay (Chang et al., 2007; Isshiki et al., 2001). *Pepd* RNA levels were quantified to investigate the effect of the *dal* mutation on *Pepd* expression. A significant (~42%) reduction in *Pepd* expression was observed in E15.5 *dal/dal* heart RNA compared to age-matched wild-type control hearts (p=0.0066; Figure 3.19). This indicates that the *dal* mutation is most likely hypomorphic, resulting in at least a partial loss of PEPD function. Interestingly, there was greater variation in *Pepd* levels in *dal* mutant embryos: relative quantification (RQ) values of *Pepd* expression in 3 C3H control embryos were 1, 0.86 and 0.922, for a mean value of 0.9273, while those in 4 *dal/dal* embryos were 0.426, 0.72, 0.45 and 0.568, for a mean value of 0.5410.

A conserved function for PEPD in zebrafish

Cardiac phenotypes have not been reported in humans with prolidase deficiency. To test whether the phenotypes of *dal* mutant mice reflect evolutionarily conserved roles of PEPD and confirm that the *dal* mutation causes a loss of PEPD function, I used an antisense morpholino approach to determine the effect of knocking down *Pepd* expression on the phenotype of zebrafish embryos. Mouse *Pepd* is composed of 15 exons and the 4 bp (ACTG) mutation in *dal* mice is located in exon 14. Zebrafish *Pepd* consists of 21 exons and the same sequence (ACTG) that is mutated in *dal* mice is conserved (located in exon 20) in zebrafish *Pepd*. The goal of the study described in this section was to generate a loss-of-function mutation in

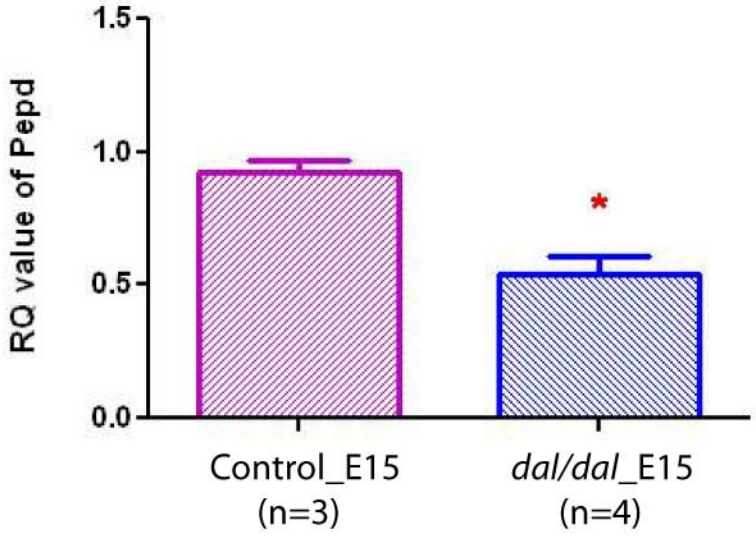

Figure 3.19. The *dal* mutation results in reduced *Pepd* RNA levels.
Relative quantitative RT-PCR was used to determine whether the *dal* mutation affects *Pepd* expression. As compared to control embryonic hearts, *Pepd* mRNA levels were reduced ~42% in *dal/dal* E15.5 hearts. The mean RQ value was significantly different between the two groups (* Student's *t*-test, p=0.0066)

zebrafish *Pepd* that would be similar in nature to the *dal* mutation (introduce a premature stop codon and a frame shift at approximately the same location). Pepd_MO was designed against the splice acceptor site of exon 20. This was predicted to cause either insertion of intron 19 into or deletion of exon 20 from the spliced mRNA product (Figure 3.20). This strategy was preferred over translational blocking because the targeted intronic insertion or exon deletion could be easily screened for by RT-PCR, while there is no antibody available against PEPD to use in monitoring the success and efficiency of translation blocking. Pepd_MO injection successfully modified splicing events, resulting in larger RT-PCR products in which intron 19 was inserted into the *Pepd* transcript (Figure 3.21). Insertion of intron 19 was confirmed by sequencing the RT-PCR products (data not shown) and is expected to introduce a frame shift and premature stop codon (Figure 3.20). Control_MO did not change *Pepd* transcription (Figure 3.21).

Zebrafish embryos injected with Pepd_MO or Control_MO on day 0 dpf were collected on 5 dpf for phenotype analyses as this is the time point at which cardiogenesis is complete in zebrafish (Sprague et al., 2001). Gross examination revealed multiple developmental abnormalities in PEPD_MO-injected embryos that were not present in embryos injected with control_MO. These abnormalities included defective pigmentation, small body and eye size, and a swollen pericardial sac (Figures 3.22 and 3.23). Defective pigmentation and small eyes were observed in 67.6% of embryos with small body size. Among those with defective pigmentation, the majority (71%) were hyper-pigmented (darker pigment patches on dorsal and ventral body surface), while pigment cells were disorganized in the rest (29%) (Table 3.6).

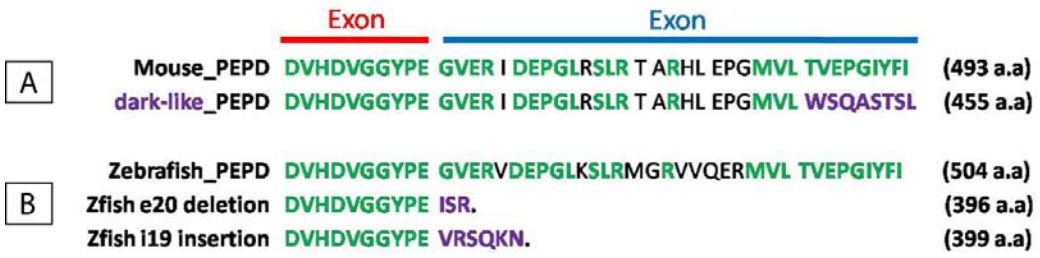

Figure 3.20. Predicted outcomes of zebrafish morpholino strategy. (A) Wild-type mouse PEPD consists of 493 amino acids, while the 4-bp deletion present in exon 14 (indicated by blue bar above sequence) of *Pepd* gene in *dal* mutant mice results in a frame shift (indicated by purple sequence) starting at 410th amino acid and a premature stop codon, which produces a truncated PEPD protein. (B) Morpholino antisense oligonucleotides targeting the acceptor donor site of exon 20 in zebrafish *Pepd* gene could result either in deletion of exon 20 or insertion of intron 19, either of which will successfully introduce a frame shift and premature stop codon into the RNA exon 20.

Figure 3.21. Antisense morpholino (MO) oligonucleotides knockdown of zebrafish *Pepd.* (A) Pepd_MO specifically targeted the splice acceptor sequence of exon 20 of the zebrafish *Pepd* gene. (B) Injection of Pepd_MO into zebrafish embryos was predicted to result in either deletion of exon 20 or insertion of intron 19. The wild-type mRNA is 502 bp. Deletion of exon 20 would shorten this to 294 bp, while insertion of intron 19 would add 241 bp to the transcript and result in a 743 bp RT-PCR product using primers indicated (F and R). (C) RT-PCR using RNA extracted from embryos injected with Control_MO or Pepd_MO was performed to confirm successful modification of *Pepd* pre-mRNA. A 502 bp RT-PCR product was observed using Control_MO RNA, while a 743 bp product was produced from Pepd_MO RNA. This indicates that Pepd_MO successfully modified the splicing of pre-mRNA sequences by inserting intron 19. The reduced intensity of RT-PCR product from Pepd_MO in comparison to that of Control_MO suggests nonsense-mediated decay of the disrupted transcript.

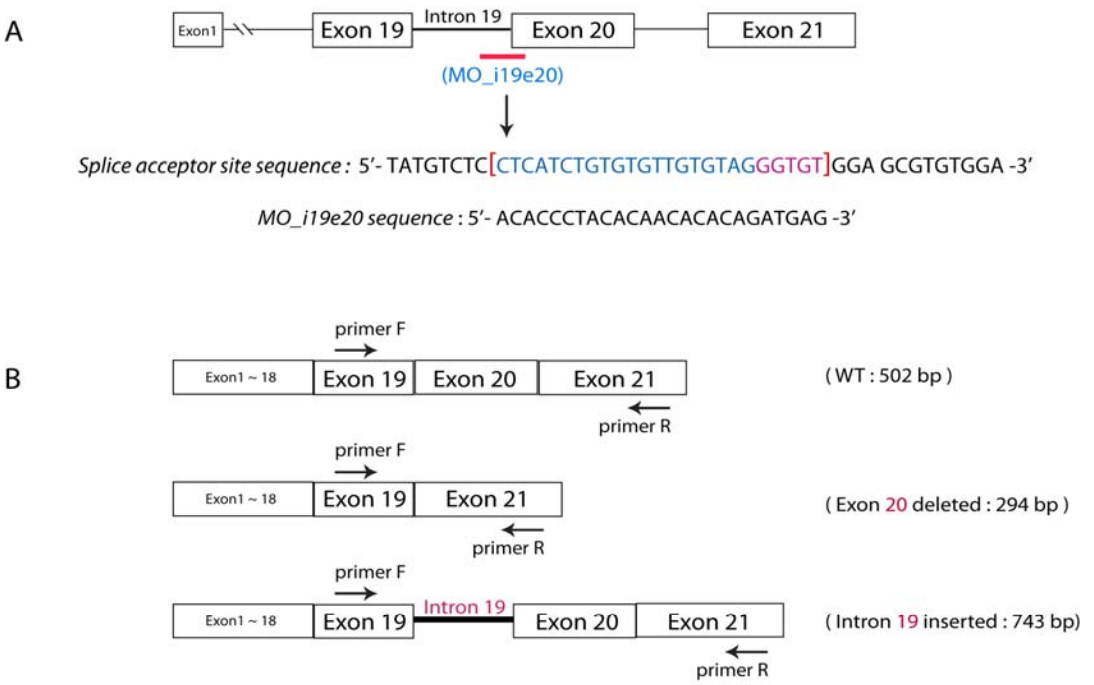
A
Exon1
Exon 19
Intron 19
Exon 20
Exon 21
(MO_i19e20)
Splice acceptor site sequence : 5'- TATGTCTC[CTCATCTGTGTGTTGTGTAGGGTGT]GGA GCGTGTGGA -3'
MO_i19e20 sequence : 5'- ACACCCTACACAACACACAGATGAG -3'
B
primer F
Exon1 ~ 18
Exon 19
Exon 20
Exon 21
primer R
(WT : 502 bp)
(Exon 20 deleted : 294 bp)
Intron 19
(Intron 19 inserted : 743 bp)
C
Control_MO
Pepd_MO
743 bp
502 bp
294 bp

Figure 3.22. Pepd_MO-treated zebrafish showed hyperpigmentation and small body size. (A,B) Stereomicroscopic views of Control_MO (A) and Pepd_MO (B) injected embryos. Normal body size and pigment distribution were observed in Control_MO injected embryos (A), while Pepd_MO –injected embryos often exhibited a small body and eye size (B). Note that pigment is clumped on the surface of chest area and at the tail of the Pepd_MO-injected embryo (B). (C,D) Magnified view of chest area in A and B. Normally distributed pigment was evenly spaced and aligned along the body surface of Control_MO injected zebrafish (C), while Pepd_MO-treated embryos had patches of hyperpigmentation and/or a disorganized distribution of pigment cells.

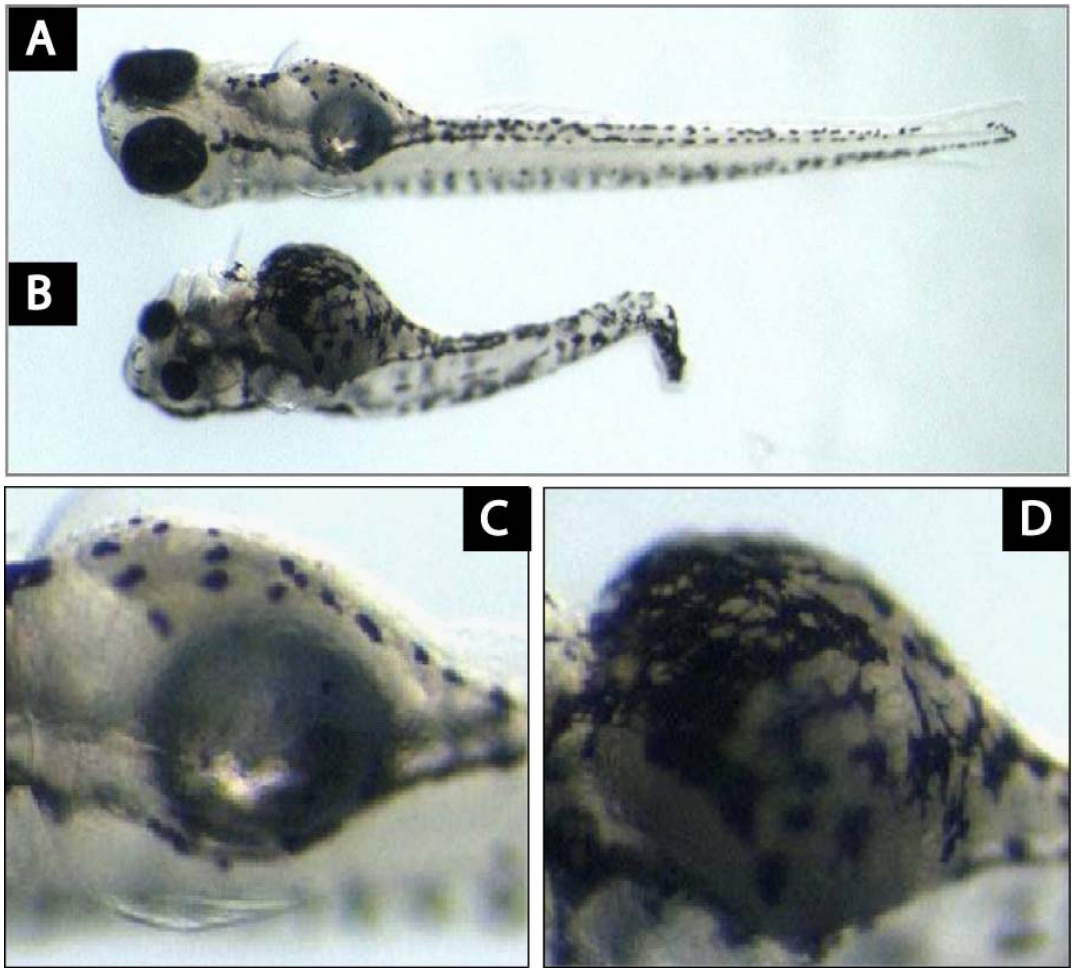
A
B
C
D

Figure 3.23. A swollen pericardial sac was observed in some Pepd_MO-injected zebrafish. Stereomicroscopic views of Control_MO (A) and Pepd_MO (B) injected embryos (B). PEPD_MO treated embryos often displayed a swollen pericardial sac (black arrow) at 5 days post fertilization (dpf).

Table 3.6. Morpholino knockdown of *Pepd* in zebrafish embryos causes multiple developmental defects

	Control_MO injected embryos (n=63)	Pepd_MO injected embryos (n=97)
	n	n (%)
Small body size	0	63 (65)
Small eye size	0	63 (65)
Unhatched eggs	0	15 (15)
Swollen pericardial sac	0	47 (48)
Defective pigmentation	0	63 (65)
-Hyperpigmentation	0	45 (46)
-Disorganized pigmentation	0	18 (19)

A swollen pericardial sac was observed in 48% of PEPD_MO-injected embryos. The dysmorphic appearance of Pepd_MO-injected embryos altered the position of landmark structures (relative to control embryos), making histological analysis difficult. Therefore, in order to examine the effect of Pepd_MO on heart development, cardiac MLC-GFP transgenic zebrafish were injected and examined by confocal microscopy. Relative to the hearts of control_MO-injected embryos, the Pepd_MO-injected fish had multiple developmental cardiac defects including homogeneously thickened ventricular free walls with less trabeculation, a smaller ventricular chamber and a narrower atrioventricular annulus (Figures 3.24 and 3.25). The diameter of the ventricular outflow tract was not different, which indicates that disrupting PEPD affects normal myocardial development but not vasculogenesis.

Linking Pepd to cardiac hypertrophy

The studies described above demonstrate that loss of PEPD function underlies the cardiac and pigmentation defects observed in *dal* mutant mice and that PEPD has an evolutionarily conserved role in heart development and pigmentation. The next logical question was: what is the function of PEPD (prolidase) in cardiomyocyte development? Since prolidase has been implicated in collagen biosynthesis and recycling, I hypothesized that the *dal* mutation disrupts the extracellular collagen content, which in turn affects integrin signaling and organization of the cytoskeleton to trigger premature hypertrophic cardiomyocyte growth. Loss of prolidase would be predicted to alter ECM collagen content. Picrosirius red staining on cardiac sections of 2 month-old controls and *dal* mutants showed that collagen in wild-type hearts

Figure 3.24. Thickened ventricular walls were observed in cardiac MLC-GFP transgenic zebrafish injected with Pepd_MO. Confocal sections of Control_MO-injected (A-D) and Pepd_MO-injected (E-H) zebrafish embryonic hearts. Ventricular walls of Pepd_MO-injected embryos (E-H) were consistently thicker, with reduced ventricular trabeculation, than those of control embryos (A-D) throughout multiple serial images.

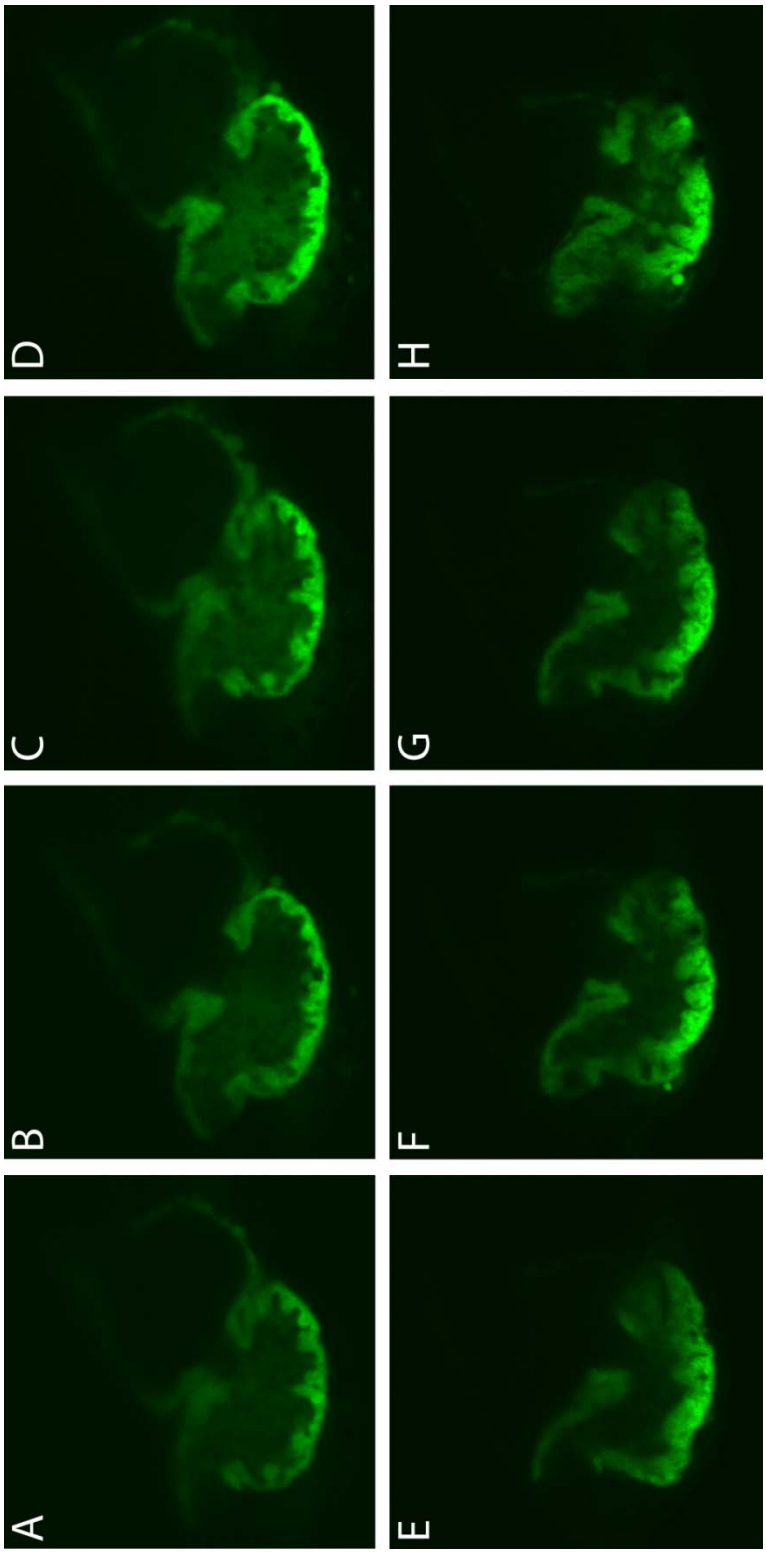
A
B
C
D
E
F
G
H

Figure 3.25. Developmental cardiac phenotypes observed in *dal* mutant mice were recapitulated by Pepd_MO knockdown in zebrafish embryos. The following features of cardiac anatomy were measured (as indicated on panel E): ventricular wall thickness (A), ventricular chamber dimension (B), AV annulus diameter (C), and ventricular outflow tract diameter (D). The ventricular myocardium (A) of Pepd_MO injected embryos was homogeneously thicker than that of Control_MO injected zebrafish ($p<0.0001$). The diameters of the internal ventricular chamber (B) and AV annulus (C) of Pepd_MO-injected zebrafish were much smaller than those of Control_MO injected zebrafish hearts ($p<0.0001$ and $p=0.0003$, respectively). The diameter of the ventricular outflow tract (D) was equivalent between the two groups ($p=0.9618$).

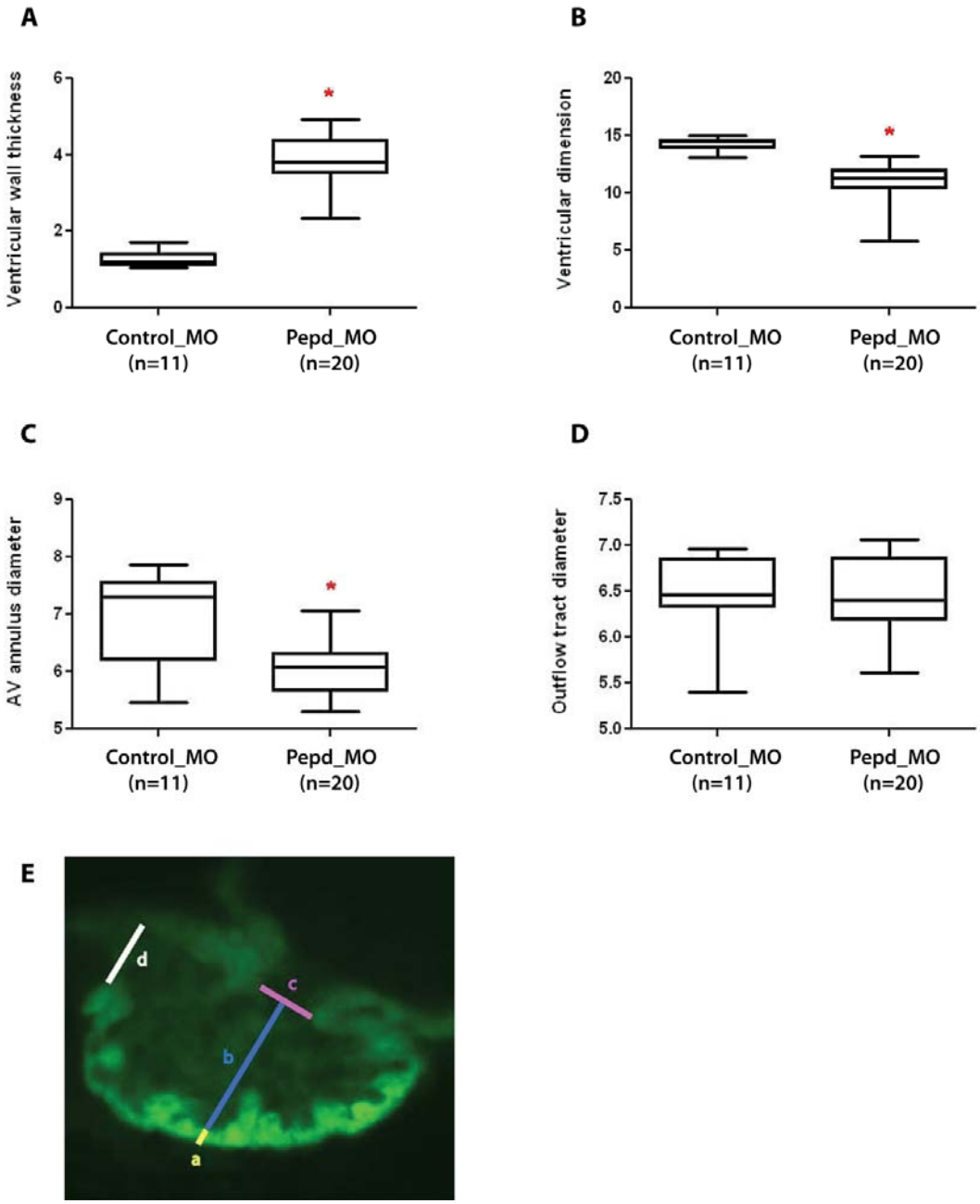
A
Ventricular wall thickness
6
4
2
0
*
Control_MO
(n=11)
Pepd_MO
(n=20)
B
Ventricular dimension
20
15
10
5
0
*
Control_MO
(n=11)
Pepd_MO
(n=20)
C
AV annulus diameter
9
8
7
6
5
*
Control_MO
(n=11)
Pepd_MO
(n=20)
D
Outflow tract diameter
7.5
7.0
6.5
6.0
5.5
5.0
Control_MO
(n=11)
Pepd_MO
(n=20)
E
d
c
b
a

was regularly polymerized and well distributed, whereas there was a reduction in the total amount and extent of polymerization of collagen in *dal/dal* heart (Figure 3.26). The Picrosirius red staining method was not able to visualize collagen in embryonic heart sections.

Collagen is the major ligand of integrin receptors (specifically α1β1, α2β1, α10β1, α11β1) which transmit extracellular information to subcellular cytoskeletal structures through signal transducers such as FAK (focal adhesion kinase), Src (cytoplasmic tyrosine kinase) and paxillin (adaptor protein of integrin-actin link complexes). Western analysis was performed to determine whether the level of integrin transducer proteins was altered in *dal* mutant embryonic hearts. Phospho-FAK, phospho-Src, total Src and paxillin were all significantly reduced ($p<0.05$) in E15.5 *dal/dal* hearts relative to controls (Figure 3.27).

Altered integrin signaling would be expected to affect the structure and/or organization of actin filament structures to which integrin signaling is transmitted. Wild-type and *dal* mutant cardiomyocytes were stained with fluorescently-conjugated phalloidin, which specifically binds F-actin. Confocal microscopic examination of wild-type cardiomyocytes showed a linear and continuous alignment of actin filaments (Figure 3.28 A and C). In contrast, *dal/dal* embryonic cardiomyocytes had an unusual pattern of F-actin distribution and organization, with an interrupted alignment of the sarcomeric actin banding pattern as well as a disorganized arrangement of actin filaments (Figure 3.28 B and D). Western blot analysis showed a significant reduction of filamentous actin (F-Actin) in E15.5 *dal* hearts relative to controls (Figure 3.29).

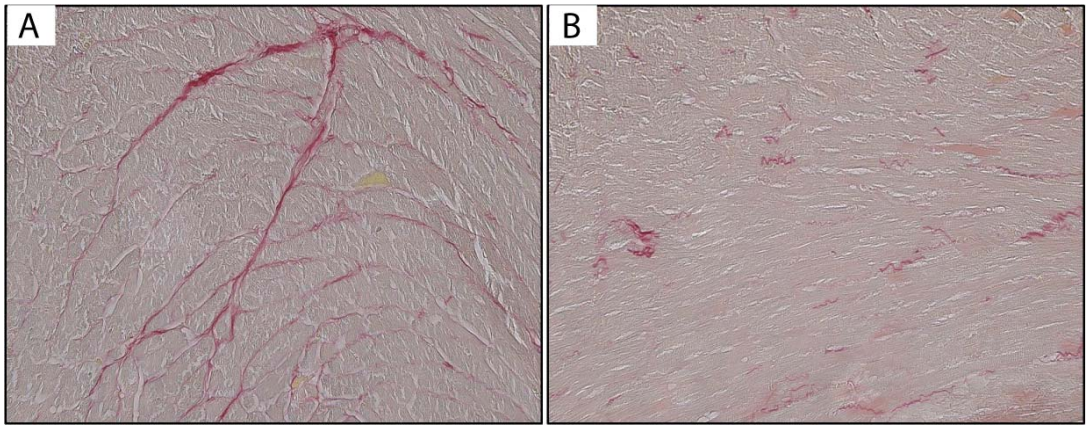

Figure 3.26. Extracellular collagen is reduced in *dal* mutant hearts. The content and distribution of extracellular collagen was examined by Picrosirius red staining of paraffin-embedded cardiac sections of 2 month-old mice. (A) Red-stained collagen was normally polymerized and distributed throughout the myocardium of control mice. (B) In *dal/dal* hearts, there was a strong reduction in the amount of collagen and it did not form long polymers.

Figure 3.27. Integrin signaling was altered in *dal/dal* embryonic hearts. (A) The protein expression level of total Src, phospho-Src, phospho-FAK and Paxillin was reduced in hearts of E15.5 *dal* embryos compared to controls. Total FAK was not changed. (B) The signal intensity of each protein was normalized against GAPDH. The mean relative intensity of total Src, phospho-Src, phospho-FAK and Paxillin was significantly lower in *dal* mutant hearts than in control hearts (* Student's *t*-test p-value: 0.001, 0.0026, 0.0088 and 0.0002, respectively). No significant change was detected in the level of total FAK protein between controls and *dal* embryonic hearts (Student's *t*-test p=0.4).

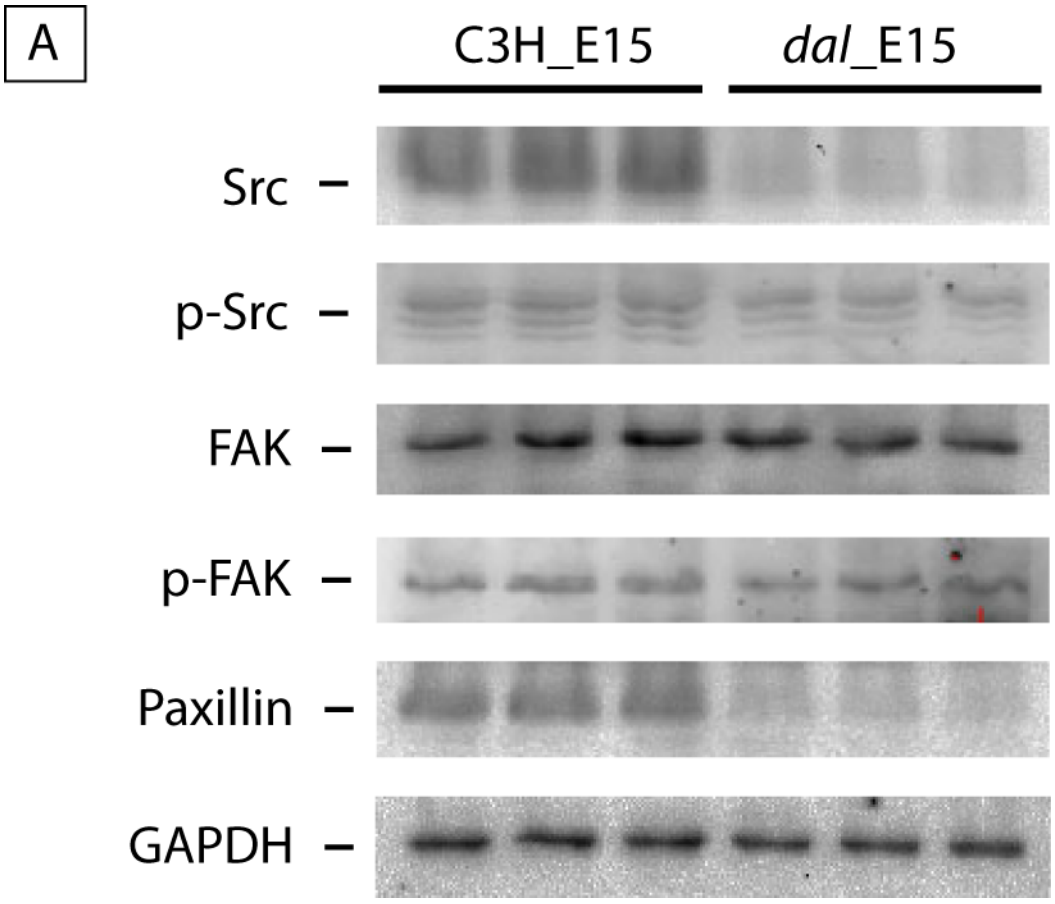
A
C3H_E15
dal_E15
Src
p-Src
FAK
p-FAK
Paxillin
GAPDH

B

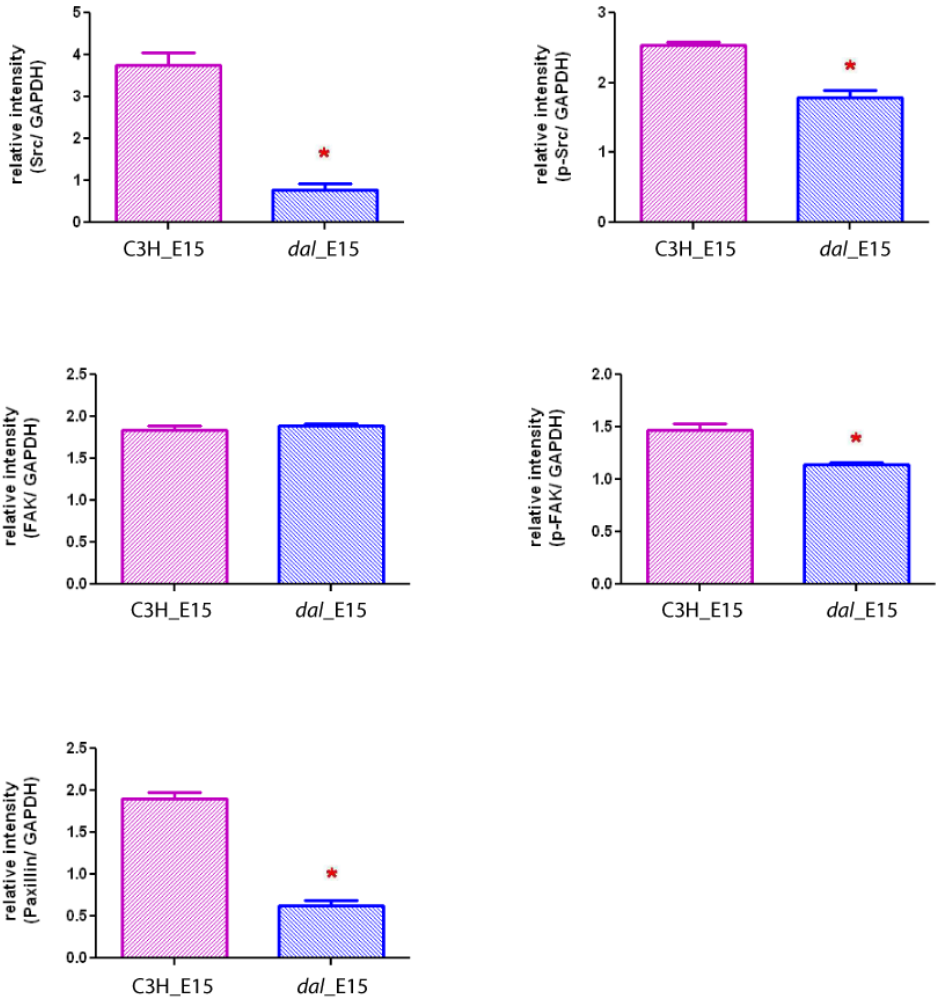
relative intensity (Src/ GAPDH)
5
4
3
2
1
0
*
C3H_E15
dal_E15
relative intensity (p-Src/ GAPDH)
3
2
1
0
*
C3H_E15
dal_E15
relative intensity (FAK/ GAPDH)
2.5
2.0
1.5
1.0
0.5
0.0
C3H_E15
dal_E15
relative intensity (p-FAK/ GAPDH)
2.0
1.5
1.0
0.5
0.0
*
C3H_E15
dal_E15
relative intensity (Paxillin/ GAPDH)
2.5
2.0
1.5
1.0
0.5
0.0
*
C3H_E15
dal_E15

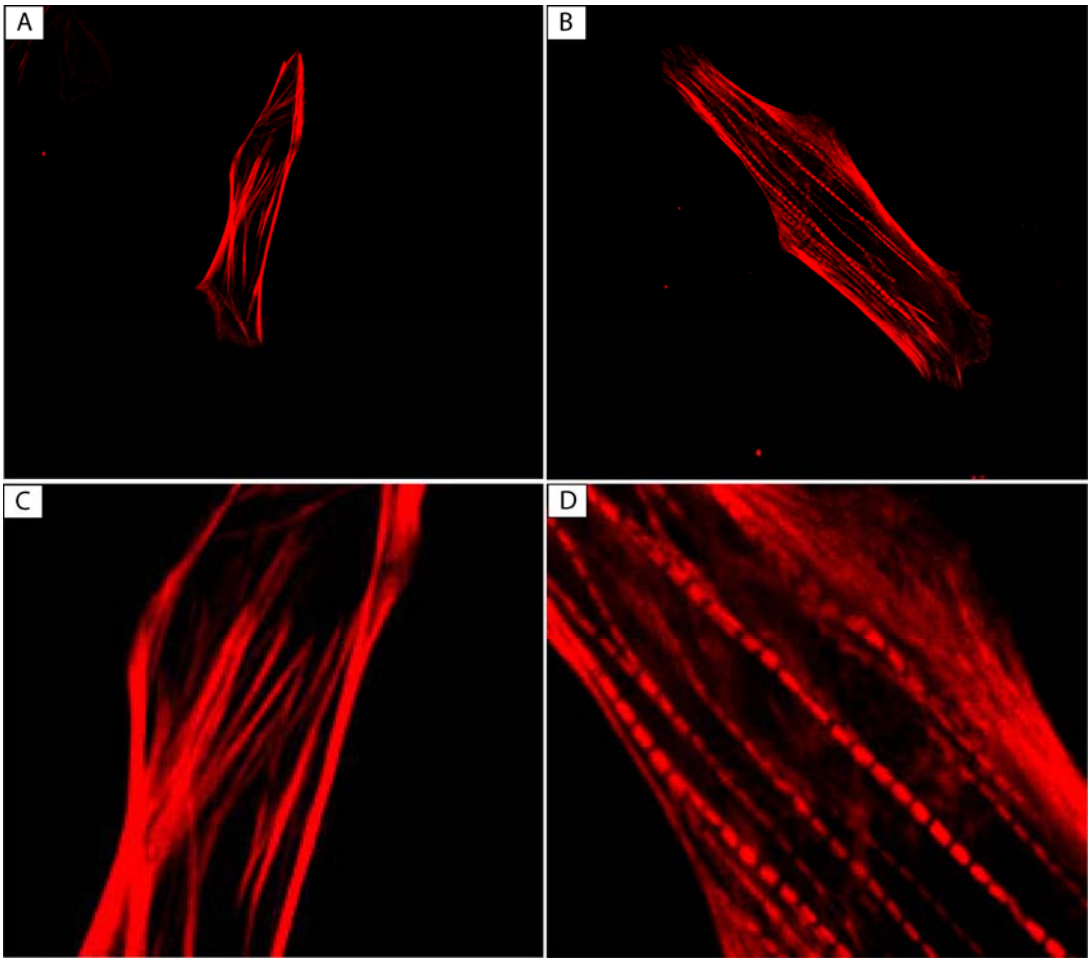

Figure 3.28. Actin cytoskeleton abnormalities in *dal* mutant embryonic cardiomyocytes. The actin cytoskeleton, which is the major sarcomeric structure of cardiomyocytes, was stained with fluorescently labeled Phalloidin and imaged by confocal microscopy. (A,C) A representative wild-type cardiomyocyte, showing linear stretches of normal actin filaments. (B,D) A representative *dal/dal* mutant cardiomyocyte, displaying an abnormal, interrupted banding pattern of actin filaments.

A.

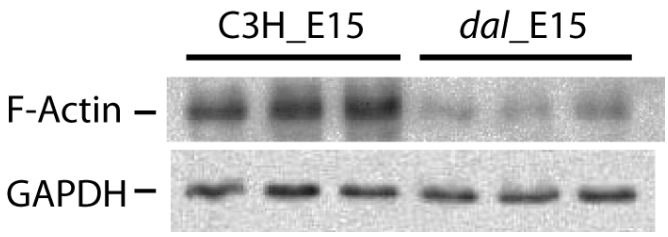

B.

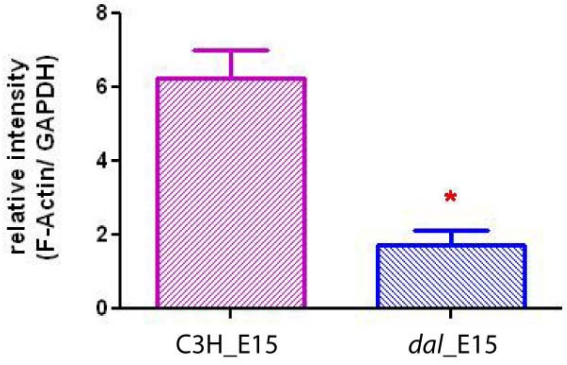

Figure 3.29. Actin was reduced in *dal/dal* embryonic hearts. (A) Western blot analysis revealed reduced levels of filamentous actin (F-Actin) in the hearts of E15.5 *dal* embryos compared to controls. (B) The signal intensity of F-Actin signal was quantified and normalized against GAPDH. The mean relative intensity of F-Actin signal in *dal* mutant samples was significantly lower than that of controls (* Student's *t*-test p=0.0092).

Discussion

Hemodynamic overload chronically imposed to the heart is known as a major trigger of adult-onset cardiac hypertrophy in clinical cardiac diseases. It was quite surprising to discover cardiac hypertrophic changes in embryonic hearts, particularly because it is known that embryonic cardiac growth is mainly accomplished by hyperplasia, with hypertrophic changes in cardiomyocytes not normally starting until postnatal day 3 in mice (Oparil et al., 1984). The *dal* mutant mouse therefore represents a novel model for decoding the genetic and molecular mechanisms of myocardial hypertrophic changes, as well as the normal transition from proliferative to hypertrophic cardiomyocyte growth.

Cardiac hypertrophy can be abnormally induced by numerous stimuli such as ECM proteins, growth factors, neurohormones, mechanical stress and cytokines. Cardiac ECM consists of structural proteins (collagen, elastin), adhesive proteins (fibronectin, laminin) and proteoglycans (Corda et al., 2000). Proliferating cardiac fibroblasts produce type I and III collagen as well as fibronectin. Cardiomyocytes synthesize type IV collagen and laminin (Klewer et al., 1998). Collagen as a ligand is sensed by integrin receptors to influence a downstream signaling pathway that connects the ECM to the sarcomeric contractile apparatus (Kempiak et al., 2005). There are 18 integrin α-subunits and 8 β-subunits. Cardiomyocytes express integrins α-1,3,5,6,7,9,10 and β-1,3,5, to (theoretically) form 18 different heterodimers (Brancaccio et al., 2006; Lal et al., 2007). Different heterodimers bind to different types of collagen protein and are involved in distinct physiological functions.

My data suggest that the mechanism underlying developmental cardiac hypertrophy in *dal* mutant embryos involves the ECM-integrin-sarcomere axis. Since the actin cytoskeleton is a dynamic structure that changes its shape and organization in response to upstream signaling transduction (Fuller et al., 1998), I propose a model in which alteration of the extracellular collagen matrix due to loss-of-function of PEPD in *dal* mutant embryonic hearts signals through integrin receptors and transducers to modify the subcellular cytoskeletal structure, leading to cardiomyocyte hypertrophy. This observation is consistent with the previous finding that abnormal cytoskeletal sarcomeric remodeling is the subcellular phenotype that underlies acquired hypertrophic cardiomyopathy (Kim et al., 2003). Ieda *et al.* recently reported that integrin signaling and ECM proteins are involved in embryonic myocardial development (Ieda et al., 2009). ECM proteins such as collagen and fibronectin secreted from cardiac fibroblasts collaboratively enhanced the proliferation of embryonic cardiomyocytes via β1 integrin signaling. Interestingly, the study showed that *integrin β1* and *fibronectin* mRNA levels peak at mid-gestation and drastically subside over the remaining gestation period (Ieda et al., 2009). A question remains as to whether the reduced expression of these genes in late gestation is a prerequisite to providing an environment in which myocardial growth switches from hyperplasia to hypertrophy after birth.

Does prolidase control extracellular matrix production from cardiac fibroblasts, regulating cardiomyocyte growth during the transition phase? Based on the finding that cardiomyocyte hypertrophy is manifested in *dal* mutant embryonic hearts, where the level of *Pepd* mRNA, integrin transducers and extracellular

collagen proteins is reduced, I hypothesize that prolidase may be a critical determinant of normal transition process that triggers hypertrophic changes. Further studies are needed to test whether integrin signaling and/or prolidase plays a crucial role in the normal postnatal hypertrophic transition process in an integrin-dependent manner. This could be accomplished by determining whether there is a significant reduction in the expression level of integrin and/or *Pepd* transducers in normal hearts over the period during which this transition takes place (postnatal day 1-5 in mice).

Lipid microdomains play important roles in localizing Src and FAK for integrin-dependent interaction with the ECM. Two major lipid microdomains include lipid rafts and caveolae (Galbiati et al., 2001). A study showed that Src is largely localized to cholesterol-enriched lipid raft domains (Liang et al., 2001). In *dal* mutant embryonic hearts, the extent of the change in the level of Src was more remarkable than that of FAK, while caveolin-1 levels were equivalent to controls (data not shown). The level of the lipid raft marker, flotillin, is reduced in adult *dal/dal* testis (Cota et al., 2008), but has not been examined in *dal/dal* embryonic hearts. Further studies to determine whether lipid rafts are disrupted in *dal* mutant embryonic hearts would provide useful information to test the hypothesis that Src kinase levels are significantly reduced due to loss of lipid rafts in addition to reduced ligand binding of extracellular collagen to integrin receptors.

There was incomplete penetrance of cardiac phenotypes in *dal* mutant animals, with ~67.6% of mutant embryonic hearts being hypertrophic. Although it cannot be proven without histological analysis, it is tempting to

speculate that the hearts of the *dal* mutant embryos with higher *Pepd* expression might have had a normal cardiac structure while those with lower values might have had thickened ventricles and higher *Anp* expression. In other words, variation in *Pepd* expression among *dal* embryos could explain the incomplete penetrance of cardiac phenotypes. When *Pepd* expression falls below the threshold required for a normal cardiac development, cardiogenesis would be disrupted and result in abnormal production of extracellular collagen and altered integrin signaling in *dal* embryos. Further studies are warranted to correlate the expression of *Pepd* and *Anp* with ventricular thickness.

Some *dal* embryos showed cardiac defects in addition to cardiac hypertrophy, including ASDs, VSDs and enlarged endocardial cushions. Many genetic mutations have been shown to cause septal defects in animal models and humans, and they are known to compromise normal growth and fusion of septum primum and septum secondum. An epithelial-to-mesenchymal transition (EMT) process takes place in the endocardial cushion, where endocardial cells are transformed into mesenchymal cells. These cells eventually give rise to cardiac valves and portions of AV septae. The ECM plays an important role in multiple cellular processes such as cell-to-cell communication, adhesion, migration and growth. Interaction between mesenchymal cells and ECM is known to regulate mesenchymal cell migration and expansion into endocardial cushions. Reduced collagen due to loss of prolidase in *dal* mutant embryonic hearts would be expected to attenuate the expansion of endocardial cushions, however, which is opposite to what was observed in some *dal* embryonic hearts. Further studies are needed to determine whether enlarged endocardial cushions in *dal* mutant embryonic

hearts result from increased number of cellular proliferation, larger cell size or cell migration defects.

In humans, prolidase deficiency (PD) caused by mutations in *PEPD* has been reported as a rare autosomal recessive disorder associated with skin ulceration, developmental delay, imidodipeptiduria and skeletal deformities (Endo and Matsuda, 1991; Falik-Zaccai et al., 2009). Interestingly, no cardiac phenotypes have been reported in human PD patients, while skin ulcerations and skeletal deformities have not been observed in *dal* mice. This might be due to differences in the types or location of mutations in human *PEPD* which could have distinct effects on collagen production and metabolism, or may reflect genetic background effects and/or species differences. Cardiac defects and dark fur in *dal* mutants were incompletely penetrant, and cardiac defects often resulted in embryonic lethality in *dal* mutant embryos. By analogy, cardiac defects might not be present in all humans with PD and when they are, they may be lethal during fetal development. Loss-of-function of *Pepd* affected myocardial development, pigmentation and body size in zebrafish, indicating a conserved role for prolidase between zebrafish and mouse.

Differences exist in human and mouse pigmentary systems. Pigment-type switching process, which results in transient expression of agouti, does not take place in human hairs. This might explain the absence of coat color phenotypes associated with human PD. Interestingly, premature aging of the skin due to photoaging not only induces the synthesis of collagenase, but also upregulates α-MSH, which signals through MC1R to promote eumelanin production (Kiss et al., 1995). α-MSH is known to attenuate the synthesis of

collagen production in human dermal fibroblasts (Bohm et al., 2004) and a microarray study revealed that melanocytes treated with agouti signal protein (ASP) upregulate genes involved in extracellular matrix-integrin receptor interactions and cell adhesion and migration (Le Pape et al., 2009). This suggests that there may be a close relationship between the expression level of ASP, extracellular matrix and integrin signaling. Since *dal* mutation acts downstream of *agouti* transcripts and upstream of *Mc1r*, it is possible that the effect of the *dal* mutation is to suppress ASP binding to the MC1R. Further studies are needed to test whether extracellular collagen is needed for ASP to reach melanocytes or promotes ASP binding to MC1R.

Collagen proteins, which maintain tissue homeostasis and integrity, account for about 70~80 percentage of the skin (Stadelmann et al., 1998). The etiology of skin ulceration in human PD remains defined. Although collagen deprivation may be a contributing factor, a lack of collagen production does not necessarily result in skin ulceration. It is rather a combination of metabolic disorders, abnormal skin integrity, immune-mediated inflammatory response and susceptibility to infectious organisms. The pathogen-free environment of a laboratory animal facility as well as the fur on their skin may protect *dal* mutant mice from agents that can cause skin damage. It would be interesting to test whether loss of prolidase delays the wound healing time in *dal* mutant mice. This information would provide useful insights into understanding a different mechanism of phenotypic expression between humans and mice.

Summary

This chapter identifies the mouse *dark-like* (*dal*) pigmentation mutant as a novel model for studying the genetic and molecular basis of developmental cardiomyocyte hypertrophy and for understanding the normal transition process of cardiomyocyte growth. I identified a mutation in *Pepd* that underlies these defects in *dal* mutant mice and used a reverse genetic approach in zebrafish to confirm that loss-of-function of *Pepd* has conserved effects on cardiogenesis, pigmentation and growth. *Pepd* encodes an enzyme called prolidase, which is integral to normal collagen biosynthesis and recycling. This work provides novel insights into the role of *Pepd* in developmental cardiac hypertrophy via remodeling of extracellular collagen, integrin signaling and actin organization in *dal* mutant embryonic hearts.

CHAPTER 4

SUMMARY AND CONCLUSIONS

Cardiovascular disease is the leading cause of death in the United States (Lloyd-Jones *et al.*, 2009). In particular, cardiac hypertrophy and arrhythmias are major risk factors for sudden cardiac death (Wachtell *et al.*, 2008). These diseases are genetically and phenotypically heterogeneous, which complicates studies to elucidate the genetic and molecular causes. Animal models therefore provide valuable opportunities to study the mechanisms underlying human cardiac disorders and offer critical insights that will be useful for developing both diagnostic tests and therapeutic treatments for both human and animal heart diseases. In the work presented here, a comprehensive investigation was performed to unravel the genetic and molecular mechanisms behind arrhythmias and cardiac hypertrophy in dogs and mice.

Inherited ventricular arrhythmias in German shepherd dogs

Young German shepherd dogs (GSDs) are predisposed to inherited ventricular arrhythmias and sudden cardiac death. Peak affectedness occurs between 20 and 28 weeks of age after birth. The cardiac autonomic system does not develop or mature properly as there is reduced sympathetic innervation of the left anterior apical region (Dae et al., 1997). Such sympathetic denervation has been proposed to be one of the predispositions for familial ventricular arrhythmias in humans (Vincent, 1998). Cardiac

electrophysiology in GSDs showed evidence of abnormal calcium transients such as EADs and DADs (Steinberg et al., 2002), which are also known to be a prerequisite substrate for developing fatal ventricular arrhythmias (Michael et al., 2009). Phenotypic and etiologic similarity between GSDs and human patients with familial ventricular arrhythmias suggests that identifying the genetic and molecular mechanisms underlying arrhythmogenicity in GSDs will benefit human health. It will also allow for the development of genetic tests and therapies to benefit the GSD population.

A genome-wide linkage analysis was performed to detect genomic region(s) linked to arrhythmias in GSDs. However, both parametric and non-parametric linkage analyses failed to discover any regions of strong linkage. As discussed in Chapter 2, a genome-wide association study of severely affected and unaffected dogs using SNP chips may be more successful in identifying a haplotype block that segregates with ventricular arrhythmias in GSDs, although pinpointing the specific genes/mutations may still be difficult since related affected breeds are not obviously available. My work identifying a significant inverse correlation between *ATP2A2*/SERCA2 levels and affectedness in GSDs may assist in the identification of candidate genes within a haplotype block, however, as this implicates at least one gene that acts upstream of *ATP2A2* transcription. The genes that underlie susceptibility to ventricular arrhythmias in GSDS will be candidates for modifiers of human familial ventricular arrhythmias, and their identity will help us understand the molecular mechanism(s) that underlie this disease.

Developmental cardiac hypertrophy in dark-like mice

Pleiotropic roles of genes that regulate pigment-switching pathway have demonstrated that coat color phenotype can be a visible marker of perturbed homeostasis in systemic organ development and maturation (Cota et al., 2006; Gunn et al., 2001; He et al., 2003). The recessive *dark-like* (*dal*) mutation causes a darkened coat color, gonad abnormalities, and small body size, (Cota et al., 2008; Harris, 2003). Here, I report that the *dal* mutation also causes heart defects, including markedly thickened cardiac ventricular walls and septa and atrial and ventricular septal defects. These defects would account for the reduced viability of *dal* embryos that was previously observed, and led me to hypothesize that the gene mutated in *dal* mice plays a pivotal role in myocardial development. Analysis of the proliferation status and size of *dal* mutant cardiomyocytes confirmed hypertrophy as the cause of the thickened myocardium. In fact, cardiomyocytes from *dal* mutant embryonic hearts were almost twice as large as those from control embryos. In addition, histological analysis of 3 month old *dal* hearts showed myocardial disarray, which is a typical sign of cardiac hypertrophy in humans and cats (Ly et al., 2005). Embryonic cardiac hypertrophy was shown to have physiological and functional consequences as that the hearts of *dal/dal* embryos displayed abnormal calcium cycling with early afterdepolarization (EAD) and irregular intervals in calcium cycling.

While many genetic mutations implicated in septal defects have been identified (Srivastava and Olson, 2000), little is known about the genes that can cause developmental cardiac hypertrophy or that regulate the normal

transition from proliferative to hypertrophic cardiomyocyte growth. To the best of my knowledge, *dal* mutants represent the first mouse model with the unique phenotype of premature (developmental) cardiac hypertrophy. Identification of the *dal* gene as *Pepd* (*peptidase D*), which encodes the enzyme prolidase, implicates collagen metabolism and integrin signaling in developmental cardiomyocyte hypertrophy. Reduced *Pepd* levels in *dal* mutant mice suggested that the *dal* mutation is hypomorphic (partial loss-of-function), and morpholino knock-down of *Pepd* in zebrafish confirmed that reduced levels of normal *Pepd* during embryonic development results in pigmentation and cardiac defects and small body size. I demonstrated that collagen was reduced in the hearts of *dal* mutant mice, as would be expected if prolidase activity was compromised. As predicted (since collagen signals through integrin receptors), expression of the major integrin transducers (FAK, Paxillin, Src) was reduced in the hearts of *dal* mutant embryos. This was associated with a disrupted pattern of collagen polymerization in *dal* mutant cardiomyocytes.

Based on my results, I propose the following model for cardiomyocyte growth (Figure 4.1): during normal cardiac development, prolidase plays a critical role in the proper metabolism of collagen, which in turn functions as a signaling molecule that regulates normal myocardial growth and intracellular cytoskeletal organization through integrin pathways. Collagen and integrin expression is maintained during active cardiogenesis, gradually declines over the late gestation, and shortly after birth undergoes a drastic reduction. That causes hyperplastic growth to be terminated and hypertrophic growth to be activated. In *dal* mutant embryos, however, prolidase levels are always

Figure 4.1. Proposed model for the development of cardiac hypertrophy in *dal* mutant hearts. (A) Integrin α/β heterodimeric receptors sense and bind extracellular matrix proteins and transmit the extracellular information to the subcellular cytoskeleton via integrin transducers. (B) Loss of prolidase function in *dal* mutant mice alters the content and distribution of extracellular collagen. Integrin receptors sense the modified ligand binding of collagen, which is transmitted through integrin transducers (FAK, Src, Paxillin) to sarcomeres. The cytoskeletal sarcomere accordingly changes its shape and organization in response to the upstream signaling stimuli. Remodeling processes in the ECM-Integrin-Sarcomere axis thus result in cardiomyocyte hypertrophy during embryonic development in *dal* mutant mice.

A.

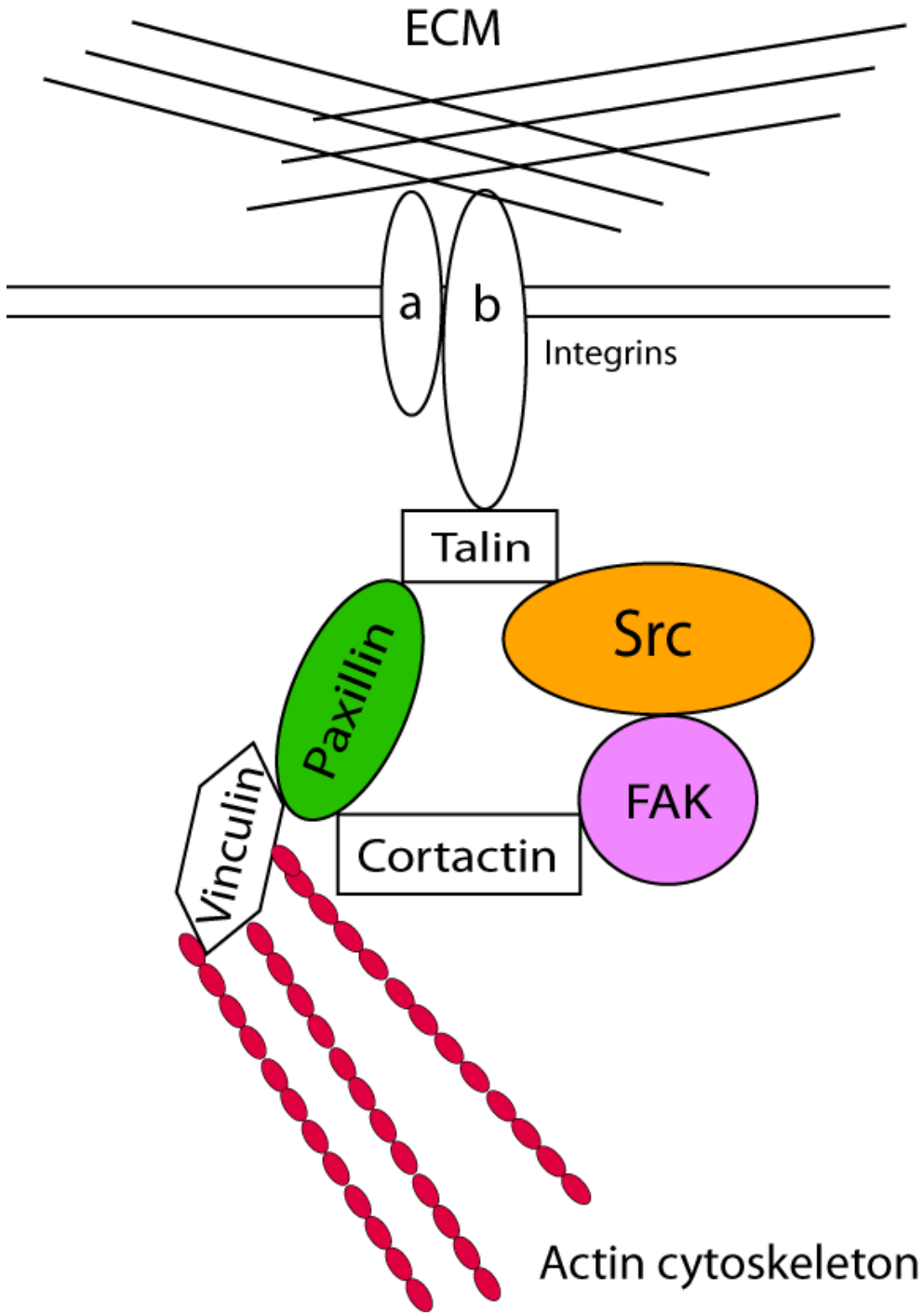
ECM
a
b
Integrins
Talin
Src
Paxillin
FAK
Vinculin
Cortactin
Actin cytoskeleton

B.

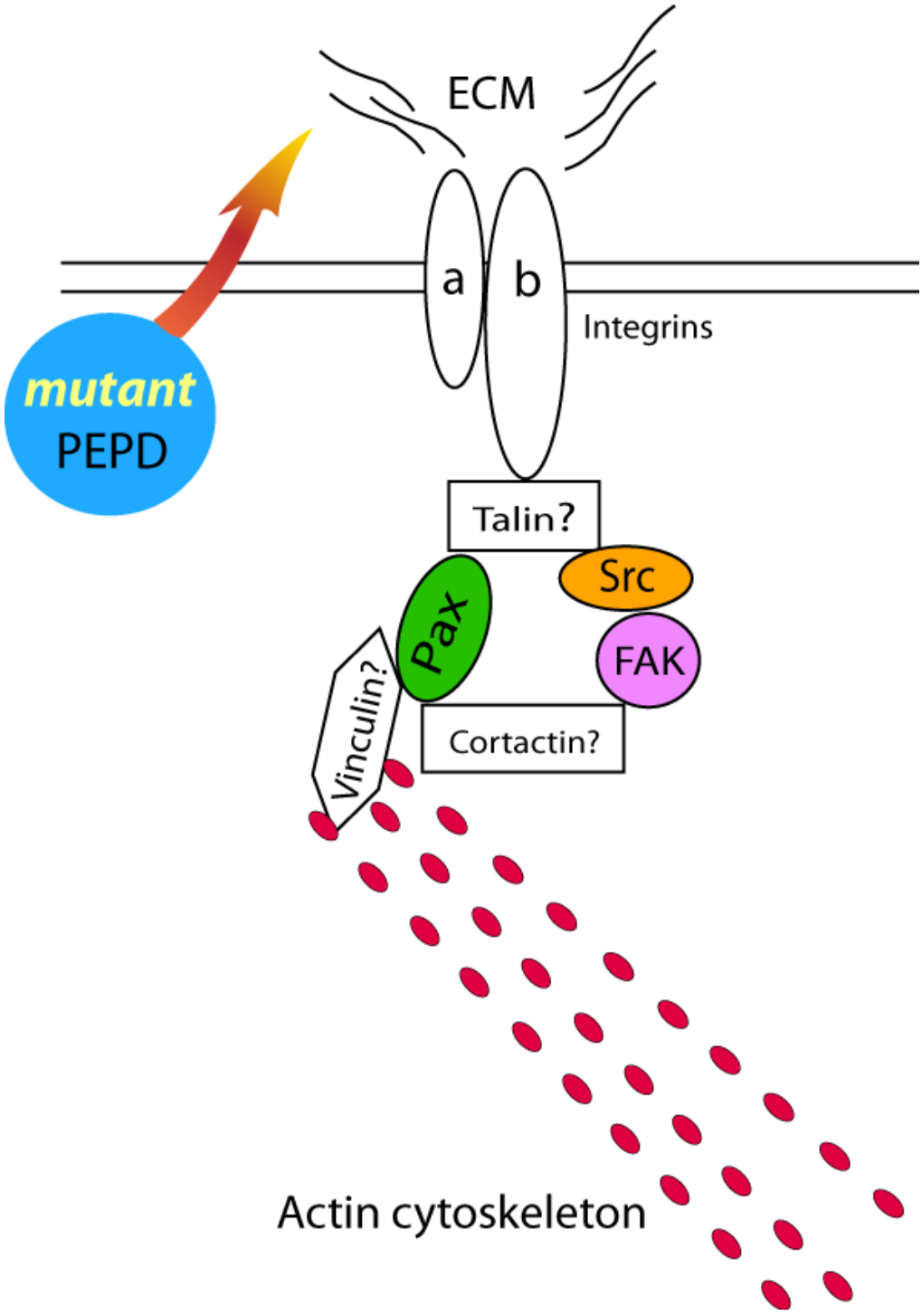
ECM
a
b
Integrins
mutant
PEPD
Talin?
Src
Pax
FAK
Vinculin?
Cortactin?
Actin cytoskeleton

reduced. This reduced prolidase activity would result in a series of alterations in a developing heart. In *dal* embryonic heats, reduced extracellular collagen levels would act as a signal that would prematurely change integrin signaling. Integrin receptors, so called mechanosensors on the cell surface, would recognize the changes in ECM composition and signaling to downstream transducers would be altered. The cytoskeletal sarcomere would change its shape and organization accordingly, causing cardiomyocytes to become larger. This reduced level of extracellular collagen and integrin that is predicted to normally take place in early postnatal period would occur early during cardiac development in *dal* mutant embryos to prematurely activate cardiomyocyte hypertrophy. This, however, might occur independent of terminating cardiomyocyte proliferation since normal myocardial proliferation was observed in *dal* embryos. This implies that the level or activity of prolidase is one of major determinants that turns on the transitional switching process of cardiomyocyte growth. This provides a series of testable hypotheses. For example: does *Pepd* expression or activity change during the early postnatal period? Is integrin signaling reduced at the onset of the transition from proliferative to hypertrophic cardiomyocyte growth? Future studies are needed to address these questions.

Conclusion

Understanding normal and abnormal cardiac development promises to have an impact on the diagnosis and treatment of human and animal heart diseases. My studies of cardiac hypertrophy in the *dark-like* mutant mouse provide new insight into the developmental development and transition pathway from

proliferative to hypertrophic cardiomyocyte growth. While my genetic studies of arrhythmias in German shepherd dogs did not reveal any chromosomal regions that were strongly linked to susceptibility to ventricular arrhythmias in young dogs, I did demonstrate a significant reduction in *ATP2A2*/SERCA2 levels in the hearts of affected dogs. To the best of my knowledge, my studies are the first to demonstrate a relationship between the expression *ATP2A2*/SERCA2 and the severity of ventricular arrhythmias. This implicates abnormal calcium handling as a key determinant of the severity of inherited ventricular arrhythmias and suggests that future genetic studies of these animals should pay close attention to genes upstream of *ATP2A2* transcription as likely candidates.

REFERENCES

Abdelmalek, N.F., Gerber, T.L., and Menter, A. (2002). Cardiocutaneous syndromes and associations. J Am Acad Dermatol *46*, 161-183; quiz 183-166.

Aikawa, R., Nagai, T., Kudoh, S., Zou, Y., Tanaka, M., Tamura, M., Akazawa, H., Takano, H., Nagai, R., and Komuro, I. (2002). Integrins play a critical role in mechanical stress-induced p38 MAPK activation. Hypertension *39*, 233-238.

Albers, K.M., Wright, D.E., and Davis, B.M. (1994). Overexpression of nerve growth factor in epidermis of transgenic mice causes hypertrophy of the peripheral nervous system. J Neurosci *14*, 1422-1432.

Almasy, L., and Blangero, J. (1998). Multipoint quantitative-trait linkage analysis in general pedigrees. Am J Hum Genet *62*, 1198-1211.

Anderson, D.J. (1993). Molecular control of cell fate in the neural crest: the sympathoadrenal lineage. Annu Rev Neurosci *16*, 129-158.

Andersson, L. (2008). Genome-wide association analysis in domestic animals: a powerful approach for genetic dissection of trait loci. Genetica.

Anversa, P., and Nadal-Ginard, B. (2002). Myocyte renewal and ventricular remodelling. Nature *415*, 240-243.

Azouz, A., Gunn, T.M., and Duke-Cohan, J.S. (2007). Juvenile-onset loss of lipid-raft domains in attractin-deficient mice. Exp Cell Res *313*, 761-771.

Berridge, M.J. (2006). Remodelling Ca2+ signalling systems and cardiac hypertrophy. Biochem Soc Trans *34*, 228-231.

Bisaha, J.G., and Bader, D. (1991). Identification and characterization of a ventricular-specific avian myosin heavy chain, VMHC1: expression in differentiating cardiac and skeletal muscle. Dev Biol *148*, 355-364.

Blangero, J., Williams, J.T., and Almasy, L. (2000). Quantitative trait locus mapping using human pedigrees. Hum Biol *72*, 35-62.

Bloom, S., Lockard, V.G., and Bloom, M. (1996). Intermediate filament-mediated stretch-induced changes in chromatin: a hypothesis for growth initiation in cardiac myocytes. J Mol Cell Cardiol *28*, 2123-2127.

Bohm, M., Raghunath, M., Sunderkotter, C., Schiller, M., Stander, S., Brzoska, T., Cauvet, T., Schioth, H.B., Schwarz, T., and Luger, T.A. (2004). Collagen metabolism is a novel target of the neuropeptide alpha-melanocyte-stimulating hormone. J Biol Chem *279*, 6959-6966.

Brady, M., Koban, M.U., Dellow, K.A., Yacoub, M., Boheler, K.R., and Fuller, S.J. (2003). Sp1 and Sp3 transcription factors are required for trans-activation of the human SERCA2 promoter in cardiomyocytes. Cardiovasc Res *60*, 347-354.

Brancaccio, M., Hirsch, E., Notte, A., Selvetella, G., Lembo, G., and Tarone, G. (2006). Integrin signalling: the tug-of-war in heart hypertrophy. Cardiovasc Res *70*, 422-433.

Bronson, R.T., Donahue, L.R., Samples, R., Kim, J.H., and Naggert, J.K. (2001). Mice with mutations in the mahogany gene Atrn have cerebral spongiform changes. J Neuropathol Exp Neurol *60*, 724-730.

Brown, D.D., Martz, S.N., Binder, O., Goetz, S.C., Price, B.M., Smith, J.C., and Conlon, F.L. (2005). Tbx5 and Tbx20 act synergistically to control vertebrate heart morphogenesis. Development *132*, 553-563.

Chang, Y.F., Imam, J.S., and Wilkinson, M.F. (2007). The nonsense-mediated decay RNA surveillance pathway. Annu Rev Biochem *76*, 51-74.

Chen, H., Yong, W., Ren, S., Shen, W., He, Y., Cox, K.A., Zhu, W., Li, W., Soonpaa, M., Payne, R.M.*, et al.* (2006). Overexpression of bone morphogenetic protein 10 in myocardium disrupts cardiac postnatal hypertrophic growth. J Biol Chem *281*, 27481-27491.

Cheng, C.F., Kuo, H.C., and Chien, K.R. (2003). Genetic modifiers of cardiac arrhythmias. Trends Mol Med *9*, 59-66.

Chetboul, V., Sampedrano, C.C., Gouni, V., Nicolle, A.P., and Pouchelon, J.L. (2006). Two-dimensional color tissue Doppler imaging detects myocardial dysfunction before occurrence of hypertrophy in a young Maine Coon cat. Vet Radiol Ultrasound *47*, 295-300.

Christoffels, V.M., Habets, P.E., Franco, D., Campione, M., de Jong, F., Lamers, W.H., Bao, Z.Z., Palmer, S., Biben, C., Harvey, R.P.*, et al.* (2000). Chamber formation and morphogenesis in the developing mammalian heart. Dev Biol *223*, 266-278.

Chugh, S.S., Reinier, K., Teodorescu, C., Evanado, A., Kehr, E., Al Samara, M., Mariani, R., Gunson, K., and Jui, J. (2008). Epidemiology of sudden cardiac death: clinical and research implications. Prog Cardiovasc Dis *51*, 213-228.

Clark, L.A., Tsai, K.L., Steiner, J.M., Williams, D.A., Guerra, T., Ostrander, E.A., Galibert, F., and Murphy, K.E. (2004). Chromosome-specific microsatellite multiplex sets for linkage studies in the domestic dog. Genomics *84*, 550-554.

Clusin, W.T. (2003). Calcium and cardiac arrhythmias: DADs, EADs, and alternans. Crit Rev Clin Lab Sci *40*, 337-375.

Corda, S., Samuel, J.L., and Rappaport, L. (2000). Extracellular matrix and growth factors during heart growth. Heart Fail Rev *5*, 119-130.

Cota, C.D., Bagher, P., Pelc, P., Smith, C.O., Bodner, C.R., and Gunn, T.M. (2006). Mice with mutations in Mahogunin ring finger-1 (Mgrn1) exhibit abnormal patterning of the left-right axis. Dev Dyn *235*, 3438-3447.

Cota, C.D., Liu, R.R., Sumberac, T.M., Jung, S., Vencato, D., Millet, Y.H., and Gunn, T.M. (2008). Genetic and phenotypic studies of the dark-like mutant mouse. Genesis *46*, 562-573.

Cruickshank, J., Quaas, R.L., Li, J., Hemsley, S., Gunn, T.M., and Moise, N.S. (2009). Genetic analysis of ventricular arrhythmia in young German Shepherd Dogs. J Vet Intern Med *23*, 264-270.

Curley, G.P., Blum, H., and Humphries, M.J. (1999). Integrin antagonists. Cell Mol Life Sci *56*, 427-441.

Dae, M.W., Lee, R.J., Ursell, P.C., Chin, M.C., Stillson, C.A., and Moise, N.S. (1997). Heterogeneous sympathetic innervation in German shepherd dogs with inherited ventricular arrhythmia and sudden cardiac death. Circulation *96*, 1337-1342.

DeSimone, D.W., Stepp, M.A., Patel, R.S., and Hynes, R.O. (1987). The integrin family of cell surface receptors. Biochem Soc Trans *15*, 789-791.

Eisenberg, L.M., and Markwald, R.R. (1995). Molecular regulation of atrioventricular valvuloseptal morphogenesis. Circ Res *77*, 1-6.

Endo, F., and Matsuda, I. (1991). Molecular basis of prolidase (peptidase D) deficiency. Mol Biol Med *8*, 117-127.

Falconer (1956). New mutants. Mouse News Letter *15*, 23.

Falik-Zaccai, T.C., Khayat, M., Luder, A., Frenkel, P., Magen, D., Brik, R., Gershoni-Baruch, R., and Mandel, H. (2009). A broad spectrum of developmental delay in a large cohort of prolidase deficiency patients demonstrates marked interfamilial and intrafamilial phenotypic variability. Am J Med Genet B Neuropsychiatr Genet.

Frey, N., and Olson, E.N. (2003). Cardiac hypertrophy: the good, the bad, and the ugly. Annu Rev Physiol *65*, 45-79.

Fuller, S.J., Gillespie-Brown, J., and Sugden, P.H. (1998). Oncogenic src, raf, and ras stimulate a hypertrophic pattern of gene expression and increase cell size in neonatal rat ventricular myocytes. J Biol Chem *273*, 18146-18152.

Galbiati, F., Razani, B., and Lisanti, M.P. (2001). Emerging themes in lipid rafts and caveolae. Cell *106*, 403-411.

Goldhaber, J.I., Xie, L.H., Duong, T., Motter, C., Khuu, K., and Weiss, J.N. (2005). Action potential duration restitution and alternans in rabbit ventricular myocytes: the key role of intracellular calcium cycling. Circ Res *96*, 459-466.

Groves, A.K., George, K.M., Tissier-Seta, J.P., Engel, J.D., Brunet, J.F., and Anderson, D.J. (1995). Differential regulation of transcription factor gene expression and phenotypic markers in developing sympathetic neurons. Development *121*, 887-901.

Gunn, T.M., Inui, T., Kitada, K., Ito, S., Wakamatsu, K., He, L., Bouley, D.M., Serikawa, T., and Barsh, G.S. (2001). Molecular and phenotypic analysis of Attractin mutant mice. Genetics *158*, 1683-1695.

Harris, B., Ward-Bailey, PF., Johnson, KR., Elcher, EM., Washburn, L., Gagnon, L., Bronson, RT.,and Davisson, MT. (2003). A New Recessive Color Mutation on Mouse Chromosome 7, dark-like. MGI Direct Data Submission.

He, L., Eldridge, A.G., Jackson, P.K., Gunn, T.M., and Barsh, G.S. (2003). Accessory proteins for melanocortin signaling: attractin and mahogunin. Ann N Y Acad Sci *994*, 288-298.

He, L., Gunn, T.M., Bouley, D.M., Lu, X.Y., Watson, S.J., Schlossman, S.F., Duke-Cohan, J.S., and Barsh, G.S. (2001). A biochemical function for attractin in agouti-induced pigmentation and obesity. Nat Genet *27*, 40-47.

Hilenski, L.L., Terracio, L., and Borg, T.K. (1991). Myofibrillar and cytoskeletal assembly in neonatal rat cardiac myocytes cultured on laminin and collagen. Cell Tissue Res *264*, 577-587.

Howe, A., Aplin, A.E., Alahari, S.K., and Juliano, R.L. (1998). Integrin signaling and cell growth control. Curr Opin Cell Biol *10*, 220-231.

Icardo, J.M., and Fernandez-Teran, A. (1987). Morphologic study of ventricular trabeculation in the embryonic chick heart. Acta Anat (Basel) *130*, 264-274.

Ieda, M., Tsuchihashi, T., Ivey, K.N., Ross, R.S., Hong, T.T., Shaw, R.M., and Srivastava, D. (2009). Cardiac fibroblasts regulate myocardial proliferation through beta1 integrin signaling. Dev Cell *16*, 233-244.

Isshiki, M., Yamamoto, Y., Satoh, H., and Shimamoto, K. (2001). Nonsense-mediated decay of mutant waxy mRNA in rice. Plant Physiol *125*, 1388-1395.

Jervell, A., and Lange-Nielsen, F. (1957). Congenital deaf-mutism, functional heart disease with prolongation of the Q-T interval and sudden death. Am Heart J *54*, 59-68.

Jiang, X., Rowitch, D.H., Soriano, P., McMahon, A.P., and Sucov, H.M. (2000). Fate of the mammalian cardiac neural crest. Development *127*, 1607-1616.

Jiao, J., Kim, H.Y., Liu, R.R., Hogan, C.A., Sun, K., Tam, L.M., and Gunn, T.M. (2009). Transgenic analysis of the physiological functions of Mahogunin ring finger-1 isoforms. Genesis.

Katz, G., Arad, M., and Eldar, M. (2009). Catecholaminergic polymorphic ventricular tachycardia from bedside to bench and beyond. Curr Probl Cardiol *34*, 9-43.

Kelly, R.G., and Buckingham, M.E. (2002). The anterior heart-forming field: voyage to the arterial pole of the heart. Trends Genet *18*, 210-216.

Kempiak, S.J., Yamaguchi, H., Sarmiento, C., Sidani, M., Ghosh, M., Eddy, R.J., Desmarais, V., Way, M., Condeelis, J., and Segall, J.E. (2005). A neural Wiskott-Aldrich Syndrome protein-mediated pathway for localized activation of actin polymerization that is regulated by cortactin. J Biol Chem *280*, 5836-5842.

Kim, B.Y., Olzmann, J.A., Barsh, G.S., Chin, L.S., and Li, L. (2007). Spongiform neurodegeneration-associated E3 ligase Mahogunin ubiquitylates TSG101 and regulates endosomal trafficking. Mol Biol Cell *18*, 1129-1142.

Kim, D.J., Park, S.H., Lim, C.S., Chun, J.S., Kim, J.K., and Song, W.K. (2003). Cellular localization of integrin isoforms in phenylephrine-induced hypertrophic cardiac myocytes. Cell Biochem Funct *21*, 41-48.

Kiss, M., Wlaschek, M., Brenneisen, P., Michel, G., Hommel, C., Lange, T.S., Peus, D., Kemeny, L., Dobozy, A., Scharffetter-Kochanek, K.*, et al.* (1995). Alpha-melanocyte stimulating hormone induces collagenase/matrix metalloproteinase-1 in human dermal fibroblasts. Biol Chem Hoppe Seyler *376*, 425-430.

Klewer, S.E., Krob, S.L., Kolker, S.J., and Kitten, G.T. (1998). Expression of type VI collagen in the developing mouse heart. Dev Dyn *211*, 248-255.

Kuppuswamy, D., Kerr, C., Narishige, T., Kasi, V.S., Menick, D.R., and Cooper, G.t. (1997). Association of tyrosine-phosphorylated c-Src with the cytoskeleton of hypertrophying myocardium. J Biol Chem *272*, 4500-4508.

Kuramoto, T., Kitada, K., Inui, T., Sasaki, Y., Ito, K., Hase, T., Kawagachi, S., Ogawa, Y., Nakao, K., Barsh, G.S.*, et al.* (2001). Attractin/mahogany/zitter plays a critical role in myelination of the central nervous system. Proc Natl Acad Sci U S A *98*, 559-564.

Lal, H., Guleria, R.S., Foster, D.M., Lu, G., Watson, L.E., Sanghi, S., Smith, M., and Dostal, D.E. (2007). Integrins: novel therapeutic targets for cardiovascular diseases. Cardiovasc Hematol Agents Med Chem *5*, 109-132.

Le Pape, E., Passeron, T., Giubellino, A., Valencia, J.C., Wolber, R., and Hearing, V.J. (2009). Microarray analysis sheds light on the dedifferentiating role of agouti signal protein in murine melanocytes via the Mc1r. Proc Natl Acad Sci U S A *106*, 1802-1807.

Lee, J.K., and Thomas, D.C. (2000). Performance of Markov chain-Monte Carlo approaches for mapping genes in oligogenic models with an unknown number of loci. Am J Hum Genet *67*, 1232-1250.

Lee, K.F., Simon, H., Chen, H., Bates, B., Hung, M.C., and Hauser, C. (1995). Requirement for neuregulin receptor erbB2 in neural and cardiac development. Nature *378*, 394-398.

Lehmann, L.H., Schaeufele, T., Buss, S.J., Balanova, M., Hartschuh, W., Ehlermann, P., and Katus, H.A. (2009). IMAGE CARDIO MED. A patient with LEOPARD syndrome and PTPN11 mutation. Circulation *119*, 1328-1329.

Lehnart, S.E., Schillinger, W., Pieske, B., Prestle, J., Just, H., and Hasenfuss, G. (1998). Sarcoplasmic reticulum proteins in heart failure. Ann N Y Acad Sci *853*, 220-230.

Liang, X., Nazarian, A., Erdjument-Bromage, H., Bornmann, W., Tempst, P., and Resh, M.D. (2001). Heterogeneous fatty acylation of Src family kinases with polyunsaturated fatty acids regulates raft localization and signal transduction. J Biol Chem *276*, 30987-30994.

Lindblad-Toh, K., Wade, C.M., Mikkelsen, T.S., Karlsson, E.K., Jaffe, D.B., Kamal, M., Clamp, M., Chang, J.L., Kulbokas, E.J., 3rd, Zody, M.C.*, et al.*

(2005). Genome sequence, comparative analysis and haplotype structure of the domestic dog. Nature *438*, 803-819.

Livak, K.J., and Schmittgen, T.D. (2001). Analysis of relative gene expression data using real-time quantitative PCR and the 2(-Delta Delta C(T)) Method. Methods *25*, 402-408.

Lloyd-Jones, D., Adams, R., Carnethon, M., De Simone, G., Ferguson, T.B., Flegal, K., Ford, E., Furie, K., Go, A., Greenlund, K.*, et al.* (2009). Heart disease and stroke statistics--2009 update: a report from the American Heart Association Statistics Committee and Stroke Statistics Subcommittee. Circulation *119*, 480-486.

Lupi, A., Tenni, R., Rossi, A., Cetta, G., and Forlino, A. (2008). Human prolidase and prolidase deficiency: an overview on the characterization of the enzyme involved in proline recycling and on the effects of its mutations. Amino Acids *35*, 739-752.

Ly, H.Q., Greiss, I., Talakic, M., Guerra, P.G., Macle, L., Thibault, B., Dubuc, M., and Roy, D. (2005). Sudden death and hypertrophic cardiomyopathy: a review. Can J Cardiol *21*, 441-448.

Mackay, T.F. (2001). Quantitative trait loci in Drosophila. Nat Rev Genet *2*, 11-20.

Marian, A.J., and Roberts, R. (1995). Recent advances in the molecular genetics of hypertrophic cardiomyopathy. Circulation *92*, 1336-1347.

Marks, A.R. (2000). Cardiac intracellular calcium release channels: role in heart failure. Circ Res *87*, 8-11.

Michael, G., Xiao, L., Qi, X.Y., Dobrev, D., and Nattel, S. (2009). Remodelling of cardiac repolarization: how homeostatic responses can lead to arrhythmogenesis. Cardiovasc Res *81*, 491-499.

Miller, K.A., Gunn, T.M., Carrasquillo, M.M., Lamoreux, M.L., Galbraith, D.B., and Barsh, G.S. (1997). Genetic studies of the mouse mutations mahogany and mahoganoid. Genetics *146*, 1407-1415.

Moise, N.S., Gilmour, R.F., Jr., and Riccio, M.L. (1997a). An animal model of spontaneous arrhythmic death. J Cardiovasc Electrophysiol *8*, 98-103.

Moise, N.S., Gilmour, R.F., Jr., Riccio, M.L., and Flahive, W.F., Jr. (1997b). Diagnosis of inherited ventricular tachycardia in German shepherd dogs. J Am Vet Med Assoc *210*, 403-410.

Moise, N.S., Meyers-Wallen, V., Flahive, W.J., Valentine, B.A., Scarlett, J.M., Brown, C.A., Chavkin, M.J., Dugger, D.A., Renaud-Farrell, S., Kornreich, B.*, et al.* (1994). Inherited ventricular arrhythmias and sudden death in German shepherd dogs. J Am Coll Cardiol *24*, 233-243.

Nguyen-Tran, V.T., Kubalak, S.W., Minamisawa, S., Fiset, C., Wollert, K.C., Brown, A.B., Ruiz-Lozano, P., Barrere-Lemaire, S., Kondo, R., Norman, L.W.*, et al.* (2000). A novel genetic pathway for sudden cardiac death via defects in the transition between ventricular and conduction system cell lineages. Cell *102*, 671-682.

Okada, Y., Takeda, S., Tanaka, Y., Belmonte, J.C., and Hirokawa, N. (2005). Mechanism of nodal flow: a conserved symmetry breaking event in left-right axis determination. Cell *121*, 633-644.

Olson, T.M., Michels, V.V., Thibodeau, S.N., Tai, Y.S., and Keating, M.T. (1998). Actin mutations in dilated cardiomyopathy, a heritable form of heart failure. Science *280*, 750-752.

Oparil, S., Bishop, S.P., and Clubb, F.J., Jr. (1984). Myocardial cell hypertrophy or hyperplasia. Hypertension *6*, III38-43.

Peng, X., Wu, X., Druso, J.E., Wei, H., Park, A.Y., Kraus, M.S., Alcaraz, A., Chen, J., Chien, S., Cerione, R.A.*, et al.* (2008). Cardiac developmental defects and eccentric right ventricular hypertrophy in cardiomyocyte focal adhesion kinase (FAK) conditional knockout mice. Proc Natl Acad Sci U S A *105*, 6638-6643.

Ramsdell, A.F., Moreno-Rodriguez, R.A., Wienecke, M.M., Sugi, Y., Turner, D.K., Mjaatvedt, C.H., and Markwald, R.R. (1998). Identification of an autocrine signaling pathway that amplifies induction of endocardial cushion tissue in the avian heart. Acta Anat (Basel) *162*, 1-15.

Roberts, R., and Brugada, R. (2003). Genetics and arrhythmias. Annu Rev Med *54*, 257-267.

Roden, D.M., Lazzara, R., Rosen, M., Schwartz, P.J., Towbin, J., and Vincent, G.M. (1996). Multiple mechanisms in the long-QT syndrome. Current knowledge, gaps, and future directions. The SADS Foundation Task Force on LQTS. Circulation *94*, 1996-2012.

Sato, T., Hirao, K., and Hiejima, K. (1993). The relationship between early afterdepolarization and the occurrence of torsades de pointes--an in vivo canine model study. Jpn Circ J *57*, 543-552.

Schultz Jel, J., Glascock, B.J., Witt, S.A., Nieman, M.L., Nattamai, K.J., Liu, L.H., Lorenz, J.N., Shull, G.E., Kimball, T.R., and Periasamy, M. (2004). Accelerated onset of heart failure in mice during pressure overload with chronically decreased SERCA2 calcium pump activity. Am J Physiol Heart Circ Physiol *286*, H1146-1153.

Seth, M., Sumbilla, C., Mullen, S.P., Lewis, D., Klein, M.G., Hussain, A., Soboloff, J., Gill, D.L., and Inesi, G. (2004). Sarco(endo)plasmic reticulum Ca2+ ATPase (SERCA) gene silencing and remodeling of the Ca2+ signaling mechanism in cardiac myocytes. Proc Natl Acad Sci U S A *101*, 16683-16688.

Sicouri, S., and Antzelevitch, C. (1993). Drug-induced afterdepolarizations and triggered activity occur in a discrete subpopulation of ventricular muscle cells (M cells) in the canine heart: quinidine and digitalis. J Cardiovasc Electrophysiol *4*, 48-58.

Sicouri, S., Antzelevitch, D., Heilmann, C., and Antzelevitch, C. (1997). Effects of sodium channel block with mexiletine to reverse action potential prolongation in in vitro models of the long term QT syndrome. J Cardiovasc Electrophysiol *8*, 1280-1290.

Sosunov, E.A., Anyukhovsky, E.P., Shvilkin, A., Hara, M., Steinberg, S.F., Danilo, P., Jr., Rosen, M.R., Moise, N.S., Merot, J., Probst, V.*, et al.* (1999). Abnormal cardiac repolarization and impulse initiation in German shepherd dogs with inherited ventricular arrhythmias and sudden death. Cardiovasc Res *42*, 65-79.

Spier, A.W., and Meurs, K.M. (2004). Evaluation of spontaneous variability in the frequency of ventricular arrhythmias in Boxers with arrhythmogenic right ventricular cardiomyopathy. J Am Vet Med Assoc *224*, 538-541.

Sprague, J., Doerry, E., Douglas, S., and Westerfield, M. (2001). The Zebrafish Information Network (ZFIN): a resource for genetic, genomic and developmental research. Nucleic Acids Res *29*, 87-90.

Srivastava, D. (2006). Making or breaking the heart: from lineage determination to morphogenesis. Cell *126*, 1037-1048.

Srivastava, D., Cserjesi, P., and Olson, E.N. (1995). A subclass of bHLH proteins required for cardiac morphogenesis. Science *270*, 1995-1999.

Srivastava, D., and Olson, E.N. (2000). A genetic blueprint for cardiac development. Nature *407*, 221-226.

Stadelmann, W.K., Digenis, A.G., and Tobin, G.R. (1998). Physiology and healing dynamics of chronic cutaneous wounds. Am J Surg *176*, 26S-38S.

Steinberg, S.F., Alcott, S., Pak, E., Hu, D., Protas, L., Moise, N.S., Robinson, R.B., and Rosen, M.R. (2002). beta(1)-Receptors increase cAMP and induce abnormal Ca(i) cycling in the German shepherd sudden death model. Am J Physiol Heart Circ Physiol *282*, H1181-1188.

Steingrimsson, E., Copeland, N.G., and Jenkins, N.A. (2006). Mouse coat color mutations: from fancy mice to functional genomics. Dev Dyn *235*, 2401-2411.

Sun, K., Johnson, B.S., and Gunn, T.M. (2007). Mitochondrial dysfunction precedes neurodegeneration in mahogunin (Mgrn1) mutant mice. Neurobiol Aging *28*, 1840-1852.

Takahashi, M., Kojima, M., Nakajima, K., Suzuki-Migishima, R., Motegi, Y., Yokoyama, M., and Takeuchi, T. (2004). Cardiac abnormalities cause early lethality of jumonji mutant mice. Biochem Biophys Res Commun *324*, 1319-1323.

Takizawa, T., Arai, M., Tomaru, K., Koitabashi, N., Baker, D.L., Periasamy, M., and Kurabayashi, M. (2003). Transcription factor Sp1 regulates SERCA2 gene expression in pressure-overloaded hearts: a study using in vivo direct gene transfer into living myocardium. J Mol Cell Cardiol *35*, 777-783.

Tallini, Y.N., Ohkura, M., Choi, B.R., Ji, G., Imoto, K., Doran, R., Lee, J., Plan, P., Wilson, J., Xin, H.B.*, et al.* (2006). Imaging cellular signals in the heart in vivo: Cardiac expression of the high-signal Ca2+ indicator GCaMP2. Proc Natl Acad Sci U S A *103*, 4753-4758.

Tam, P.P., Parameswaran, M., Kinder, S.J., and Weinberger, R.P. (1997). The allocation of epiblast cells to the embryonic heart and other mesodermal lineages: the role of ingression and tissue movement during gastrulation. Development *124*, 1631-1642.

Thomas, G., Killeen, M.J., Gurung, I.S., Hakim, P., Balasubramaniam, R., Goddard, C.A., Grace, A.A., and Huang, C.L. (2007). Mechanisms of ventricular arrhythmogenesis in mice following targeted disruption of KCNE1 modelling long QT syndrome 5. J Physiol *578*, 99-114.

Verdi, J.M., Groves, A.K., Farinas, I., Jones, K., Marchionni, M.A., Reichardt, L.F., and Anderson, D.J. (1996). A reciprocal cell-cell interaction mediated by NT-3 and neuregulins controls the early survival and development of sympathetic neuroblasts. Neuron *16*, 515-527.

Vincent, G.M. (1998). The molecular genetics of the long QT syndrome: genes causing fainting and sudden death. Annu Rev Med *49*, 263-274.

Visscher, P.M., Haley, C.S., Heath, S.C., Muir, W.J., and Blackwood, D.H. (1999). Detecting QTLs for uni- and bipolar disorder using a variance component method. Psychiatr Genet *9*, 75-84.

Wachtell, K., Devereux, R.B., Lyle, P.A., Okin, P.M., and Gerdts, E. (2008). The left atrium, atrial fibrillation, and the risk of stroke in hypertensive patients with left ventricular hypertrophy. Ther Adv Cardiovasc Dis *2*, 507-513.

Walker, W.P., Aradhya, S., Hu, C.L., Shen, S., Zhang, W., Azarani, A., Lu, X., Barsh, G.S., and Gunn, T.M. (2007). Genetic analysis of attractin homologs. Genesis *45*, 744-756.

Wan, X., Laurita, K.R., Pruvot, E.J., and Rosenbaum, D.S. (2005). Molecular correlates of repolarization alternans in cardiac myocytes. J Mol Cell Cardiol *39*, 419-428.

Wright, A., Charlesworth, B., Rudan, I., Carothers, A., and Campbell, H. (2003). A polygenic basis for late-onset disease. Trends Genet *19*, 97-106.

Zaffran, S., and Frasch, M. (2002). Early signals in cardiac development. Circ Res *91*, 457-469.